DOKUZ EYLÜL UNIVERSITY
GRADUATE SCHOOL OF NATURAL AND APPLIED SCIENCES

DYNAMIC STABILITY ANALYSIS OF A CURVED BEAM WITH SUSPENDED SPRING-MASS SYSTEMS

by
Seda VATAN

June, 2019
İZMİR

DYNAMIC STABILITY ANALYSIS OF A CURVED BEAM WITH SUSPENDED SPRING-MASS SYSTEMS

A Thesis Submitted to the
Graduate School of Natural and Applied Sciences of Dokuz Eylül University
In Partial Fulfillment of the Requirements for the Degree of Master of Science
in Mechanical Engineering, Machine Theory and Dynamics Program

by
Seda VATAN

June, 2019
İZMİR

M.Sc. THESIS EXAMINATION RESULT FORM

We have read the thesis entitled **"DYNAMIC STABILITY ANALYSIS OF A CURVED BEAM WITH SUSPENDED SPRING-MASS SYSTEMS"** completed by **SEDA VATAN** under supervision of **PROF. DR. HASAN ÖZTÜRK** and we certify that in our opinion it is fully adequate, in scope and in quality, as a thesis for the degree of Master of Science.

Prof. Dr. Hasan ÖZTÜRK

Supervisor

Prof. Dr. Zeki KIRAL

(Jury Member)

Dr. Öğr. Ü. Aysun BALTACI

(Jury Member)

Prof. Dr. Kadriye ERTEKİN
Director
Graduate School of Natural and Applied Sciences

ACKNOWLEDGMENTS

I would like to express my respect and gratitude to esteemed mentor Prof. Dr. Mustafa SABUNCU who I started this study with, for guidance, encouragement and clarifying me with his knowledge. I will always remember him and his advice.

I would also like to thank my supervisor Prof. Dr. Hasan ÖZTÜRK who always support me and help in every respect, for giving the chance to study with him.

I owe thanks to Research Assistant Salih DEMİRTAŞ for his valuable help throughout this study.

I am remarkably indebted to my husband Mr. Onur CAN and all of my family for their patience and support during my education.

Finally, I am grateful to my workmate Research Assistant Kübra TURAL, Research Assistant İpek ŞAMLI LÖK, and all of my friends for encouraging me in my challenging time.

Seda VATAN

DYNAMIC STABILITY ANALYSIS OF A CURVED BEAM WITH SUSPENDED SPRING-MASS SYSTEMS

ABSTRACT

In this study, the dynamic stability of a curved beam with the suspended spring-mass system is investigated for both isotropic material and layered composite. The beam is considered to Euler-Bernoulli beam and uniform cross-section. The effective flexural modulus have been employed for the composite curved beam. The curved beam fixed both ends and subjected to a uniformly distributed periodic axial load. The curved beam modeled by using the finite element model based on energy equations in conjunction with Bolotin's approach.

The developed MATLAB finite element code is used to determine the dynamic instability regions. The natural frequencies and critical buckling load parameters of the curved beam are also determined. Those are compared with the results of ANSYS model and other studies existing literature and very good agreement is found. The effect of the stiffness coefficients, position of the spring-mass system, dynamic load parameter, and static load parameter on the dynamic regions are investigated for various subtended angle and radius of the curved beam. The results are presented by tables and graphics.

Keywords: Dynamic stability, Finite element method, suspended spring-mass

ASILI KÜTLE-YAY SİSTEMLERİNE SAHİP EĞRİ KİRİŞİN DİNAMİK KARARLILIK ANALİZİ

ÖZ

Bu çalışmada, asılı kütle-yay sistemine sahip eğri bir kirişin dinamik kararlılığı hem izotropik malzeme hem de tabakalı kompozit için incelenmiştir. Kiriş, Euler-Bernoulli kirişi ve sabit kesit alana sahiptir. Kompozit eğri kiriş için etkin esneklik modülü kullanılmıştır. Eğri kiriş, iki ucundan sabitlenmiş ve düzgün dağılan periyodik eksenel bir yüke maruz bırakılmıştır. Eğri kiriş modeli, Bolotin yaklaşımı ve enerji denklemlerine dayanan sonlu elemanlar modeli kullanılarak oluşturulmuştur.

Geliştirilen MATLAB sonlu elemanlar kodu kullanılarak dinamik kararsızlık bölgeleri belirlenmiştir. Kirişin doğal frekansları ve kritik burkulma yükü parametreleri de belirlenmiştir. Bunlar, ANSYS programında oluşturulan modelin ve literatürde var olan çalışmaların sonuçları ile karşılaştırılmış ve sonuçların yakın olduğu görülmüştür. Eğri kirişin çeşitli açı ve radyus değerleri için asılı kütle-yay sisteminin konumunun, yay katsayısının, dinamik yük parametresinin ve statik yük parametresinin kirişin kararsızlık bölgelerine etklileri incelenmiştir. Sonuçlar tablo ve grafiklerle sunulmuştur.

Anahtar kelimeler: Dinamik kararlılık, Sonlu elemanlar methodu, asılı kütle-yay

CONTENTS

Page

M.Sc. THESIS EXAMINATION RESULT FORM ii
ACKNOWLEDGMENTS... iii
ABSTRACT iv
ÖZ v
LIST OF FIGURES ix
LIST OF TABLES.. xvi

CHAPTER ONE - INTRODUCTION 1

1.1 Introduction 1
1.2 Literature about the Issue 2
1.3 Objective of the Thesis 4
1.4 Organization of the Thesis 5

CHAPTER TWO - THEORY OF DYNAMIC STABILITY 6

2.1 Theory of Stability.. 6
2.2 The System with Periodic Load 10

CHAPTER THREE - THEORY OF FINITE ELEMENT METHOD...............12

3.1 What is the Finite Element Method? 12
3.2 Process of the Finite Element Method...13
3.2.1 Bar Element 14
3.2.2 Beam Element...17
3.3 Transformation Matrix...20
3.4 Global Matrices 22

CHAPTER FOUR - THEORETICAL ANALYSIS 24

4.1 Determination of the Problem 24

4.2 The Finite Element Model 25
4.2.1 Energy Equations for a Finite Curved Element 25
4.2.2 Energy Equations for the spring-mass system......................................29
4.2.2 The Assembly Procedure of the spring-mass system.............................30
4.3 Investigation of Dynamic Stability..31

CHAPTER FIVE - DYNAMIC STABILITY ANALYSIS.................................34

5.1 Vibration Analysis..34
5.2 Dynamic Stability Regions of a Curved Beam 40
5.1.1 The Effect of Subtended Angle (θ) 40
5.1.2 The Effect of Radius of the Curved Beam 43
5.3 Dynamic Stability of Curved Beam with Suspended Spring-Mass System 45
5.2.1 The Effect of Subtended Angle (θ) 51
5.2.2 The Effect of Radius of the Curved Beam 54
5.2.3 The Effect of the Stiffness Coefficient of the Suspended Spring-Mass System...56

CHAPTER SIX - DYNAMIC STABILITY ANALYSIS FOR A COMPOSITE CURVED BEAM 62

6.1 Composite Structures...62
6.1.1 The effective flexural modulus for a two-dimensional unidirectional lamina..62
6.2 Free Vibration Analysis of a Composite Curved Beam 67
6.3 Dynamic Stability Region of the Composite Curved Beam 68
6.4 Dynamic Stability Region of the Curved Composite Beam with Suspended System 71

CHAPTER SEVEN - CONCLUSION 81

REFERENCES 83

APPENDICES..**86**

LIST OF FIGURES

Page

Figure 1.1 Different examples of a structure containing curved beams 1

Figure 2.1 Mechanical System 7

Figure 2.2 Two Solutions of Mathieu's Equation 9

Figure 2.3 A system with Periodic Change in Loading 11

Figure 3.1 Finite element model of Plano-milling machine.....................................12

Figure 3.2 A Bar Element 14

Figure 3.3 A Beam Element 17

Figure 3.4 L-Beam involving two beam element 21

Figure 3.5 Two elements of L-Beam in Figure 3.4 21

Figure 3.6 A beam consisted of two elements...22

Figure 3.7 Elements of the beam 22

Figure 4.1 Model of the curved beam with the suspended spring-mass system 24

Figure 4.2 A curved finite element 25

Figure 4.3 The joints of the suspended spring-mass system 29

Figure 5.1 Convergence curve...34

Figure 5.2 The node numbers of the curved beam and spring-mass systems in different cases ; (a) no spring-mass system, (b) one spring-mass system on the 25th node, (c) three spring-mass system on 13th, 25th, and 36th nodes. 37

Figure 5.3 The effect of suspended spring-mass location and k_{ratio} on the first four natural frequencies of the curved beam (E=2.069x10^{11}N/m^2, ν=0.3, ρ=7836.8 kg/m^3, b=0.02m, t=0.01m, θ=120º, R=1m.)............................38

Figure 5.4 The effect of the subtended angle on the first stability regions of the curved beam, α=0 (E=2.069x10^{11}N/m^2, ν=0.3, ρ=7836.8 kg/m^3, b=0.02m, t=0.01m, R=1m) 41

Figure 5.5 The effect of the subtended angle on the second stability regions of the curved beam, α=0 (E=2.069x10^{11}N/m^2, ν=0.3, ρ=7836.8 kg/m^3, b=0.02m, t=0.01m, R=1m) 41

Figure 5.6 The effect of the subtended angle on the first stability regions of the curved beam, α=0.5 (E=2.069x10^{11}N/m^2, ν=0.3, ρ=7836.8 kg/m^3, b=0.02m, t=0.01m, R=1m) 42
Figure 5.7 The effect of the subtended angle on the second stability regions of the curved beam, α=0.5 (E=2.069x10^{11}N/m^2, ν=0.3, ρ=7836.8 kg/m^3, b=0.02m, t=0.01m, R=1m) 42
Figure 5.8 The effect of the radius of the curved beam on the first stability regions of the curved beam, α=0 (E=2.069x10^{11}N/m^2, ν=0.3, ρ=7836.8 kg/m^3, b=0.02m, t=0.01m, θ=120º) 43
Figure 5.9 The effect of the radius of the curved beam on the second stability regions of the curved beam, α=0 (E=2.069x10^{11}N/m^2, ν=0.3, ρ=7836.8 kg/m^3, b=0.02m, t=0.01m, θ=120º) 44
Figure 5.10 The effect of the radius of the curved beam on the first stability regions of the curved beam, α=0.5 (E=2.069x10^{11}N/m^2, ν=0.3, ρ=7836.8 kg/m^3, b=0.02m, t=0.01m, θ=120º) 44
Figure 5.11 The effect of the radius of the curved beam on the second stability regions of the curved beam, α=0.5 (E=2.069x10^{11}N/m^2, ν=0.3, ρ=7836.8 kg/m^3, b=0.02m, t=0.01m, θ=120º) 45
Figure 5.12 The effect of the spring-mass system on the first stability regions of the curved beam, α=0 (E=2.069x10^{11}N/m^2, ν=0.3, ρ=7836.8 kg/m^3, b=0.02m, t=0.01m, θ=120º, R=1m, m_s=2 kg, k_{ratio}=1)..46
Figure 5.13 The effect of the spring-mass system on the second stability regions of the curved beam, α=0 (E=2.069x10^{11}N/m^2, ν=0.3, ρ=7836.8 kg/m^3, b=0.02m, t=0.01m, θ=120º, R=1m, m_s=2 kg, k_{ratio}=1)..47
Figure 5.14 The effect of the spring-mass system on the first stability regions of the curved beam, α=0.5 (E=2.069x10^{11}N/m^2, ν=0.3, ρ=7836.8 kg/m^3, b=0.02m, t=0.01m, θ=120º, R=1m, m_s=2 kg, k_{ratio}=1)..47
Figure 5.15 The effect of the spring-mass system on the second stability regions of the curved beam, α=0.5 (E=2.069x10^{11}N/m^2, ν=0.3, ρ=7836.8 kg/m^3, b=0.02m, t=0.01m, θ=120º, R=1m, m_s=2 kg, k_{ratio}=1)..48
Figure 5.16 The effect of the location of the spring-mass system on the first stability regions of the curved beam with one suspended spring-mass system, α=0

($E=2.069x10^{11}N/m^2$, $\nu=0.3$, $\rho=7836.8$ kg/m^3, b=0.02m, t=0.01m, $\theta=120^o$, R=1m, $m_s=2$ kg, $k_{ratio}=1$) 49
Figure 5.17 The effect of the location of the spring-mass system on the second stability regions of the curved beam with one suspended spring-mass system, $\alpha=0$ ($E=2.069x10^{11}N/m^2$, $\nu=0.3$, $\rho=7836.8kg/m^3$, b=0.02m, t=0.01m, $\theta=120^o$, R=1m, $m_s=2$ kg, $k_{ratio}=1$) 49
Figure 5.18 The effect of the location of the spring-mass system on the first stability regions of the curved beam with one suspended spring-mass system, $\alpha=0.5$ ($E=2.069x10^{11}N/m^2$, $\nu=0.3$, $\rho=7836.8$ kg/m^3, b=0.02m, t=0.01m, $\theta=120^o$, R=1m, $m_s=2$ kg, $k_{ratio}=1$) 50
Figure 5.19 The effect of the location of the spring-mass system on the second stability regions of the curved beam with one suspended spring-mass system, $\alpha=0.5$ ($E=2.069x10^{11}N/m^2$, $\nu=0.3$, $\rho=7836.8kg/m^3$, b=0.02m, t=0.01m, $\theta=120^o$, R=1m, $m_s=2$ kg, $k_{ratio}=1$) 50
Figure 5.20 The effect of the subtended angle on the first stability regions of the curved beam with one suspended spring-mass system, $\alpha=0$ ($E=2.069x10^{11}N/m^2$, $\nu=0.3$, $\rho=7836.8$ kg/m^3, b=0.02m, t=0.01m, R=1m, $m_s=2$ kg, $k_{ratio}=1$) 51
Figure 5.21 The effect of the subtended angle on the second stability regions of the curved beam with one suspended spring-mass system, $\alpha=0$ ($E=2.069x10^{11}N/m^2$, $\nu=0.3$, $\rho=7836.8$ kg/m^3, b=0.02m, t=0.01m, R=1m, $m_s=2$ kg, $k_{ratio}=1$) 52
Figure 5.22 The effect of the subtended angle on the first stability regions of the curved beam with one suspended spring-mass system $\alpha=0.5$, ($E=2.069x10^{11}N/m^2$, $\nu=0.3$, $\rho=7836.8$ kg/m^3, b=0.02m, t=0.01m, R=1m, $m_s=2$ kg, $k_{ratio}=1$) 52
Figure 5.23 The effect of the subtended angle on the second stability regions of the curved beam with one suspended spring-mass system $\alpha=0.5$, ($E=2.069x10^{11}N/m^2$, $\nu=0.3$, $\rho=7836.8$ kg/m^3, b=0.02m, t=0.01m, R=1m, $m_s=2$ kg, $k_{ratio}=1$) 53
Figure 5.24 The effect of the radius of the curved beam on the first stability regions of the curved beam with one suspended spring-mass system, $\alpha=0$ ($E=2.069x10^{11}N/m^2$, $\nu=0.3$, $\rho=7836.8$ kg/m^3, b=0.02m, t=0.01m, $\theta=120^o$, $m_s=2$ kg, $k_{ratio}=1$) 54

Figure 5.25 The effect of the radius of the curved beam on the second stability regions of the curved beam with one suspended spring-mass system, α=0 (E=2.069x10^{11}N/m^2, ν=0.3, ρ=7836.8 kg/m^3, b=0.02m, t=0.01m, θ=120º, m_s=2 kg, k_{ratio}=1) 55
Figure 5.26 The effect of the radius of the curved beam on the first stability regions of the curved beam with one suspended spring-mass system, α=0 (E=2.069x10^{11}N/m^2, ν=0.3, ρ=7836.8 kg/m^3, b=0.02m, t=0.01m, θ=120º, m_s=2 kg, k_{ratio}=1) 55
Figure 5.27 The effect of the radius of the curved beam on the second stability regions of the curved beam with one suspended spring-mass system, α=0 (E=2.069x10^{11}N/m^2, ν=0.3, ρ=7836.8 kg/m^3, b=0.02m, t=0.01m, θ=120º, m_s=2 kg, k_{ratio}=1) 56
Figure 5.28 The effect of stiffness ratio of suspended spring on the first stability regions of the curved beam with one suspended spring-mass system, α=0 (E=2.069x10^{11}N/m^2, ν=0.3, ρ=7836.8 kg/m^3, b=0.02m, t=0.01m, θ=120º, R=1m, m_s=2 kg) 57
Figure 5.29 The effect of stiffness ratio of suspended spring on the second stability regions of the curved beam with one suspended spring-mass system, α=0 (E=2.069x10^{11}N/m^2, ν=0.3, ρ=7836.8 kg/m^3, b=0.02m, t=0.01m, θ=120º, R=1m, m_s=2 kg) 58
Figure 5.30 The effect of stiffness ratio of suspended spring on the first stability regions of the curved beam with one suspended spring-mass system, α=0 (E=2.069x10^{11}N/m^2, ν=0.3, ρ=7836.8 kg/m^3, b=0.02m, t=0.01m, θ=120º, R=1m, m_s=2 kg) 58
Figure 5.31 The effect of stiffness ratio of suspended spring on the second stability regions of the curved beam with one suspended spring-mass system, α=0 (E=2.069x10^{11}N/m^2, ν=0.3, ρ=7836.8 kg/m^3, b=0.02m, t=0.01m, θ=120º, R=1m, m_s=2 kg) 59
Figure 5.32 The effect of stiffness ratio of suspended spring on the first stability regions of the curved beam with one suspended spring-mass system, α=0.5 (E=2.069x10^{11}N/m^2, ν=0.3, ρ=7836.8 kg/m^3, b=0.02m, t=0.01m, θ=120º, R=1m, m_s=2 kg) 59

Figure 5.33 The effect of stiffness ratio of suspended spring on the second stability regions of the curved beam with one suspended spring-mass system, α=0.5 ($E=2.069x10^{11}N/m^2$, ν=0.3, ρ=7836.8 kg/m^3, b=0.02m, t=0.01m, θ=120º, R=1m, m_s=2 kg) 60
Figure 5.34 The effect of stiffness ratio of suspended spring on the first stability regions of the curved beam with one suspended spring-mass system, α=0.5 ($E=2.069x10^{11}N/m^2$, ν=0.3, ρ=7836.8 kg/m^3, b=0.02m, t=0.01m, θ=120º, R=1m, m_s=2 kg) 60
Figure 5.35 The effect of stiffness ratio of suspended spring on the second stability regions of the curved beam with one suspended spring-mass system, α=0.5 (E=2.069x1011N/m2, ν=0.3, ρ=7836.8 kg/m3, b=0.02m, t=0.01m, θ=120º, R=1m, ms=2 kg)..61

Figure 6.1 The coordinates of an orthotropic lamina...65
Figure 6.2 The layers of a beam 67
Figure 6.3 The effect of the orientation angle on the first stability regions of the curved composite beam, α=0 ($E_1=3.5x10^{10}N/m^2$, $E_2=9x10^9N/m^2$, $G_{12}=4.7x10^9N/m^2$, $G_{23}=3.5x10^9N/m^2$, ν_{12}=0.28, ρ=1850 kg/m^3, b=0.02m, t=0.01m, θ=120º, R=1m) 69
Figure 6.4 The effect of the orientation angle on the second stability regions of the curved composite beam, α=0 ($E_1=3.5x10^{10}N/m^2$, $E_2=9x10^9N/m^2$, $G_{12}=4.7x10^9N/m^2$, $G_{23}=3.5x10^9N/m^2$, ν_{12}=0.28, ρ=1850 kg/m^3, b=0.02m, t=0.01m, θ=120º, R=1m) 70
Figure 6.5 The effect of the orientation angle on the first stability regions of the curved composite beam, α=0.5 ($E_1=3.5x10^{10}N/m^2$, $E_2=9x10^9N/m^2$, $G_{12}=4.7x10^9N/m^2$, $G_{23}=3.5x10^9N/m^2$, ν_{12}=0.28, ρ=1850 kg/m^3, b=0.02m, t=0.01m, θ=120º, R=1m) 70
Figure 6.6 The effect of the orientation angle on the second stability regions of the curved composite beam angles, α=0.5 ($E_1=3.5x10^{10}N/m^2$, $E_2=9x10^9N/m^2$, $G_{12}=4.7x10^9N/m^2$, $G_{23}=3.5x10^9N/m^2$, ν_{12}=0.28, ρ=1850 kg/m^3, b=0.02m, t=0.01m, θ=120º, R=1m) 71

Figure 6.7 The effect of number of the spring-mass system on the first stability regions of the curved composite beam, α=0 (E_1=3.5x10^{10}N/m^2, E_2=9x10^9N/m^2, G_{12}=4.7x10^9N/m^2, G_{23}=3.5x10^9N/m^2, ν_{12}=0.28, ρ=1850 kg/m^3, b=0.02m, t=0.01m, θ=120º, R=1m, m_s=2 kg, k_{ratio}=1)...72
Figure 6.8 The effect of number of the spring-mass system on the second stability regions of the curved composite beam, α=0 (E_1=3.5x10^{10}N/m^2, E_2=9x10^9N/m^2, G_{12}=4.7x10^9N/m^2, G_{23}=3.5x10^9N/m^2, ν_{12}=0.28, ρ=1850 kg/m^3, b=0.02m, t=0.01m, θ=120º, R=1m, m_s=2 kg, kratio=1)................73
Figure 6.9 The effect of number of the spring-mass system on the first stability regions of the curved composite beam, α=0.5 (E_1=3.5x10^{10}N/m^2, E_2=9x10^9N/m^2, G_{12}=4.7x10^9N/m^2, G_{23}=3.5x10^9N/m^2, ν_{12}=0.28, ρ=1850 kg/m^3, b=0.02m, t=0.01m, θ=120º, R=1m, m_s=2 kg, k_{ratio}=1)...73
Figure 6.10 The effect of number of the spring-mass system on the second stability regions of the curved composite beam, α=0.5 (E_1=3.5x10^{10}N/m^2, E_2=9x10^9N/m^2, G_{12}=4.7x10^9N/m^2, G_{23}=3.5x10^9N/m^2, ν_{12}=0.28, ρ=1850 kg/m^3, b=0.02m, t=0.01m, θ=120º, R=1m, m_s=2 kg, k_{ratio}=1).................74
Figure 6.11 The effect of the fiber angles on the first stability regions of the curved composite beam with one suspended system, α=0 (E_1=3.5x10^{10}N/m^2, E_2=9x10^9N/m^2, G_{12}=4.7x10^9N/m^2, G_{23}=3.5x10^9N/m^2, ν_{12}=0.28, ρ=1850 kg/m^3, b=0.02m, t=0.01m, θ=120º, R=1m, m_s=2 kg, k_{ratio}=1).................75
Figure 6.12 The effect of the fiber angles on the second stability regions of the curved composite beam with one suspended system, α=0 (E_1=3.5x10^{10}N/m^2, E_2=9x10^9N/m^2, G_{12}=4.7x10^9N/m^2, G_{23}=3.5x10^9N/m^2, ν_{12}=0.28, ρ=1850 kg/m^3, b=0.02m, t=0.01m, θ=120º, R=1m, m_s=2 kg, k_{ratio}=1).................76
Figure 6.13 The effect of the fiber angles on the first stability regions of the curved composite beam with one suspended system, α=0.5 (E_1=3.5x10^{10}N/m^2, E_2=9x10^9N/m^2, G_{12}=4.7x10^9N/m^2, G_{23}=3.5x10^9N/m^2, ν_{12}=0.28, ρ=1850 kg/m^3, b=0.02m, t=0.01m, θ=120º, R=1m, m_s=2 kg, k_{ratio}=1).................77
Figure 6.14 The effect of the fiber angles on the second stability regions of the curved composite beam with one suspended system, α=0.5 (E_1=3.5x10^{10}N/m^2, E_2=9x10^9N/m^2, G_{12}=4.7x10^9N/m^2, G_{23}=3.5x10^9N/m^2, ν_{12}=0.28, ρ=1850 kg/m^3, b=0.02m, t=0.01m, θ=120º, R=1m, m_s=2 kg, k_{ratio}=1).................78

Figure 6.15 The effect of the fiber angles on the first stability regions of the curved composite beam with three suspended systems, α=0 (E_1=3.5x10^{10}N/m^2, E_2=9x10^9N/m^2, G_{12}=4.7x10^9N/m^2, G_{23}=3.5x10^9N/m^2, ν_{12}=0.28, ρ=1850 kg/m^3, b=0.02m, t=0.01m, θ=120º, R=1m, m_s=2 kg, k_{ratio}=1)..................79
Figure 6.16 The effect of the fiber angles on the second stability regions of the curved composite beam with three suspended systems, α=0 (E_1=3.5x10^{10}N/m^2, E_2=9x10^9N/m^2, G_{12}=4.7x10^9N/m^2, G_{23}=3.5x10^9N/m^2, ν_{12}=0.28, ρ=1850 kg/m^3, b=0.02m, t=0.01m, θ=120º, R=1m, m_s=2 kg, k_{ratio}=1)..................79
Figure 6.17 The effect of the fiber angles on the first stability regions of the curved composite beam with three suspended systems, α=0.5 (E_1=3.5x10^{10}N/m^2, E_2=9x10^9N/m^2, G_{12}=4.7x10^9N/m^2, G_{23}=3.5x10^9N/m^2, ν_{12}=0.28, ρ=1850 kg/m^3, b=0.02m, t=0.01m, θ=120º, R=1m, m_s=2 kg, k_{ratio}=1)..................80
Figure 6.18 The effect of the fiber angles on the second stability regions of the curved composite beam with three suspended systems, α=0.5 (E_1=3.5x10^{10}N/m^2, E_2=9x10^9N/m^2, G_{12}=4.7x10^9N/m^2, G_{23}=3.5x10^9N/m^2, ν_{12}=0.28, ρ=1850 kg/m^3, b=0.02m, t=0.01m, θ=120º, R=1m, m_s=2 kg, k_{ratio}=1)..................80

LIST OF TABLES

Page

Table 5.1 The comparison of frequency results between the present model and Öztürk's FEM results (A=8.387 mm^2, L = 101.6 mm, R = 762 mm, $t^2/12R^2$ = 0.154 x 10^{-7}, E = 6.89 x 10^{10} N/m^2, ρ=2770kg/m^3)..............................35

Table 5.2 The comparison of k_{cr} ratio critical buckling load parameters between the present model and Öztürk's FEM results (θ = 60°, R = 762 mm, b = 25.4 mm, t = 2 mm, E = 6.89 x 10^{10} N/m^2, ρ = 2770 kg/m^3)............................35

Table 5.3 The comparison of the first four natural frequencies of the curved beam with respect to the different number of the suspended spring-mass systems between the present model, ANSYS and Çankaya's FEM results (E=2.069x10^{11}N/m², ν=0.3, ρ=7836.8 kg/m^3, b=0.02m, t=0.01m, θ=120º, R=1m, k_s=10kN/m, m_s=2 kg) 36

Table 5.4 The natural frequencies of the suspended spring-mass system according to the stiffness coefficients ratios 38

Table 6.1 The comparison of frequency results between the present composite curved beam and ANSYS models (E_1=35x10^9 N/m^2, E_2=9x10^9 N/m^2 , G_{12} = 4.7x10^9 N/m^2 , ν_{12}=0.28, ρ=1850 kg/m^3, b=0.02m, t=0.01m, R=1m) 68

CHAPTER ONE
INTRODUCTION

1.1 Introduction

Curved beams are used in bridges, space industry, defense industry, ships, and many other areas. Dynamic problems arise since these structures are subjected to dynamic loads. For instance, vehicles constitute a dynamic load on the bridge which has a curved structure like "Figure1.1 (a)". Moreover, we can illustrate that this curved structure can be supported with a cable or rope, like spring systems, and its road acts as a mass system. Another example, planes, and ships, that have lots of curved beam elements, are constantly exposed to external loads. At the same time, their constructions hold many kinds of link and weight. We can see such an airplane structure in "Figure 1.1 (b)". Therefore, dynamic stability analysis for these structures is at least as important as their frequency analysis.

(a)

(b)

Figure 1.1 Different examples of a structure containing curved beams (Castle, 2006; Howard, 2013; Ravishankar, 2015)

1.2 Literature about the Issue

Many researchers have released important of curved structures and have investigated for a long time. If it is necessary to mention these significant surveys; Bolotin (1962) has been a brilliant guide about the determination of regions of dynamic for following researchers. In addition, his book especially includes a chapter about "Dynamic Stability of Curved Rods".

Another remarkable study is about vibration analysis of a curved beam, which Petyt and Fleisch (1971) have investigated three finite element models in order to determine the radial vibrations of a curved beam. They have shown that rigid body displacements should be represented as far as closely to the real. Besides that, using one of the models, the variation with the subtended angle of the six lowest natural frequencies have been examined with different boundary conditions.

Sabir and Ashwell (1971) have compared different shape functions each other for the finite element of a curved beam. As a result of their study, one of the shape functions have been seen to appear more rapidly converge than the others do. In this way, this result can be a reference for many following studies.

There is another study where the flexural vibration characteristics of curved sandwich beams are investigated by using the finite element displacement method. Different types of displacement models, combining an element having three, four and five degrees of freedom per node, have been used (Ahmed, 1971).

The stability problem of systems subjected to external loads has been considered by Abbas (1977). The problem has been investigated about complex structures using the finite element method. The results of study which are the natural frequencies of vibration, the static buckling load, the regions of dynamic , have been presented for unstiffened plates, eccentrically stiffened plates.

Sabuncu (1978) has investigated the vibration of turbine blade packages with shroud blade. He has modeled the shroud as a constant curvature curved beam and used to analyze the finite element method.

Seeking effect of geometric properties of curve beam on free vibration have been preferred by many researchers. For instance, some researchers have presented an approximate method, is named the Green function, to analyze horizontally curved beams. Their curved beam models were with arbitrary shapes and variable cross-sections and have been examined for both in-plane vibration and out-of-plane vibration (Kawakami et al, 1995).

In a different study, effect of the curvature of a laminated curved beam and orientation angle, variations of subtended angle, having an in-plane curvature on the natural frequencies and buckling load have been studied using finite element method with Sabir and Ashwell's displacement function (Gunyar et al. 2012).

Chidamparam and Leissa (1993) reviewed the published literature on the vibrations of curved bars, beams, rings, and arches and have organized them. They have considered in-plane, out-of-plane and coupled vibrations all of them.

In the literature, although there are many studies about the vibration of curved beam, studies about dynamic stability of the curved beams are much less. If it is necessary to address these, some of them are;

Briseghella et al. (1998) have made a study that can be a reference used the finite element method on dynamic stability analysis. They have presented a set of numerical applications concerning beams and framed structures.

Yoo et al. (1996) have investigated the lateral buckling of the horizontally curved beam by using the finite element method.

Another of these papers is about snap-through properties of a non-linear dynamic buckling response to sinusoidal excitation of a clamped-clamped curved beam (Poon et al., 2002).

Lim and Kang (2004) have developed an elastic buckling theory for thin-walled arches based on the principle of minimum total potential energy.

In another study, in-plane stability analysis of curved beam has examined by using the Finite Element Method. Non-uniform cross-sectioned curved beam has been modeled under uniformly distributed dynamic loads and obtained the first and second unstable regions for dynamic stability (Ozturk et al., 2006).

Karaağaç et al. (2011) have got a study that consists of buckling, vibration and dynamic stability analysis of a curved beam with an edge crack. They have used the finite element method based on energy approach and have examined the effect of a single-edge crack and its locations.

The other study has investigated the effect of variations of subtended angle and orientation angle of a laminated curved beam on the dynamic stability. Using the Finite Element Method, the results have been obtained and have been compared with the results obtained from the ANSYS program for the natural frequency and buckling load (Günyar, 2012).

1.3 Objective of the Thesis

Structures, consisting of curved beam, have mostly an equivalent mass-spring systems along with a dynamic load. However, in the literature, there is a lack of study about dynamic analysis of the curved beam with suspended spring-mass system. For this reason, the present subject of the thesis is necessary to both the advancement of literature and the implementation of engineering.

First of all, the curved beam with suspended spring-mass system has been modeled by using the finite element method and afterward, its system matrices have been determined based on energy equations. After its buckling and frequency analysis performed, the dynamic analysis has been examined. The effect of stiffness coefficients and position of the spring-mass system on the dynamic stability regions are investigated for various subtended angle and radius of the curved beam. The results are represented by tables and graphics.

1.4 Organization of the Thesis

This thesis consists of seven chapters to explain the way analyze the dynamic stability of curved beam. Firstly, a brief introduction to the subject and the literature survey is revealed in Chapter 1. Then, the dynamic stability theory is presented in Chapter 2. Chapter 3 presents the solution method of the issue, the Finite Element Method. Chapter 4 describes the steps of analysis and the results are given in Chapter 5. For the composite curved beam, the effective flexural modulus is explained and its results are given in Chapter 6. Finally, Chapter 7 includes the conclusion of this study.

CHAPTER TWO
THEORY OF DYNAMIC STABILITY

2.1 Theory of Stability

As a simple introduction, the elastic system shown in Figure 2.1 is considered. The concentrated mass m is fastened to the end of the weightless rod r where the free displacement of the rod is further limited by the bushing b at a distance l from the lower end of the rod. If the displacement of the mass at any instant of time t is y, the restoring force of the elasticity of the rod is given by -ky and the equation of motion of the mass is of the form (Abbas, 1977, p.51):

$$-ky = m\ddot{y} \tag{2.1}$$

where k is the coefficient of the rigidity of the system. If the bushing is long enough to give practically complete clamping of the lower part of the rod, then the coefficient k may be found from the formula (Abbas, 1977):

$$k = \frac{3EI}{l^3} \tag{2.2}$$

where E is the modulus of elasticity and I is the moment of inertia. Thus, the equation of motion can be written as:

$$\ddot{y} + \frac{3EI}{l^3} y = 0 \tag{2.3}$$

If the distance l is constant, Equation 2.3 describes the free vibration of the mass about its mean position and the fraction $3EI/ml^3$ is the square of the characteristic frequency of the vibration.

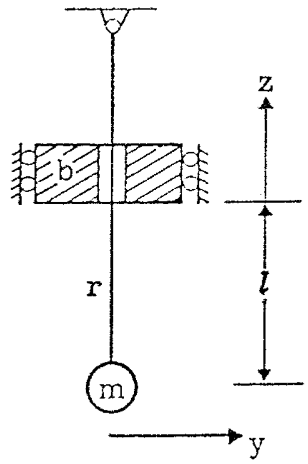

Figure 2.1 Mechanical System (Abbas, 1977, p.69)

Supposing that the bushing slides along the rod according to the fixed law:

$$z = A\cos\omega t \tag{2.4}$$

i.e., it executes harmonic oscillations with amplitude A and angular frequency ω, then the coefficient of rigidity is a function of the time:

$$k = \frac{3EI}{(l+z)^3} = \frac{3EI}{(l + A\cos\omega t)^3} \tag{2.5}$$

The differential Equation 2.3 becomes an equation with variable coefficients:

$$\ddot{y} + \frac{3EI}{m(l + A\cos\omega t)^3}\, y = 0 \tag{2.6}$$

The rigidity change of the system causes the external force, therefore the vibrations of mass m are not free vibration. Moreover, the vibrations are not forced vibrations, because the external force is not a driving force. If these vibrations arise due to the change of parameters of the system, in this case, they are called parametrically excited.

There are some ranges of the exciting frequencies in which the amplitudes of the parametric oscillation increase monotonically. This phenomenon of parametric resonance or dynamic is more dangerous than ordinary resonance which only occurs for clearly defined values of the external driving frequency.

There are many mechanical systems that are subjected to parametric excitation and in the majority of cases they are of practical importance. The differential equation of the parametric vibration may be reduced to the standard form:

$$\frac{d^2y}{d\tau^2}+(a-2b\cos 2\tau)y=0 \tag{2.7}$$

where a and b are constants.

In the mechanical system shown in Figure 2.1, if we assume that the amplitude A of the vibrations of the bushing is very small in comparison with the length l, then instead of Equation 2.5 we obtain approximately:

$$k=\frac{3EI}{(l+A\cos\omega t)^3}\simeq\frac{3EI}{l^3}(1-\frac{3A}{l}\cos\omega t) \tag{2.8}$$

and the differential Equation 2.11 takes the form:

$$\ddot{y}+\frac{3EI}{ml^3}(1-\frac{3A}{l}\cos\omega t)y=0 \tag{2.9}$$

Expressing in terms of dimensionless time τ where $2\tau = \omega t$, equation 2.9 becomes

$$\frac{d^2y}{d\tau^2}+\left(\frac{12EI}{m\omega^2l^3}-\frac{36EIA}{m\omega^2l^4}\cos 2\tau\right)y=0 \tag{2.10}$$

Now the differential Equation 2.9 takes on the standard form 2.7 with:

$$a = \frac{12EI}{m\omega^2 l^3} \qquad \text{and} \qquad b = \frac{18EIA}{m\omega^2 l^4} \tag{2.11}$$

Transformations of this type are typical of cases of small pulsations of the variable parameter of the system.

Equation 2.7 is called Mathieu's equation and its solutions are oscillatory and depend in a decisive way on the actual values of the parameters a and b. In some cases, a given combination of a and b corresponds to combinations of limited amplitude, while in other cases, the vibrations are of increasing amplitude. Essentially, the subsequent behavior of the vibrations is of little importance, since the important thing is the tendency followed by the vibrational process: if the amplitudes remain bounded, the system is dynamically stable; otherwise, parametric resonance occurs and the system is dynamically unstable.

Figure 2.2 shows two cases for the results of solving Equation 2.7. The vibrations are significantly different in spite of the same two values of parameter b (b=0.1). This is because there are a different values of the parameter a (a=1; a=1.2) in both cases. In the first case, the vibrations of the system increase, that is, the system is dynamically unstable. But in the second case, they remain bounded, that is, the system is dynamically stable.

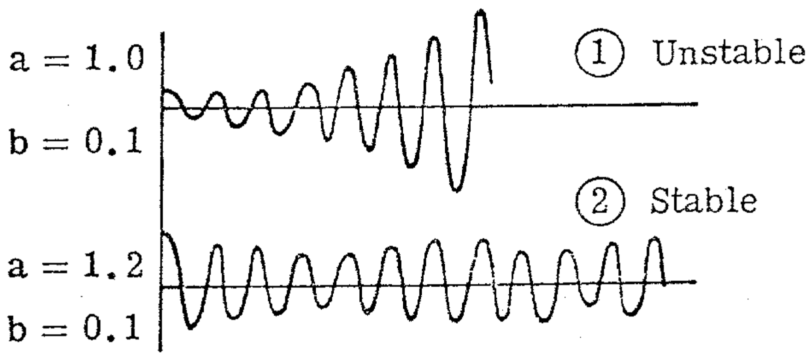

Figure 2.2 Two Solutions of Mathieu's Equation (Abbas, 1977, p.69)

Three reasons for parametric excitation may be observed as:

a) periodic change in rigidity

b) periodic change in inertia of the system and

c) periodic change in the loading of the system.

In this study, the problem includes an external periodic force to affect to the system. Thus, the view of only one of three reasons, which is periodic change in the loading the system, should be sufficient to well-understanding this study.

2.2 The System with Periodic Load

Consider the system shown in Figure 2.3. The mass m is fastened to the upper end of the vertical, perfectly rigid rod r, and at the bottom of the rod there are the supports, which offers elastic resistance to rotation. The vertical force P acts at the upper end of the rod (Abbas, 1977, p.57).

The equation of free vibration of the system is given by

$$PI\Phi - k\Phi = ml^2\ddot{\Phi} \tag{2.12}$$

where $k\Phi$ are the restoring moment (the moment of the elastic hinge) and the gravitational force due to the mass m is included in the force P.

If the force P varies according to the harmonic law

$$P(t) = P_0 + P_t \cos \omega t \tag{2.13}$$

then Equation 2.12 becomes

$$\ddot{\Phi} + \frac{1}{ml^2}\left(k - P_0 l - P_t l \cos \omega t\right)\Phi = 0 \tag{2.14}$$

This equation reduces to the standard form of the Equation 2.7 with

$$2\tau = \omega t\,, \qquad a = \frac{4}{m\omega^2 l^2}\left(\frac{k}{l} - P_0\right), \qquad b = \frac{2P_t}{m\omega^2 l} \tag{2.15}$$

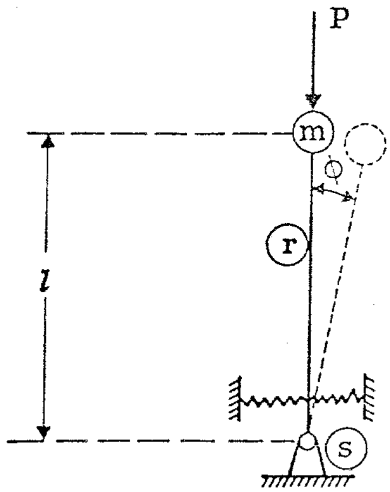

Figure 2.3 A system with Periodic Change in Loading (Abbas, 1977, p.70)

CHAPTER THREE
THEORY OF FINITE ELEMENT METHOD

3.1 What is the Finite Element Method?

The requirement of new methods shows up as complex structures become prevalent in the engineering models. By this reason, the idea of the finite element method appeared at half of the 20th century and have been improved until today. The finite element method is a useful numeric method for many kinds of disciplines, such as vibration, heat transfer or flow.

The application principle of the method is mutual for all of the variety of systems. The method is a discretization procedure of a continuous system to a finite number of continuous elements which are connected together with "nodes”. Other words, the system is an assemblage of various pieces connected together, as seen in Figure 3.1. This process is named as “meshing”. In there, each piece is named “finite element”. In the nodes (joints) between finite elements, there is a balance of forces and convenient displacements. Thus, all piece act as an entire system.

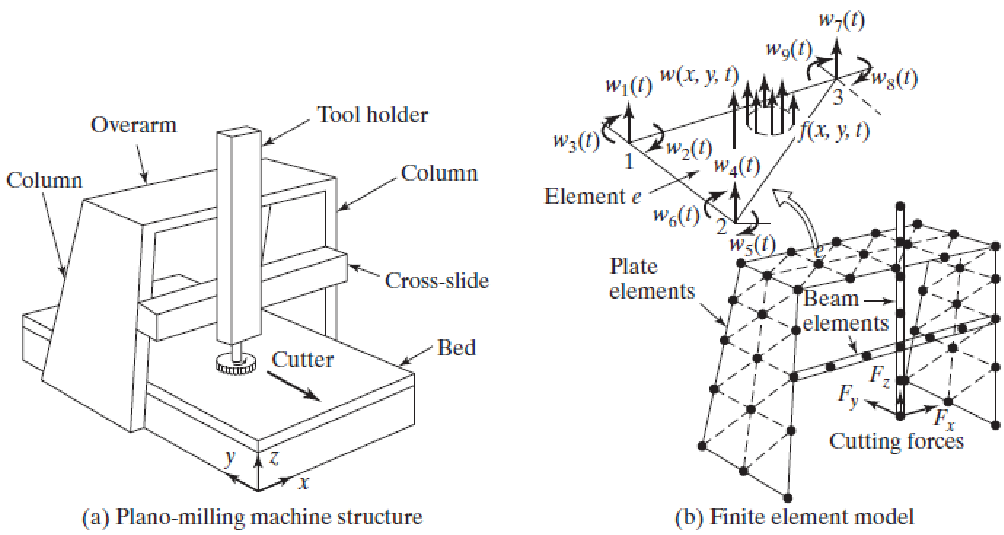

Figure 3.1 Finite element model of Plano-milling machine (Rao, 2011, p.1043)

The approximate solution of displacements is determined because the exact solution of their is very complicated. Therefore, the method gives an approximate solution. On the other hand, if the size of finite elements is reduced, the results converge to exact values.

3.2 Process of the Finite Element Method

The finite element method basically comprises of four steps, meshing, obtainment of an element matrix, obtainment of global matrices, and applying boundary conditions.

Meshing is a discretization procedure of the system. This step can be far more complicated in three dimensional systems. There are many studies that are about types of mesh and these systems can be solved with different types and sizes of meshes in various computer programs. Two dimensional systems for a vibration problem are only considered in this chapter.

In the numeric solution, each element is determined in the same length but different element size can be chosen when the solution carried out with using computer programs. After the mesh processing, the mass and stiffness matrices are obtained for each element using energy equations.

These matrices for an element is combined with each other according to joint displacements of each piece in the whole system. Thereby, the global mass matrix and the global stiffness matrix are obtained.

Thanks to these global matrices, the equation of motion, seen in Equation 3.1, of a system that is conservative and undamped, can be figured out. Thus the natural frequencies of a system can be determined.

$$\mathbf{M}\ddot{x} + \mathbf{K}x = 0 \tag{3.1}$$

In this chapter, the method is explained in terms of vibration analysis with a sample. In this aim, a bar element and a beam element have been preferred due to their similarity to the curved beam that is the element belonging to this thesis' problem.

3.2.1 Bar Element

Bar element shown in Figure 3.2 is a linkage that has two freedom degrees. This element moves only x-axis direction with time-dependent.

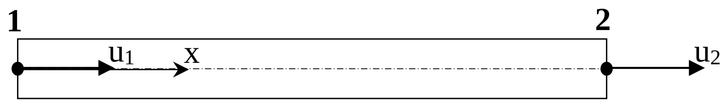

Figure 3.2 A Bar Element

The shape function which describes this behavior is like as in Equation 3.2 (Rao, 2011).

$$u(x,t) = a_1(t) + a_2(t)x \tag{3.2}$$

The element length is l. Joint displacements of this element, u_1, and u_2, are shown in Figure 3.2. This means,

$$u(0,t) = u_1(t) \tag{3.3}$$

$$u(l,t) = u_2(t) \tag{3.4}$$

The shape function satisfies the boundary conditions given in Equation 3.3 and 3.4. Depending on Equation 3.3 and 3.4, the shape function constants, a_1 and a_2, are described as in Equation 3.5 and 3.6.

$$u_1(t) = a_1(t) \quad \text{or} \quad a_1(t) = u_1(t) \tag{3.5}$$

$$u_2(t) = a_1(t) + a_2(t)l \quad \text{or} \quad a_2(t) = \frac{u_2(t) - u_1(t)}{l} \tag{3.6}$$

If these constants are substituted into Equation 3.2, the shape function is:

$$u(x,t) = u_1(t)\left(\frac{1-x}{l}\right) + u_2(t)\frac{x}{l} \tag{3.7}$$

The kinetic energy equation for the longitudinal vibration can be represented as

$$T = \frac{1}{2}\rho A\left(\frac{\partial u}{\partial t}\right)^2 dx \tag{3.8}$$

where ρ is a density of the material of bar element and A is a cross-sectional area of the bar element. If Equation 3.9 is rearranged, Equation 3.9 is obtained as

$$T = \frac{1}{2}\frac{\rho Al}{3}\left(\dot{u}_1^2 + \dot{u}_1\dot{u}_2 + \dot{u}_2^2\right) \tag{3.9}$$

where,

$$\dot{u}_1 = \frac{du_1(t)}{dt} \quad \text{and} \quad \dot{u}_2 = \frac{du_2(t)}{dt} \tag{3.10}$$

In Equation 3.9, if the joint displacements are represented as a vector,

$$\mathbf{\dot{u}} = \begin{Bmatrix} \dot{u}_1 \\ \dot{u}_2 \end{Bmatrix}$$

the kinetic energy can be rewritten as Equation 3.11

$$\mathbf{T} = \frac{1}{2}\mathbf{\dot{u}^T m \dot{u}} \tag{3.11}$$

and thus the mass matrix, for a bar element is as following:

$$\mathbf{m} = \frac{\rho A l}{6}\begin{bmatrix} 2 & 1 \\ 1 & 2 \end{bmatrix} \tag{3.12}$$

The potential energy equation is given in Equation 3.13. In there, E is the elasticity module of material. The potential energy equation also consists of the partial derivative of *u(x,t)* shape function with respect to *x* displacement.

$$V = \frac{1}{2} EA \left(\frac{\partial u}{\partial x} \right)^2 dx \tag{3.13}$$

$$V = \frac{1}{2} EA \int_0^l \left(-\frac{1}{l} u_1(t) + \frac{1}{l} u_2(t) \right)^2 dx$$

If the derivative function is written in Equation 3.13, the potential energy equation is obtained as

$$V = \frac{1}{2} \frac{EA}{l} \left(u_1^2 - 2u_1 u_2 + u_2^2 \right) \tag{3.14}$$

The displacement vector is

$$\mathbf{u} = \begin{Bmatrix} u_1 \\ u_2 \end{Bmatrix}$$

When this vector is replaced to Equation 3.14, the potential energy equation is represented as Equation 3.15

$$\mathbf{V} = \frac{1}{2} \mathbf{u}^{\mathrm{T}} \mathbf{k} \mathbf{u} \tag{3.15}$$

thereby the stiffness matrix is obtained as follows:

$$\mathbf{k} = \frac{EA}{l}\begin{bmatrix} 1 & -1 \\ -1 & 1 \end{bmatrix} \tag{3.16}$$

3.2.2 Beam Element

A beam element involves two nodes and four freedom degree, shown in Figure 3.3. Each node has one bending and one slope joint displacements.

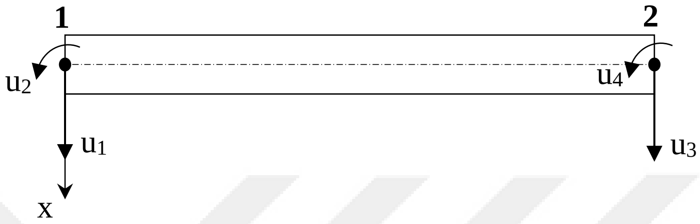

Figure 3.3 A Beam Element

The shape function which describes this behavior is like as in Equation 3.17 (Rao, 2011).

$$u(x,t) = a_1(t) + a_2(t)x + a_3(t)x^2 + a_4(t)x^3 \tag{3.17}$$

The shape function satisfies the boundary conditions given as follows:

$$u(0,t) = u_1(t) \tag{3.18a}$$

$$u'(0,t) = u_2(t) \tag{3.18b}$$

$$u(l,t) = u_3(t) \tag{3.18c}$$

$$u'(l,t) = u_4(t) \tag{3.18d}$$

Considering these boundary conditions, the shape function constants, $a_1(t)$, $a_2(t)$, $a_3(t)$, and $a_4(t)$, are described as

$$a_1(t) = u_1(t) \tag{3.19a}$$

$$a_2(t) = u_2(t) \tag{3.19b}$$

$$a_3(t) = \frac{1}{l^2}\left[-3u_1(t) - 2u_2(t)l + 3u_3(t) - u_4(t)l\right] \tag{3.19c}$$

$$a_4(t) = \frac{1}{l^3}\left[2u_1(t) + u_2(t)l - 2u_3(t) + u_4(t)l\right] \tag{3.19d}$$

Thus, the shape function is represented as

$$\begin{aligned} u(x,t) = {} & \left(1 - 3\frac{x^2}{l^2} + 2\frac{x^3}{l^3}\right)u_1(t) + \left(\frac{x}{l} - 2\frac{x^2}{l^2} + \frac{x^3}{l^3}\right)lu_2(t) \\ & + \left(3\frac{x^2}{l^2} - 2\frac{x^3}{l^3}\right)u_3(t) + \left(-\frac{x^2}{l^2} + \frac{x^3}{l^3}\right)lu_4(t) \end{aligned} \tag{3.20}$$

which is an assemblage of functions of time and displacement. If the displacement terms are renamed like Equation 3.21, 3.22, 3.23, and 3.24,

$$N_1 = 1 - 3\frac{x^2}{l^2} + 2\frac{x^3}{l^3} \tag{3.21}$$

$$N_2 = \left(\frac{x}{l} - 2\frac{x^2}{l^2} + \frac{x^3}{l^3}\right)l \tag{3.22}$$

$$N_3 = 3\frac{x^2}{l^2} - 2\frac{x^3}{l^3} \tag{3.23}$$

$$N_4 = \left(-\frac{x^2}{l^2} + \frac{x^3}{l^3} \right) l \tag{3.24}$$

the shape function can be written that equals the multiplying of displacement-depended terms matrix and time-dependent terms vector.

$$u(x,t) = \begin{bmatrix} N_1 & N_2 & N_3 & N_4 \end{bmatrix} \begin{Bmatrix} u_1 \\ u_2 \\ u_3 \\ u_4 \end{Bmatrix}$$

$$u(x,t) = \mathbf{Nu} \tag{3.25}$$

The kinetic energy equation is

$$T = \frac{1}{2} \int_0^l \rho A \left\{ \frac{\partial u(x,t)}{\partial t} \right\}^2 dx \tag{3.26}$$

If this equation is solved, the kinetic energy equation is reformed as

$$\mathbf{T} = \frac{1}{2} \dot{\mathbf{u}}^{\mathbf{T}} \mathbf{m} \dot{\mathbf{u}} \tag{3.27}$$

which consists of a mass matrix and derivative of the time vector. Hence, the mass matrix is obtained as in Equation 3.28.

$$\mathbf{m} = \frac{\rho A l}{420} \begin{bmatrix} 156 & 22l & 54 & -13l \\ 22l & 4l^2 & 13l & -3l^2 \\ 54 & 13l & 156 & -22l \\ -13l & -3l^2 & -22l & 4l^2 \end{bmatrix} \tag{3.28}$$

Therefore, the potential energy is defined as

$$V = \frac{1}{2} EI \left\{ \frac{\partial^2 u(x,t)}{\partial x^2} \right\}^2 dx \tag{3.29}$$

If the second derivative of shape function *u(x,t)* with respect to *x* displacement is written into Equation 3.29, Equation 3.30 is obtained.

$$V = \frac{1}{2} EA \int_0^l \left(-\frac{1}{l} u_1(t) + \frac{1}{l} u_2(t) \right)^2 dx \tag{3.30}$$

Then the potential energy equation is rearranged, shown in Equation 3.31 and the stiffness matrix is attained as in Equation 3.32.

$$\mathbf{V} = \frac{1}{2} \mathbf{u}^{\mathbf{T}} \mathbf{k} \mathbf{u} \tag{3.31}$$

$$\mathbf{k} = \frac{EI}{l^3} \begin{bmatrix} 12 & 6l & -12 & 6l \\ 6l & 4l^2 & -6l & 2l^2 \\ -12 & -6l & 12 & -6l \\ 6l & 2l^2 & -6l & 4l^2 \end{bmatrix} \tag{3.32}$$

3.3 Transformation Matrix

The finite element is especially used in complex structures. The elements of these structures are not mostly in the same axis, for instance, Figure 3.1. The axes in mutual node between elements should be the same directions, thence there is required a rectifier matrix named as “transformation matrix”.

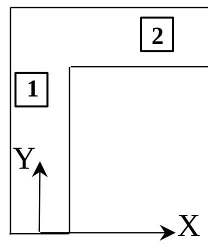

Figure 3.4 L-Beam involving two beam element

To illustrate simply, the L-beam in Figure 3.4 is taken into consideration. There are two beam element connected together in node 2 where *X* and *Y* are global coordinates.

The joint displacements of elements end shown as Figure 3.5 have a different direction. In this case, the local coordinates should be transformed to the global coordinates, *X* and *Y*, shown as Figure 3.4.

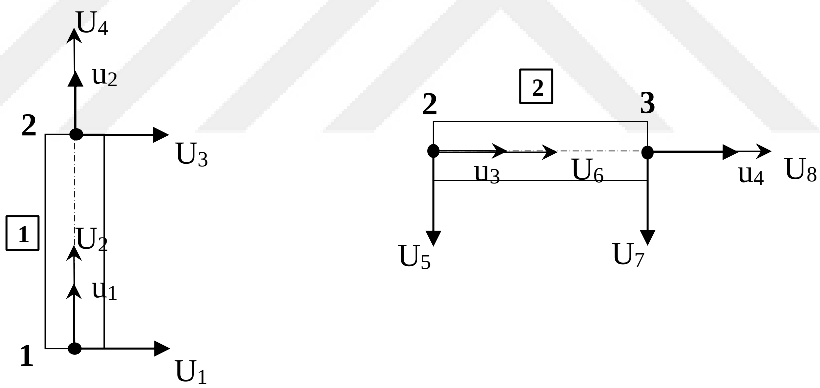

Figure 3.5 Two elements of L-Beam in Figure 3.4

To transform the coordinates, Equation 3.34 is used where **L** is the transformation matrix for the joint displacements.

$$\mathbf{u}_i = [L]\begin{Bmatrix} U_i \\ U_{i+1} \end{Bmatrix} \tag{3.34}$$

Using Equation 3.34 is not necessary for the first element since the joint displacements of element 1 are on the global coordinates. As for element 2, there is required applying to transform for the joint displacements, u_3 and u_4, on node 2. In the present case, L transformation matrix is

$$\mathbf{L} = \begin{bmatrix} \cos\theta & \sin\theta & 0 & 0 \\ 0 & 0 & \cos\theta & \sin\theta \end{bmatrix} \tag{3.35}$$

3.4 Global Matrices

After achieved matrices of an element, the matrices of whole system should be obtained to solve the equation of motion in Equation 3.1. The matrix of each element is aggregated according to mutual joint displacements. For instance, if the procedure is applied for a beam comprised of two elements in Figure 3.6,

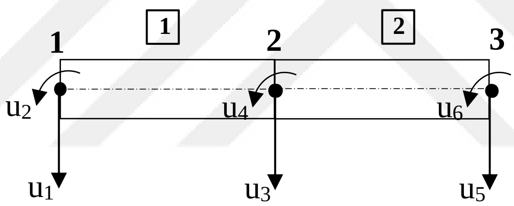

Figure 3.6 A beam consisted of two elements

the elements and displacements are as in Figure 3.7. The mass matrix of each element becomes like in Equation 3.29.

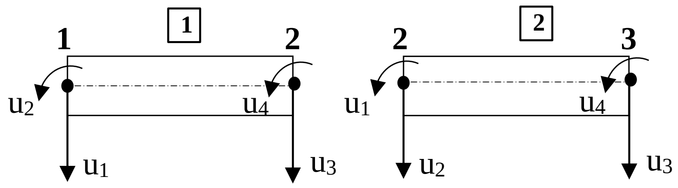

Figure 3.7 Elements of the beam

In an element matrix, each column and row belongs to a displacement in nodes. For a beam element, the mass matrix is like in Equation 3.29 and it can be enumerated following as

$$\mathbf{m} = \frac{\rho A l}{420} \begin{array}{c c} \begin{array}{cccc} 1 & 2 & 3 & 4 \end{array} & \\ \begin{bmatrix} 156 & 22l & 54 & -13l \\ 22l & 4l^2 & 13l & -3l^2 \\ 54 & 13l & 156 & -22l \\ -13l & -3l^2 & -22l & 4l^2 \end{bmatrix} & \begin{array}{c} 1 \\ 2 \\ 3 \\ 4 \end{array} \end{array} \tag{3.36}$$

The numbers (1,2,3,4) are the number of joint displacement. Namely, size of the matrix is determined by the number of joint displacement. If the global mass matrix is expressed by these element matrices, it is obtained in a form that

$$\mathbf{M} = \frac{\rho A l}{420} \begin{array}{c c} \begin{array}{cccccc} 1 & 2 & 3 & 4 & 5 & 6 \end{array} & \\ \begin{bmatrix} 156 & 22l & 54 & -13l & 0 & 0 \\ 22l & 4l^2 & 13l & -3l^2 & 0 & 0 \\ 54 & 13l & (156+156) & (-22l) & 54 & -13l \\ -13l & -3l^2 & (-22l+22l) & (4l^2+4l^2) & 13l & -3l^2 \\ 0 & 0 & 54 & 13l & 156 & -22l \\ 0 & 0 & -13l & -3l^2 & -22l & 4l^2 \end{bmatrix} & \begin{array}{c} 1 \\ 2 \\ 3 \\ 4 \\ 5 \\ 6 \end{array} \end{array} \tag{3.37}$$

Actually, the value corresponded to the number of displacement in an element shown as Figure 3.7, is written to where corresponding to the number of displacement in the global matrix shown as Figure 3.6.

Finally, this procedure remake for all elements when the system has lots of elements. Thus, the global matrices are achieved and the equation of motion for the system can be solved.

CHAPTER FOUR
THEORETICAL ANALYSIS

In this chapter, the solution steps of curved beam finite model are explained as simplistic as possible. First of all, the curved beam is assumed that Euler-Bernoulli beam and uniform cross-section. Besides that, only in-plane vibration is considered and the shape function of the curved beam is used from the references of Öztürk (2006) and Sabir (1971).

4.1 Determination of the Problem

The problem is illustrated in Figure 4.1 where the curved beam with suspended spring-mass system consists of finite curved elements. Symbols, k_s, and m_s refer to stiffness coefficient and mass of the spring-mass system, respectively. θ signifies subtended angle (or opening angle) belonging to the curved beam. Besides that, the curved beam fixed both ends, has a uniformly distributed dynamic load *P(t)* and suspended the spring-mass system.

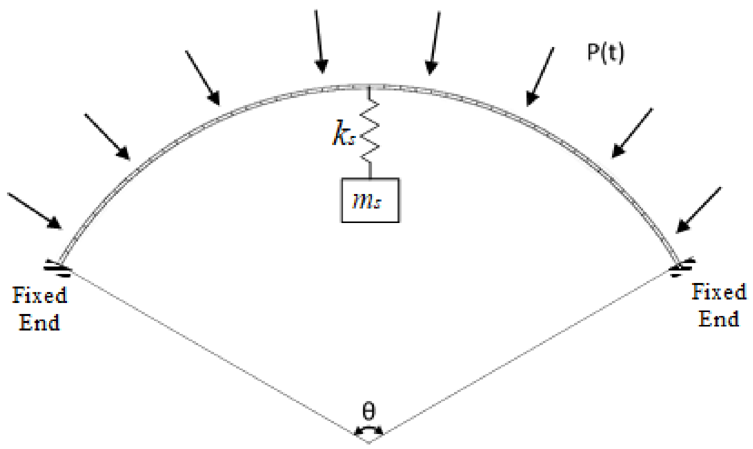

Figure 4.1 Model of the curved beam with the suspended spring-mass system

4.2 The Finite Element Model

To define the equation of motion, firstly, the curved beam should be modeled and its mass matrix, geometric stiffness matrix and stiffness matrix should be obtained. The curved beam is modeled as consisting of 48 finite elements.

4.2.1 Energy Equations for a Finite Curved Element

A finite curved element is modeled shown in Figure 4.2. There are geometric properties and deflections of the elemental finite element. *b*, *t*, *R*, and ϕ are width, thickness, radius and subtended angle (opening angle) of an element, respectively.

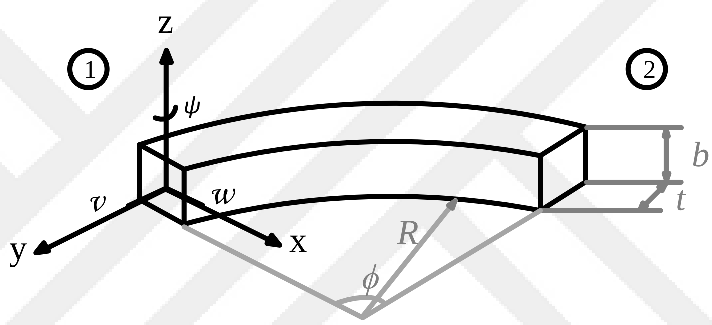

Figure 4.2 A curved finite element

The circumferential deflection is symbolized with *v*, the radial deflection is symbolized with *w* and the rotation of tangent is symbolized with ψ. The shape functions are used in this study as indicated below.

$$w = a_1 \cos\phi + a_2 \sin\phi + a_4 - a_6\phi \tag{4.1}$$

$$v = -a_1 \sin\phi + a_2 \cos\phi + a_3 + a_6\phi + \frac{1}{2} a_6\phi^2 \tag{4.2}$$

$$\psi = \frac{dw}{dy} - \frac{v}{R} \tag{4.3}$$

The deflection vector consisting of these deflections is written as

$$\mathbf{q}^T = \begin{bmatrix} v_1 & w_1 & \psi_1 & v_2 & w_2 & \psi_2 \end{bmatrix} \tag{4.4}$$

The displacement vector consists of six displacement parameters for an element that both ends has three of them. Using the displacement functions, the potential energy of the curved beam is expressed as

$$U = \frac{1}{2}\left[\int_0^l EI_{xx}\left(w'' - \frac{v'}{R}\right)^2 + EA\left(\frac{w}{R} + v'\right)^2\right]dy \tag{4.5}$$

If the potential energy equation is considered matrix form as indicated Equation 4.6, the stiffness matrix of a finite curved element is achieved.

$$U = \frac{1}{2}\mathbf{q}^T\mathbf{k}_e\mathbf{q} \tag{4.6}$$

where,

$$\mathbf{k}_e = \mathbf{C}^T\mathbf{k}\mathbf{C} \tag{4.7}$$

The elastic stiffness matrix **k** is

$$\mathbf{k} = \frac{\phi E}{R^2}\begin{bmatrix} 0 & 0 & 0 & 0 & 0 & 0 \\ 0 & 0 & 0 & 0 & 0 & 0 \\ 0 & 0 & 0 & 0 & 0 & 0 \\ 0 & 0 & 0 & A & A & 0 \\ 0 & 0 & 0 & A & \dfrac{\left(I_{XX} + AR^2\right)}{R^2} & \dfrac{\phi I_{XX}}{2R^2} \\ 0 & 0 & 0 & 0 & \dfrac{\phi I_{XX}}{2R^2} & \dfrac{\phi^2 I_{XX}}{3R^2} \end{bmatrix} \tag{4.8}$$

The constants matrix **C** is

$$\mathbf{C}=\begin{bmatrix} -B_4 & B_1 & -RB_4 & -B_5 & -B_1 & -RB_5 \\ -B_3 & B_2 & -RB_3 & B_1 & B_2 & RB_1 \\ B_1 & -B_2 & RB_3 & B_1 & B_2 & RB_1 \\ B_4 & -B_3 & RB_4 & B_5 & B_1 & RB_5 \\ B_6 & -B_7 & RB_8 & B_6 & B_7 & RB_9 \\ -B_1 & B_2 & -RB_1 & -B_1 & -B_2 & -RB_1 \end{bmatrix} \tag{4.9}$$

where

$B_1=[\cos(\phi)-1]/D$

$B_2=[\sin(\phi)]/D$

$B_3=[1-\phi\sin(\phi)-\cos(\phi)]/D$

$B_4=[\sin(\phi)-\phi\cos(\phi)]/D$

$B_5=[\phi-\sin(\phi)]/D$

$B_6=B_1\phi/2$

$B_7=B_2\phi/2$

$B_8=B_6+1/\phi$

$B_9=B_6-1/\phi$

$D=2\cos(\phi)-2+\phi\sin(\phi)$

As the above procedure can be applied for the kinetic energy equation. The kinetic energy equation of the curved beam is defined in Equation 4.10 by utilizing the displacements in Equations 4.1, 4.2 and 4.3.

$$T=\frac{1}{2}\int_0^l \rho A\left(\dot{w}^2+\dot{v}^2\right)dy \tag{4.10}$$

Substituting the displacement vector into Equation 4.9, the matrix form of the kinetic energy equation is obtained and thus the mass matrix of a curved element is taken out from Equation 4.11 as in Equation 4.12.

$$T=\frac{1}{2}\dot{\mathbf{q}}^T\mathbf{m}_e\dot{\mathbf{q}} \tag{4.11}$$

where,

$$\mathbf{m}_e = \mathbf{C}^T \mathbf{m} \mathbf{C} \tag{4.12}$$

The mass matrix is

$$\mathbf{m} = \rho A \begin{bmatrix} \phi & 0 & \mathrm{c} & -1 & \mathrm{s}+\phi\mathrm{c} & \mathrm{c}(-2+\phi^2/2)-2\phi\mathrm{s}+2 \\ 0 & \phi & \mathrm{s} & -\mathrm{c}+1 & \mathrm{c}+\phi\mathrm{s}-1 & \mathrm{s}(-2+\phi^2/2)+2\phi\mathrm{c} \\ \mathrm{c}-1 & \mathrm{s} & \phi & 0 & \phi^2/2 & \phi^3/6 \\ \mathrm{s} & -\mathrm{c}+1 & 0 & \phi & 0 & -\phi^2/2 \\ -\mathrm{s}+\phi\mathrm{c} & \mathrm{c}+\phi\mathrm{s}-1 & \phi^2/2 & 0 & \phi^3/3 & \phi^4/8 \\ \mathrm{c}(-2+\phi^2/2)-2\phi\mathrm{s}+2 & \mathrm{s}(-2+\phi^2/2)+2\phi\mathrm{c} & \phi^3/6 & -\phi^2/2 & \phi^4/8 & \phi^3/3+\phi^5/20 \end{bmatrix}$$

where c and s signify $cos\alpha$ and $sin\alpha$ terms, respectively.

The strain energy is

$$V = \int_0^l \mathrm{P(t)} R \left(\frac{dw}{dy} - \frac{v}{R} \right)^2 dy \tag{4.14}$$

The geometric stiffness matrix of a curved element arises if the strain energy equation is written as matrix-form.

$$V = \frac{1}{2} \mathbf{q}^T P(t) \mathbf{k}_g \mathbf{q} \tag{4.15}$$

where,

$$\mathbf{k}_g = \mathbf{C}^T \mathbf{k}^* \mathbf{C} \tag{4.16}$$

The elastic stiffness matrix $\mathbf{k^*}$ is

$$
\mathbf{k}^* = \frac{\phi}{R}\begin{bmatrix}
0 & 0 & 0 & 0 & 0 & 0 \\
0 & 0 & 0 & 0 & 0 & 0 \\
0 & 0 & 1 & \frac{1}{2}\phi & \frac{1}{6}(6+\phi^2) & 0 \\
0 & 0 & 0 & 0 & 0 & 0 \\
0 & 0 & \frac{1}{2}\phi & 0 & \frac{1}{3}\phi^2 & \frac{1}{8}\phi(4+\phi^2) \\
0 & 0 & \frac{1}{6}(6+\phi^2) & 0 & \frac{1}{8}\phi(4+\phi^2) & \frac{1}{60}(3\phi^4+20\phi^2+60)
\end{bmatrix} \tag{4.17}
$$

4.2.2 Energy Equations for the Spring-Mass System

The suspended spring-mass system is depicted in Figure 4.3. The system vibration is assumed that in the only vertical direction. Thus, the displacement on the mutual joint (i+1) of spring-mass elements is described as y_{i+1}. However, there are two joint displacements in a node (i) between the spring-mass system and the curved beam, since the behavior of curved beam is in-plane.

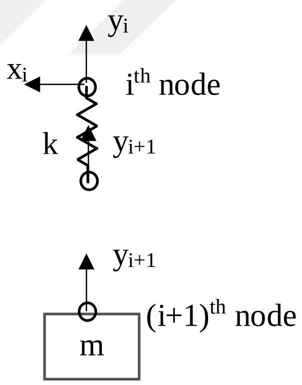

Figure 4.3 The joints of the suspended spring-mass system

In this case, the displacement vector becomes

$$
\mathbf{q}_s^T = \begin{bmatrix} x_i & y_i & x_{i+1} & y_{i+1} \end{bmatrix} \tag{4.18}
$$

where *i* denotes node number depending on the number of nodes in the whole system. The kinetic energy equation for the spring-mass system is

$$\mathbf{T} = \frac{1}{2}\dot{\mathbf{q}}_s^T \mathbf{m}_s \dot{\mathbf{q}}_s \tag{4.19}$$

in matrix form and likewise the potential energy equation is

$$\mathbf{U} = \frac{1}{2}\dot{\mathbf{q}}_s^T \mathbf{k}_s \dot{\mathbf{q}}_s \tag{4.20}$$

where $\mathbf{m}_s$ and $\mathbf{k}_s$ are the mass matrix of the spring-mass system and the stiffness matrix of the spring-mass system, respectively. From Equation 4.19 and 4.20, the mass matrix of the spring-mass system is obtained as

$$\mathbf{m}_s = m_i \begin{bmatrix} 0 & 0 \\ 0 & 1 \end{bmatrix} \tag{4.21}$$

and in the same way, the stiffness matrix of the spring-mass system is obtained following:

$$\mathbf{k}_s = k_i \begin{bmatrix} 1 & -1 \\ -1 & 1 \end{bmatrix} \tag{4.22}$$

4.2.3 Assembly Procedure of the Spring-Mass System

To complete the finite element procedure, the global matrices of the system should be reached. Because of this, all elements are assembled to arrive the system acting as a whole in respect to the finite element method. Since the directions of joint displacements of the curved beam are different to the joint displacements of spring-mass system, the element matrices should be combined with the stiffness matrix and mass matrix of the spring-mass system by utilizing L transformation matrix given in Equation 4.23.

$$\mathbf{L} = \begin{bmatrix} \cos\varphi & -\sin\varphi \\ \sin\varphi & \cos\varphi \end{bmatrix} \tag{4.23}$$

Then, the mass matrix and stiffness matrix of finite elements of the curved beam and spring-mass systems are assembled and as a result, the global matrices of the whole system are obtained.

4.3 Investigation of Dynamic Stability

Substituting the energy equations of the system into the Lagrange's Equation of motion, in case of axially loaded system, the equation of motion in matrix-form is obtained as

$$\mathbf{M}\ddot{\mathbf{q}} + \mathbf{K}_e\mathbf{q} - P(t)\mathbf{K}_g\mathbf{q} = \mathbf{0} \tag{4.24}$$

where the periodic uniformly distributed dynamic load P(t) define as

$$P(t) = P_0 + P_t \cos\Omega t \tag{4.25}$$

where P_0 and P_t are static and time-depended components of load, respectively. Besides, **Ω** is the disturbing frequency. The static buckling load P_{cr} is obtained from the solution of the eigenvalue problem in Equation 4.26.

$$\left|\mathbf{M}\ddot{\mathbf{q}} - k_{cr}\mathbf{K}_g\mathbf{q}\right| = \mathbf{0} \tag{4.26}$$

k_{cr} is described as the buckling parameter and formulated as

$$k_{cr} = \sqrt{\frac{P_{cr}R^3}{EI_{xx}}} \tag{4.27}$$

If the distributing load *P(t)* is rewritten related to the static buckling load, it becomes

$$P(t) = \alpha P_{cr} + \beta P_{cr} \cos\Omega t \tag{4.28}$$

where,

$$\alpha = \frac{P_0}{P_{cr}} \tag{4.29}$$

$$\beta = \frac{P_t}{P_{cr}} \tag{4.30}$$

where α and β are static load parameter and dynamic load parameter, respectively. Substituting the dynamic load P(t) from Equation 4.28 into Equation 4.24, the equation of motion is obtained as

$$\mathbf{M}\ddot{\mathbf{q}} + \left[\mathbf{K}_e - \alpha P_{cr}\mathbf{K}_{gs} - \beta P_{cr}\cos(\Omega t)\mathbf{K}_{gt}\right]\mathbf{q} = \mathbf{0} \tag{4.31}$$

and is called the second-order differential equation with periodic coefficients of Mathie-Hill type. In this formula, $\mathbf{K_{gs}}$ and $\mathbf{K_{gt}}$ are considered the influence of the static and time-dependent components of the load.

Equation 4.31 can be defined as a periodic function of period *T* and *2T* where $T=2\pi/\omega$. Bolotin (1962) proved that the solution with period of *2T* is significant importance and the stability regions can be determined with Equation 4.32

$$\left[\mathbf{K}_e - \alpha P_{cr}\mathbf{K}_{gs} \pm \frac{1}{2}\beta P_{cr}\mathbf{K}_{gt} - \frac{\Omega^2}{4}\mathbf{M}\right]\mathbf{q} = \mathbf{0} \tag{4.32}$$

If the static component and time-dependent component of distributing load are performed in the same manner, $\mathbf{K_{gs}}$ and $\mathbf{K_{gt}}$ become identical and these matrices are assumed to be equal to $\mathbf{K_g}$ matrix. In this case, Equation 4.32 becomes

$$\left[\mathbf{K}_e - \left(\alpha \pm \frac{1}{2}\beta\right)P_{cr}\mathbf{K}_g - \frac{\Omega^2}{4}\mathbf{M}\right]\mathbf{q} = \mathbf{0} \qquad (4.33)$$

Equation 4.33 represents the solution of three related problems below.

I. Free vibration with ω, in case of α = 0 and β = 0.

$$\left[\mathbf{K}_e - \omega^2\mathbf{M}\right]\mathbf{q} = \mathbf{0} \qquad (4.34)$$

II. Static stability with α = 1, β = 0 and ω = 0.

$$\left[\mathbf{K}_e - P_{cr}\mathbf{K}_g\right]\mathbf{q} = \mathbf{0} \qquad (4.35)$$

III. Dynamic stability in case of the existence of all terms.

$$\left[\mathbf{K}_e - \left(\alpha \pm \frac{1}{2}\beta\right)P_{cr}\mathbf{K}_g - \frac{\Omega^2}{4}\mathbf{M}\right]\mathbf{q} = \mathbf{0} \qquad (4.36)$$

CHAPTER FIVE
DYNAMIC STABILITY ANALYSIS

5.1 Vibration Analysis

The results of this study may be presented for a different number of finite element. The number of element is determined by means of the convergence curve that presents how many of them ensure the accuracy of the solution. In the convergence curve, an increasing number of the element leads to a decrease in the value of the results until a certain point and, thus converges to value of the exact solution. The result value hardly changes after a certain point where the number of finite element is sufficient in order to the accuracy of the solution.

In present work, the number of the finite element has been determined according to the convergence curve for the first natural frequency in Figure 5.1. As can be also seen there, about 20 elements are sufficient to properly figure out the problem. Nevertheless, the number of the finite element is selected 48 elements to suspend the spring-mass system for various points.

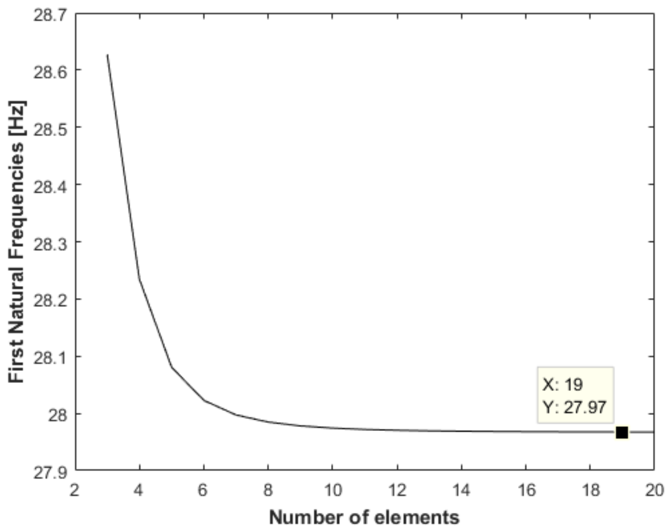

Figure 5.1 Convergence curve

The present finite element model is compared with a similar model of Öztürk (2006) for the first five natural frequencies to accurate the accuracy of the results. As seen in Table 5.1, agreements are good.

Table 5.1 The comparison of frequency results between the present model and Öztürk's FEM results (A=8.387 mm^2, L = 101.6 mm, R = 762 mm, $t^2/12R^2$ = 0.154 x 10^{-7}, E = 6.89 x 10^{10} N/m^2, ρ=2770kg/m^3)

Mode	Frequency (Hz)	
	Öztürk (2006)	Present Work
1	452	452.25
2	728	728.83
3	1084	1084.10
4	1698	1697.99
5	2818	2815.17

To accurate the present model for the dynamic analysis, the k_{cr} ratio critical buckling load parameters are figured out for various numbers of elements like as in Table 5.2 and these results are verified with the study of Öztürk's. For different element numbers, the results of the present work are satisfied the accuracy compared to Öztürk's results.

Table 5.2 The comparison of k_{cr} ratio critical buckling load parameters between the present model and Öztürk's FEM results (θ = 60°, R = 762 mm, b = 25.4 mm, t = 2 mm, E = 6.89 x 10^{10} N/m^2, ρ = 2770 kg/m^3)

Number of elements	k_{cr} ratio critical buckling load parameters	
	Öztürk (2006)	Present Work
4	8.7729	8.7727
6	8.6849	8.6848
8	8.6666	8.6664
10	8.6612	8.6611
12	8.6593	8.6591
30	8.6574	8.6573

The free vibration analysis of the curved beam with suspended spring-mass system is studied by Çankaya et al. (2017). The results of their study are shown in Table 5.3.

Table 5.3 also includes the natural frequencies of the curved beam for situations where it is with spring-mass systems and is not. These frequencies are compared with both that of ANSYS and the present work.

It can be seen from Tables 5.1 and 5.3 that the results of present work are a good agreement with both Öztürk's and Çankaya's FEM results and ANSYS results by the terms of the natural frequencies and buckling parameters.

The curved beam with one suspended spring-mass is shown as Figure 5.2 (b), in there, the spring-mass system is suspended on the 25th node. When the curved beam has three suspended systems, each suspended system is on the 13th, 25th and 36th nodes as seen in Figure 5.2 (c).

Table 5.3 The comparison of the first four natural frequencies of the curved beam with respect to the different number of the suspended spring-mass systems between the present model, ANSYS and Çankaya's FEM results ($E=2.069x10^{11}N/m^2$, $\nu=0.3$, $\rho=7836.8\ kg/m^3$, $b=0.02m$, $t=0.01m$, $\theta=120^o$, $R=1m$, $k_s=10kN/m$, $m_s=2\ kg$)

Mode	Frequency [Hz]								
	no suspended s-m system			with one suspended s-m system			with three suspended s-m system		
	Çankaya et al. [6]	ANSYS	Present Work	Çankaya et al. [6]	ANSYS	Present Work	Çankaya et al. [6]	ANSYS	Present Work
1	27.970	27.963	27.966	10.749	10.749	10.787	10.285	10.209	10.162
							10.625	10.661	10.677
				27.967	27.963	28.864	11.235	11.210	11.203
							30.504	30.715	30.854
2	55.710	55.682	55.706	58.072	58.048	56.099	58.809	58.470	58.388
3	101.353	101.270	101.356	101.353	101.274	101.558	101.615	101.290	101.375
4	151.170	150.990	151.179	151.524	151.341	151.179	151.547	151.790	152.156

According to the results of frequency shown in Table 5.3, the first natural frequency becomes the natural frequency of the spring-mass system when the spring-mass system is suspended to the curved beam. If the number of the suspended spring-mass system is more than one, the natural frequencies of the spring-mass system appear for each spring-mass system before the natural frequencies of the whole system.

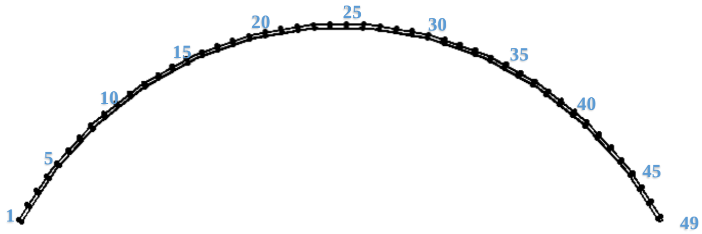

(a)

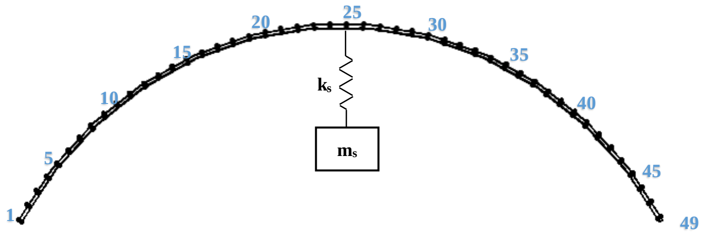

(b)

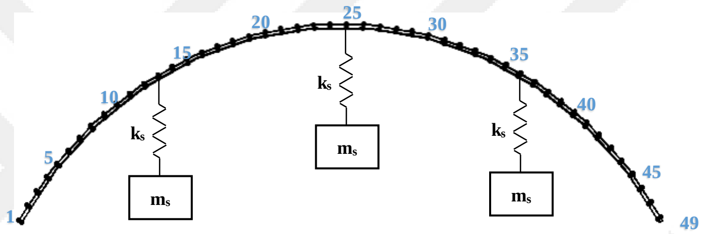

(c)

Figure 5.2 The node numbers of the curved beam and spring-mass systems in different cases ; (a) no spring-mass system, (b) one spring-mass system on the 25th node, (c) three spring-mass system on 13th, 25th, and 36th nodes

In present work, the stiffness coefficient of suspended spring is selected with respect to the equivalent stiffness coefficient of the curved beam so that the results can be evaluated independently on dimensions. The stiffness coefficient of the curved beam is determined by considering the equivalent spring-mass model. After modeling of the curved beam using ANSYS, the first natural frequency, and the mass value are obtained from there. Using natural frequency and mass values, the equivalent stiffness coefficient is determined by the equation $\omega_n^2 = k/m$. This stiffness coefficient of the curved beam is only approximate value.

The stiffness coefficient ratio k_{ratio} is the ratio of the stiffness coefficient of suspended spring k_s to the equivalent stiffness coefficient of the curved beam. The stiffness coefficient of suspended spring is determined with respect to values of k_{ratio} and analysis are realized for this value of k_s.

Table 5.4 The natural frequencies of the suspended spring-mass system according to the stiffness coefficients ratios

k_{ratio}	0.1	0.3	0.5	1	1.5	2	5
f_n [Hz]	11.33	19.62	25.33	35.82	43.87	50.66	80.09

The natural frequency values of the spring-mass system corresponding to the stiffness coefficient ratio k_{ratio} are shown in Table 5.4 where the suspended mass value is assumed 2 kg.

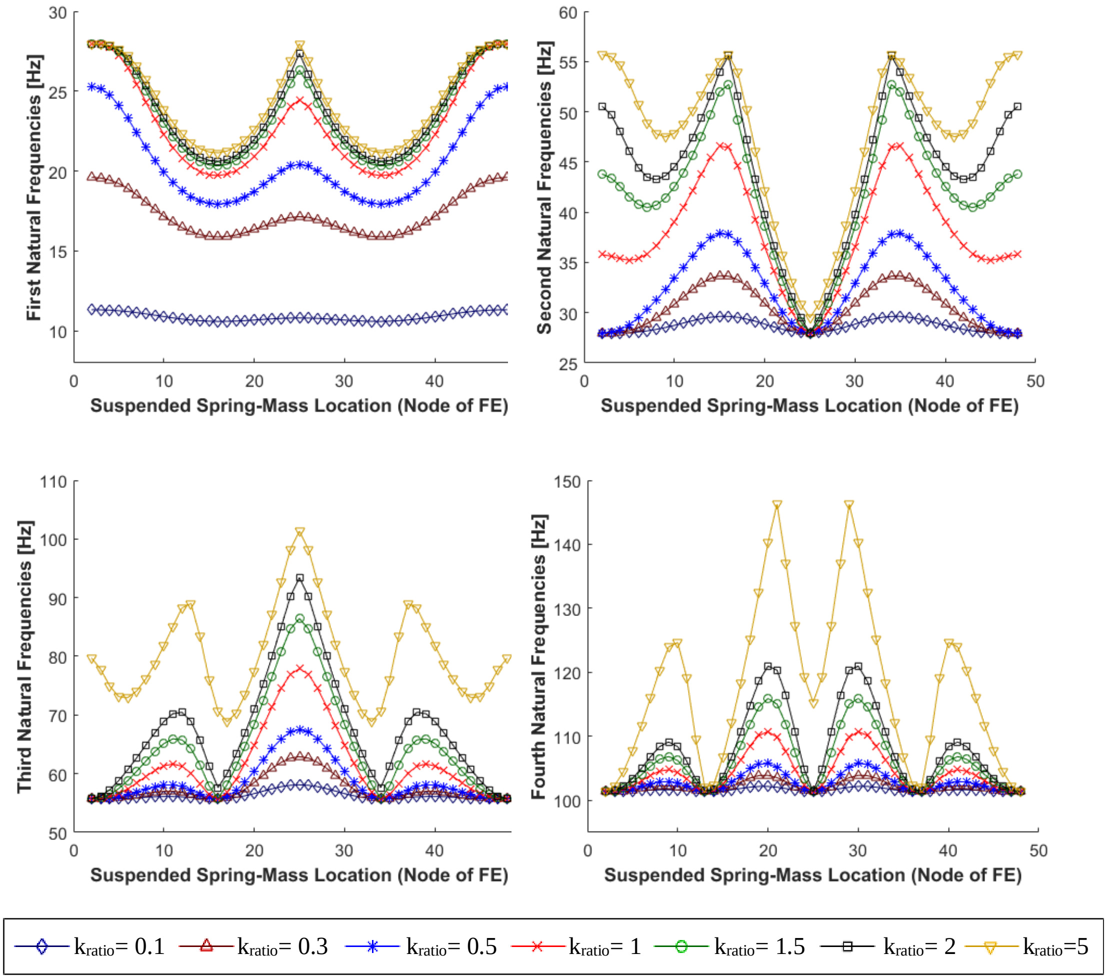

Figure 5.3 The effect of suspended spring-mass location and k_{ratio} on the first four natural frequencies of the curved beam (E=2.069x10^{11}N/m^2, ν=0.3, ρ=7836.8 kg/m^3, b=0.02m, t=0.01m, θ=120º, R=1m.)

The effect of location of the suspended spring-mass system on the natural frequencies are investigated for different k_{ratio} values and acquired results are presented in Figure 5.3.

As seen in Figure 5.3, the stiffness ratio can be seen as the most effective factor because it directly affects the natural frequency of the system. The natural frequencies of the spring-mass system are seen as the first natural frequency in cases which the stiffness ratio k_{ratio} is smaller than one. Besides that, the natural frequencies of spring-mass system change with respect to the location (node of suspending) because of the change of flexibility of the curved beam.

Conversely, if the stiffness ratio k_{ratio} is one and above, the natural frequencies of the whole system are seen in first natural frequencies. The effect of the spring-mass system on the natural frequencies of whole system change with respect to location. In these frequencies, the whole system vibrates in the first mode of curved beam, therefore the spring-mass system on the non-vibrating nodes never affects the natural frequencies of the curved beam.

As for the second frequencies, when the stiffness ratio is one and above (except for k_{ratio}=5), the natural frequencies of the spring-mass system appear. In there, the natural frequencies of the whole system corresponding to the first mode is seen for the other values of stiffness ratio.

In the case where the stiffness ratio equals five, these values of frequency represent the second natural frequencies of the whole system. For this frequency value, the effect of suspended spring-mass system change with respect to the location. When the location of the suspended spring-mass system corresponds to non-vibrational nodes of the second mode, the spring-mass system hardly affects the second natural frequencies of the whole system.

When the stiffness ratio equals five, the natural frequency of the spring-mass system is between the second and the third natural frequencies of the whole system. Therefore, this frequency value of the spring-mass system appears in the third natural frequencies where the whole system vibrates with the second mode of the curved beam.

Except for these specific cases, the natural frequencies of the whole system is seen respectively as excepted and the effect of location of suspended system change in respect to mode shapes of the curved beam.

5.2 Dynamic Stability Regions of a Curved Beam

In this section, the effect of the subtended angle and radius of a curved beam without the suspended spring-mass system on the dynamic stability are represented. These effects are given to compare that of the suspended spring-mass system.

5.1.1 The Effect of Subtended Angle (θ)

The effect of dynamic stability parameter (β) and subtended angle on the dynamic stability regions are shown with graphics in Figures 5.4 – 5.7. These effects are figured out two cases in which the static load parameter is zero and 0.5. The results are obtained for different values of subtended angle that are 60°, 90°, 120°, 150°, and 180°. There is the disturbing frequency values are given as the ratio of the natural frequency of the curved beam for θ=120°.

In case that the static load parameter is zero, change of the dynamic instability regions are represented in Figures 5.4 and 5.5. As seen from Figure 5.4 that when the subtended angle of the curved beam decreases, the first instability region widens and the initial disturbing frequency moves away origin. Figure 5.5 shows that the second instability regions are dispersed and narrower than the first instability regions.

The change of the dynamic instability regions for α=0.5 is represented in Figures 5.6 and 5.7. The dynamic load parameter is bounded between the values of zero and one. When the static load parameter increase, the initial disturbing frequency moves towards origin and the instability regions narrows in line with the increase of the subtended angle.

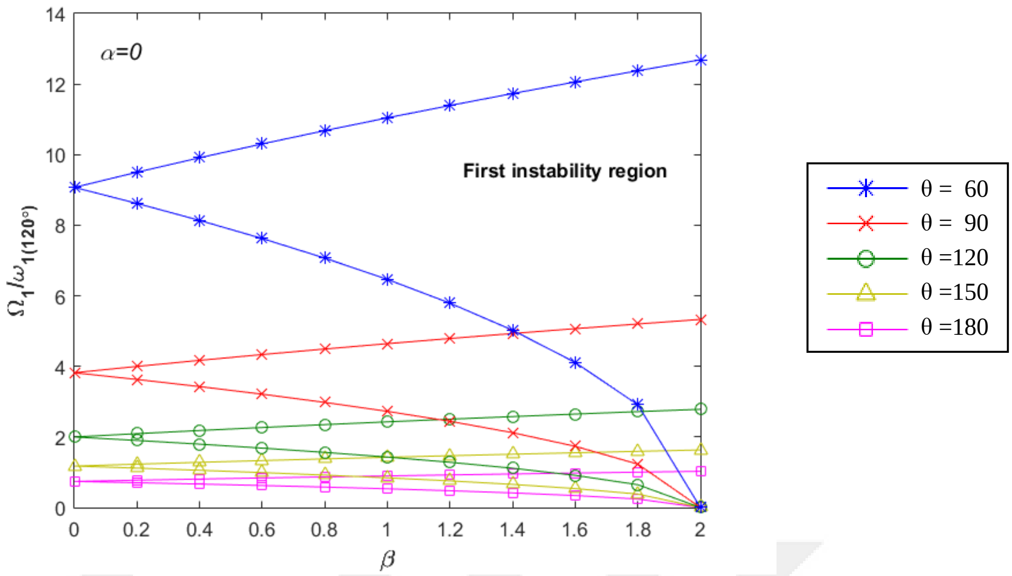

Figure 5.4 The effect of the subtended angle on the first stability regions of the curved beam, α=0 (E=2.069x10^{11}N/m^2, ν=0.3, ρ=7836.8 kg/m^3, b=0.02m, t=0.01m, R=1m)

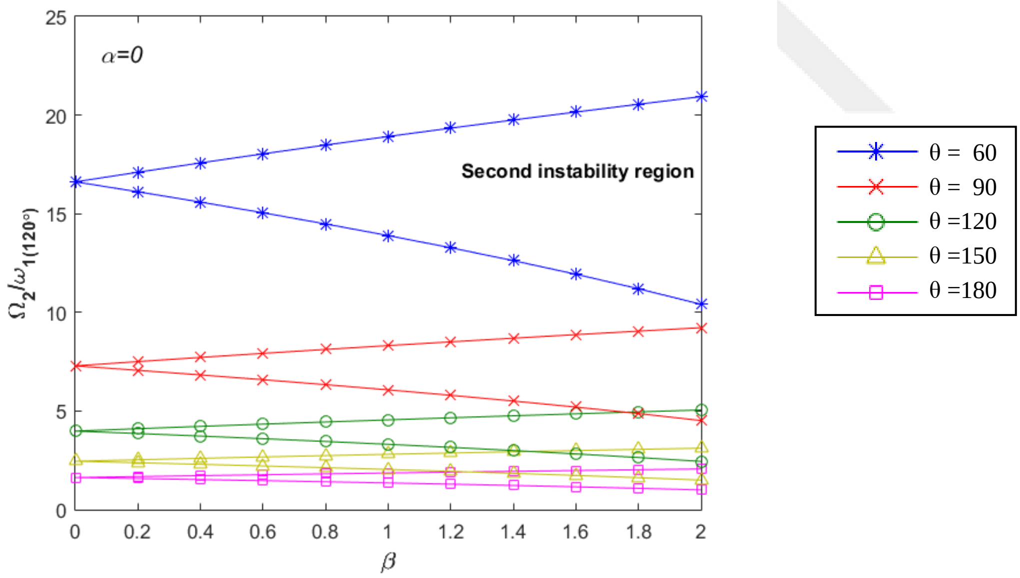

Figure 5.5 The effect of the subtended angle on the second stability regions of the curved beam, α=0 (E=2.069x10^{11}N/m^2, ν=0.3, ρ=7836.8 kg/m^3, b=0.02m, t=0.01m, R=1m)

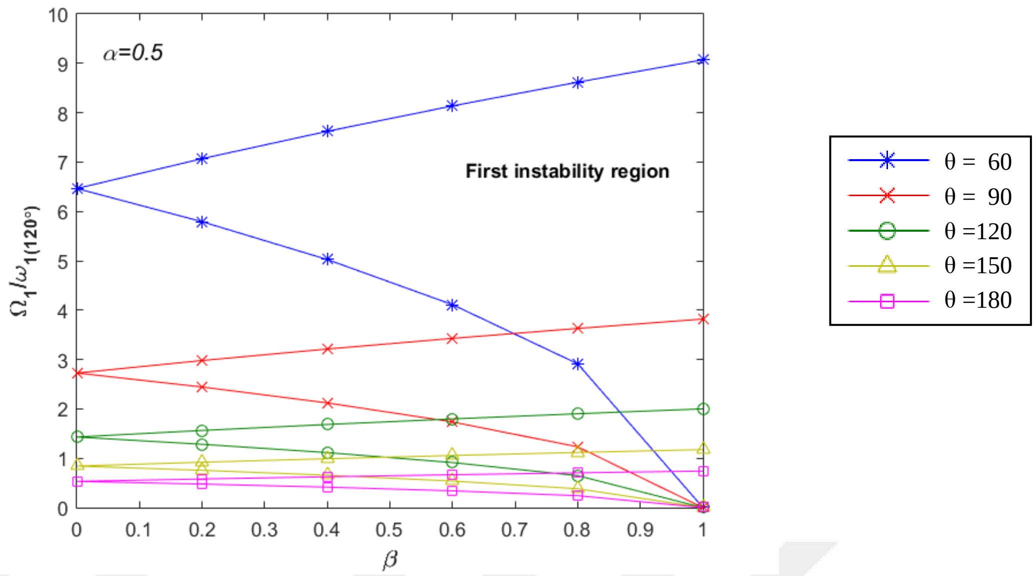

Figure 5.6 The effect of the subtended angle on the first stability regions of the curved beam, α=0.5 (E=2.069x10^{11}N/m^2, ν=0.3, ρ=7836.8 kg/m^3, b=0.02m, t=0.01m, R=1m)

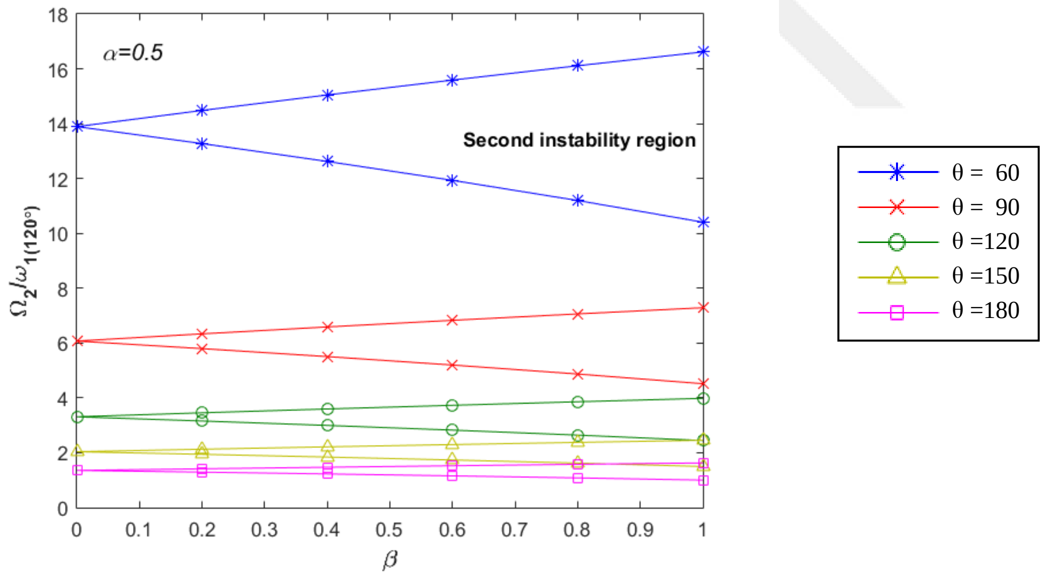

Figure 5.7 The effect of the subtended angle on the second stability regions of the curved beam, α=0.5 (E=2.069x10^{11}N/m^2, ν=0.3, ρ=7836.8 kg/m^3, b=0.02m, t=0.01m, R=1m)

5.1.2 The Effect of Radius of the Curved Beam

The effect of dynamic stability parameter (β) and radius on the dynamic stability regions are shown with graphics in Figures 5.8 – 5.11. The results are obtained for different values of radius of the curved beam that are 0.25, 0.5, 0.75, and 1 meter. There is the disturbing frequency values are given as the ratio of the natural frequency of the curved beam for *R*=1 meter.

These effects are figured out for two cases in which the static load parameter is zero and 0.5. In case that the static parameter is zero, change of the dynamic stability regions are represented in Figures 5.8 and 5.9. There is a similar effect between the radius and the curved beam. If the radius increases, the instability region narrows, and moves towards the origin.

In case that the static load parameter is 0.5, change of the dynamic stability regions are represented in Figures 5.10 and 5.11. As seen from these figures, the instability regions move towards the origin when the static load parameter increases.

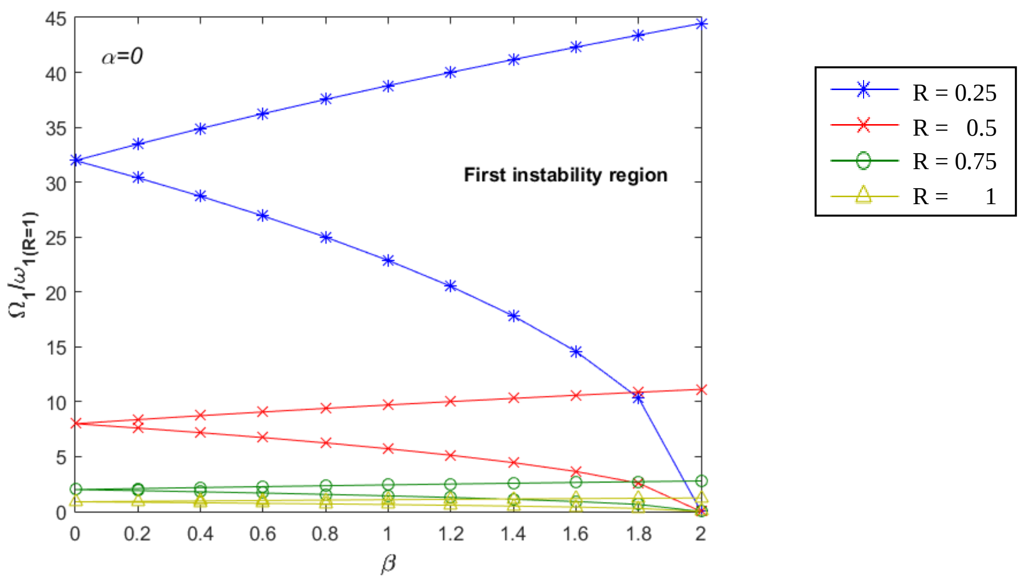

Figure 5.8 The effect of the radius of the curved beam on the first stability regions of the curved beam, α=0 (E=2.069x10^{11}N/m^2, ν=0.3, ρ=7836.8 kg/m^3, b=0.02m, t=0.01m, θ=120º)

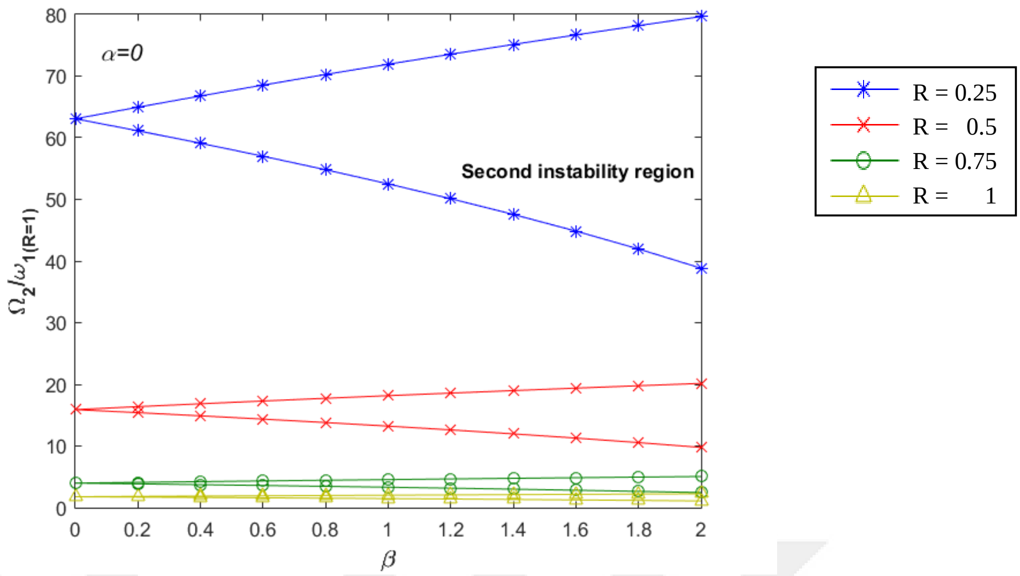

Figure 5.9 The effect of the radius of the curved beam on the second stability regions of the curved beam, α=0 (E=2.069x10^{11}N/m^2, ν=0.3, ρ=7836.8 kg/m^3, b=0.02m, t=0.01m, θ=120º)

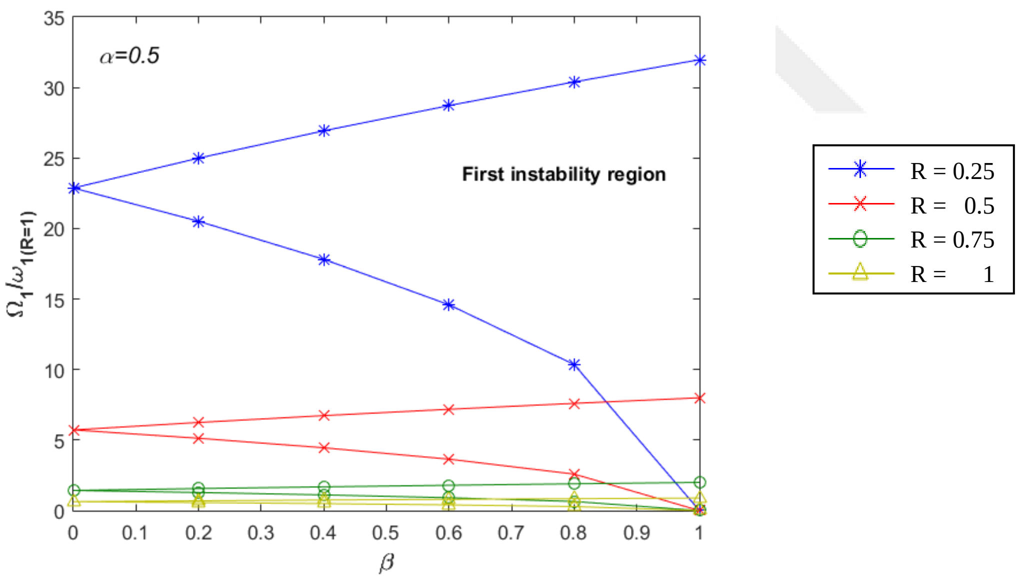

Figure 5.10 The effect of the radius of the curved beam on the first stability regions of the curved beam, α=0.5 (E=2.069x10^{11}N/m^2, ν=0.3, ρ=7836.8 kg/m^3, b=0.02m, t=0.01m, θ=120º)

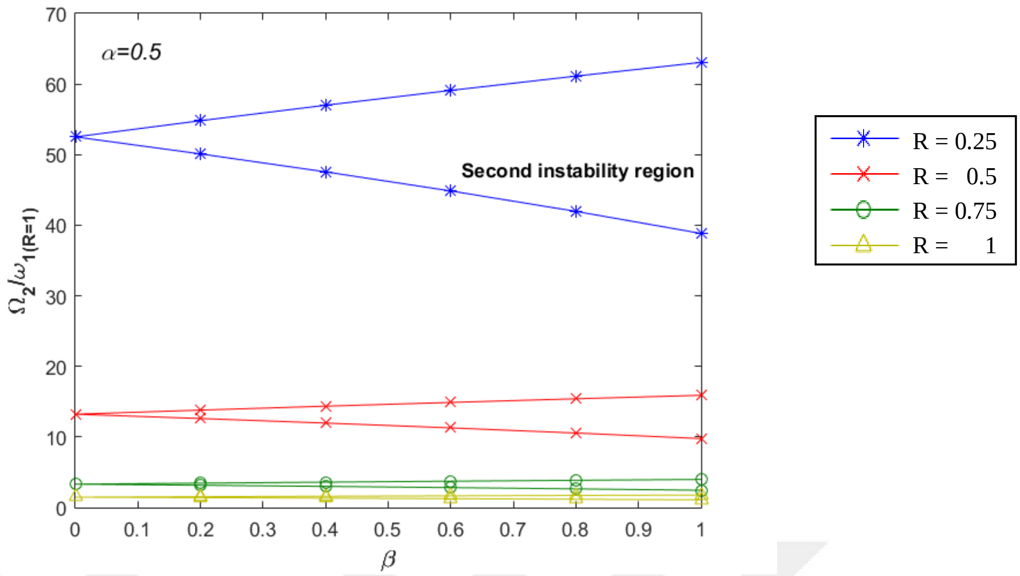

Figure 5.11 The effect of the radius of the curved beam on the second stability regions of the curved beam, α=0.5 (E=2.069x10^{11}N/m^2, ν=0.3, ρ=7836.8 kg/m^3, b=0.02m, t=0.01m, θ=120º)

5.3 Dynamic Stability of Curved Beam with Suspended Spring-Mass System

In this section, the effects of suspended spring-mass, the location of the spring-mass system, the subtended angle and radius of the curved beam, and k_{ratio} parameter are investigated on the stability regions. The dynamic stability regions are shown with respect to the ratio of disturbing frequency to the natural frequency of curved beam without a suspended spring-mass system furthermore, the radius of the curved beam is 1 meter and the subtended angle is 120°.

The graphics which are given in Figures 5.12 - 5.15, shows the effect of the number of suspended spring-mass system. For this reason, there is illustrated three different cases. In the first case, the curved beam doesn't have a suspended system, in the second one, the curved beam is with one suspended system and in the last one, the curved beam is with three suspended systems. The suspended mass is 2 kg and the stiffness coefficient ratio k_{ratio} equals 1. Figures 5.12 and 5.13 express the case of no static loading while Figures 5.14 and 5.15 show the case of static loading.

As seen from Figure 5.12, if the suspended spring-mass system is pieced on the curved beam, the dynamic instability region narrows and moves towards the origin. In case of one suspended system, the lower borders of the first unstable region intersect with the lower borders of no suspended system for β ≥ 0.8. When the static load parameter is 0.5, the intersecting points increase and the lower borders of cases that are no suspended system and one suspended system become the same; moreover, the upper borders of them intersect at $\beta = 0.2$. However, in the second dynamic instability regions shown in Figure 5.13, the location of them is scattered.

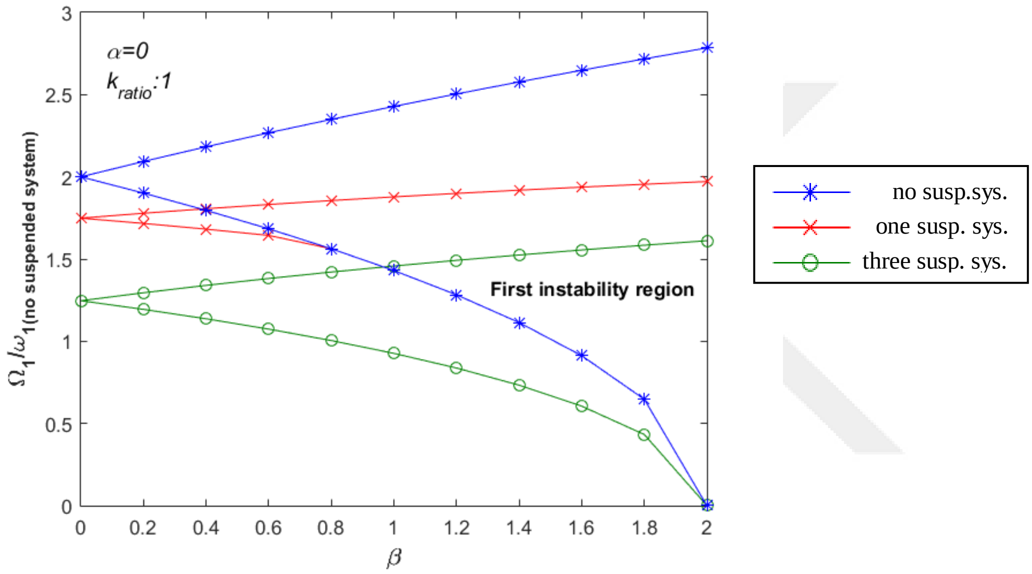

Figure 5.12 The effect of the spring-mass system on the first stability regions of the curved beam, α=0 ($E=2.069 \times 10^{11} N/m^2$, ν=0.3, ρ=7836.8 kg/m^3, b=0.02m, t=0.01m, θ=120º, R=1m, m_s=2 kg, k_{ratio}=1)

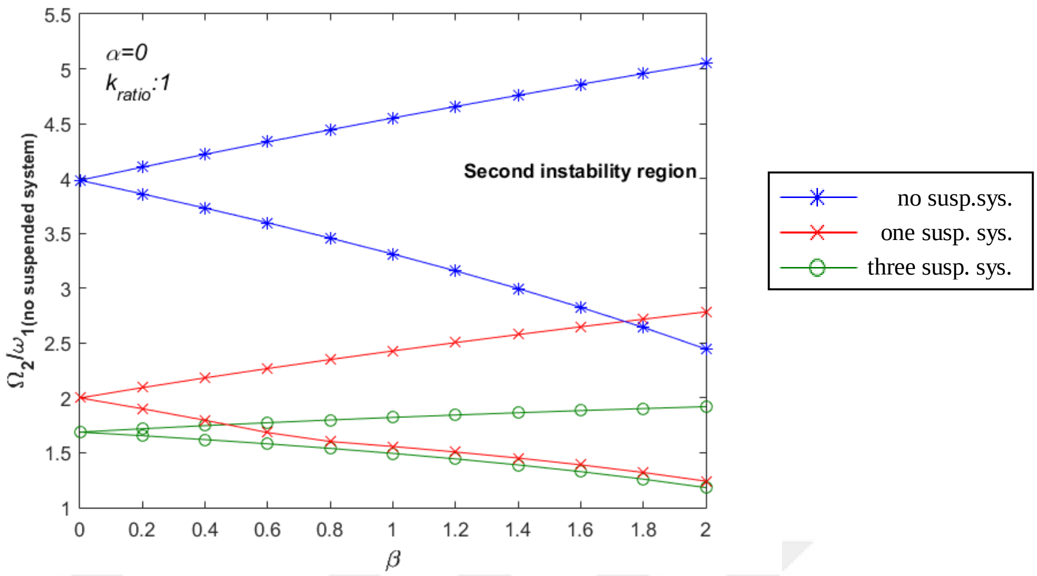

Figure 5.13 The effect of the spring-mass system on the second stability regions of the curved beam, α=0 (E=2.069x10^{11}N/m^2, ν=0.3, ρ=7836.8 kg/m^3, b=0.02m, t=0.01m, θ=120º, R=1m, m_s=2 kg, k_{ratio}=1)

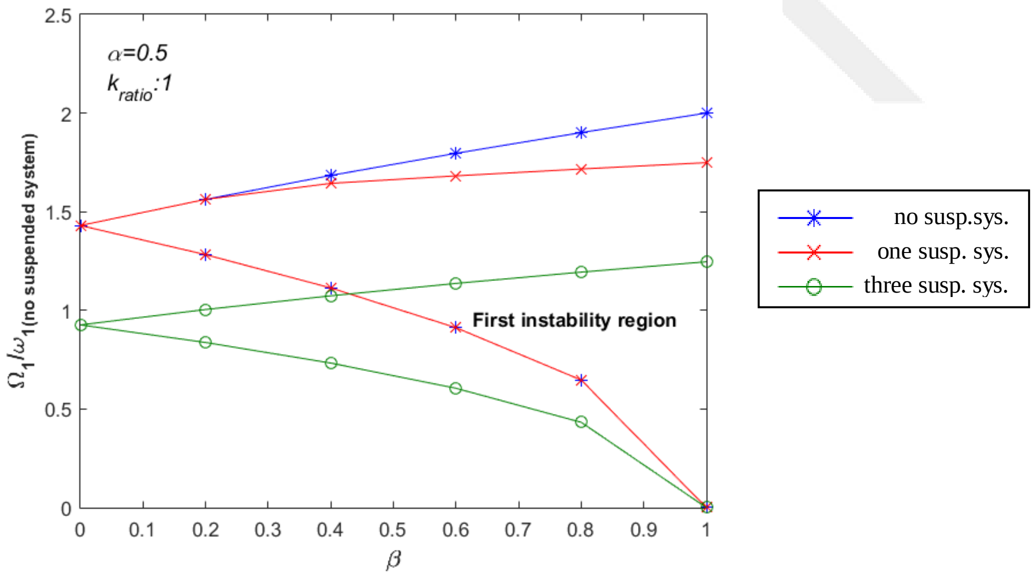

Figure 5.14 The effect of the spring-mass system on the first stability regions of the curved beam, α=0.5 (E=2.069x10^{11}N/m^2, ν=0.3, ρ=7836.8 kg/m^3, b=0.02m, t=0.01m, θ=120º, R=1m, m_s=2 kg, k_{ratio}=1)

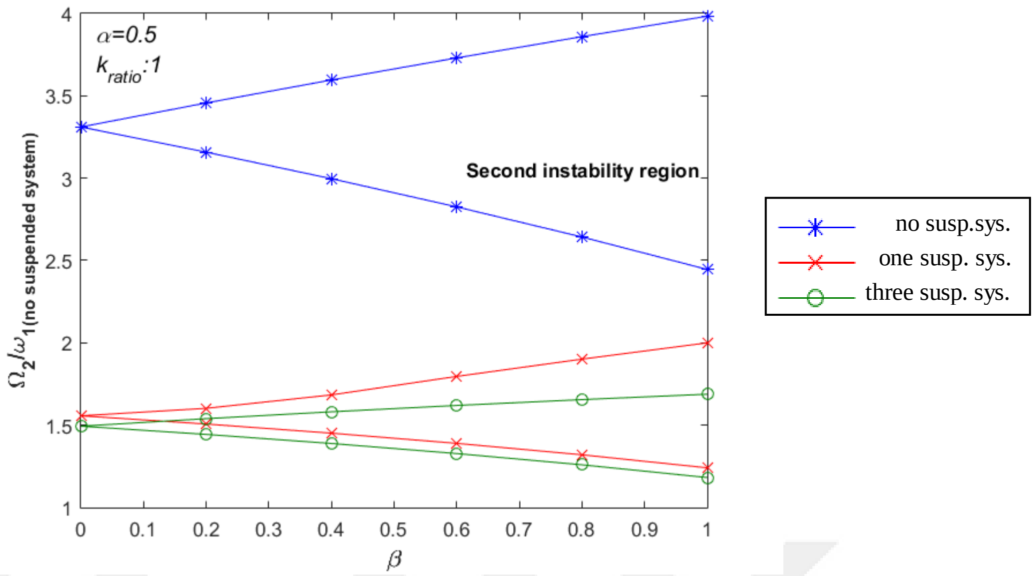

Figure 5.15 The effect of the spring-mass system on the second stability regions of the curved beam, α=0.5 (E=2.069x10^{11}N/m^2, ν=0.3, ρ=7836.8 kg/m^3, b=0.02m, t=0.01m, θ=120º, R=1m, m_s=2 kg, k_{ratio}=1)

To comprehend the effect of location of the spring-mass system on the first and second stability regions, only one spring-mass system has been suspended on various node of the system showing in Figure 5.2 (a). The effect of location of the spring-mass system on the stability regions is shown in Figures 5.16 and 5.17 for no static load. The effect of location of the spring-mass system on the stability regions for static loading is indicated in Figures 5.18 and 5.19. For both situations, having static load and no static load, the ratio of stiffness coefficient ratio k_{ratio} equals 1 and the mass of suspended spring is 2 kg.

As seen from these results, if the suspended spring-mass system is attached further away from non-vibrating nodes in terms of the mode shape of the curved beam, the dynamic instability region is narrower and closer to the origin from other cases. When the static load parameter increase, the initial disturbing frequency moves towards the origin. However, the 5th node that has a suspended spring-mass is more stable than 25th node that has a suspended spring-mass because of the decrease of rigidity on the midpoint of the curved beam.

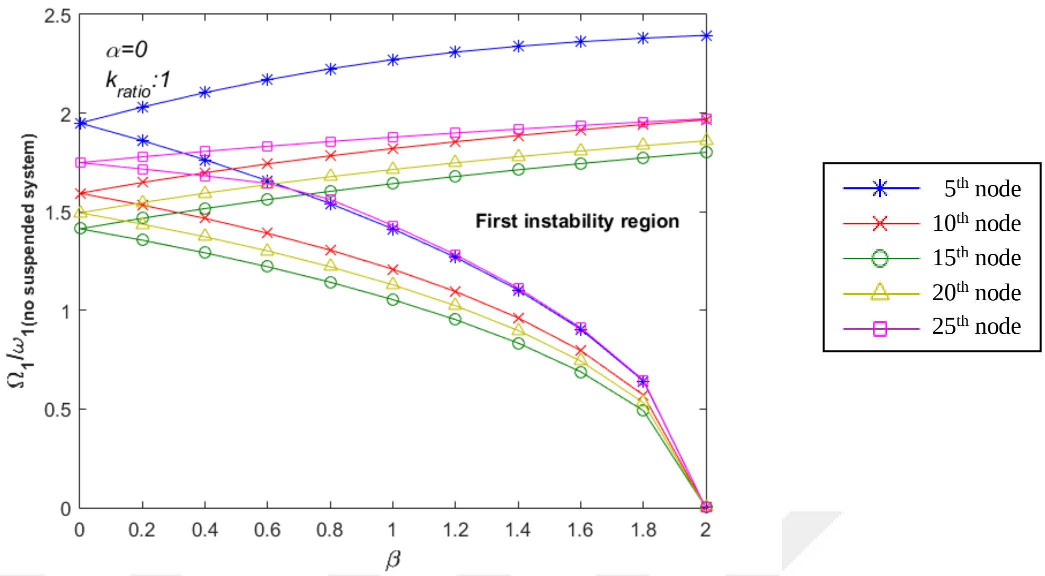

Figure 5.16 The effect of the location of the spring-mass system on the first stability regions of the curved beam with one suspended spring-mass system, α=0 (E=2.069x10^{11}N/m^2, ν=0.3, ρ=7836.8 kg/m^3, b=0.02m, t=0.01m, θ=120º, R=1m, m_s=2 kg, k_{ratio}=1)

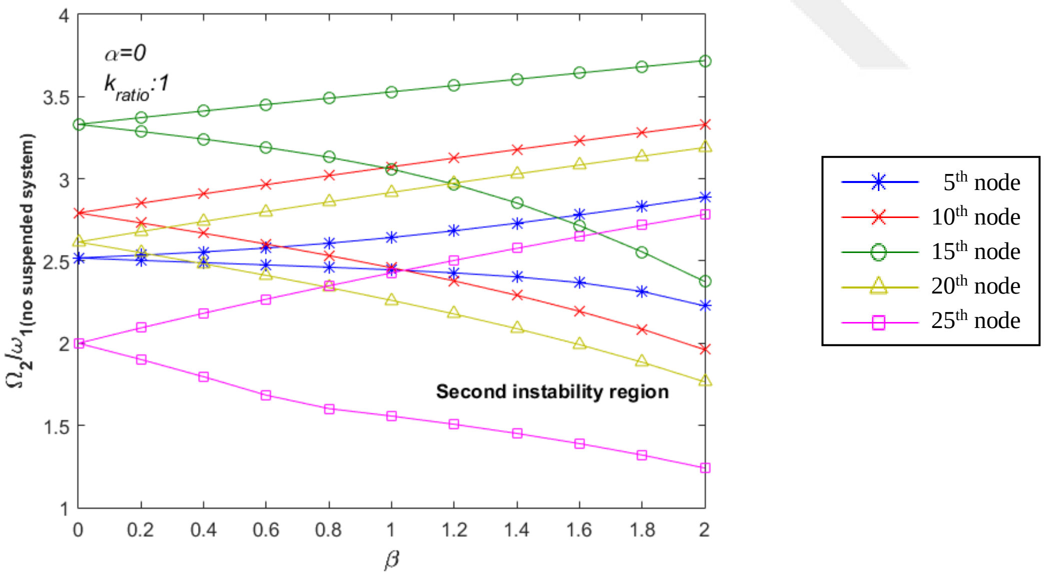

Figure 5.17 The effect of the location of the spring-mass system on the second stability regions of the curved beam with one suspended spring-mass system, α=0 (E=2.069x10^{11}N/m^2, ν=0.3, ρ=7836.8kg/m^3, b=0.02m, t=0.01m, θ=120º, R=1m, m_s=2 kg, k_{ratio}=1)

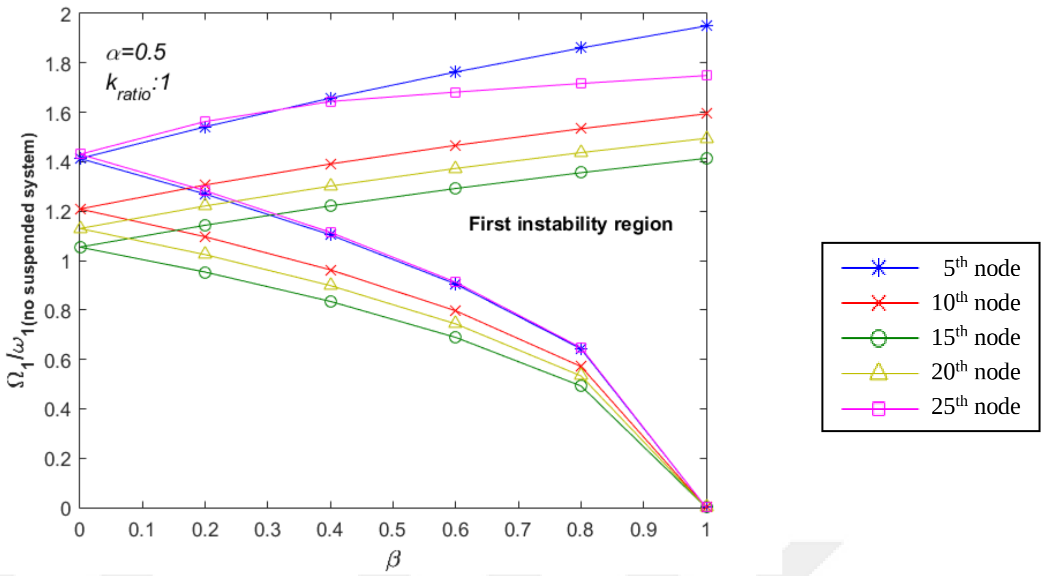

Figure 5.18 The effect of the location of the spring-mass system on the first stability regions of the curved beam with one suspended spring-mass system, α=0.5 (E=2.069x10^{11}N/m^2, ν=0.3, ρ=7836.8 kg/m^3, b=0.02m, t=0.01m, θ=120º, R=1m, m_s=2 kg, k_{ratio}=1)

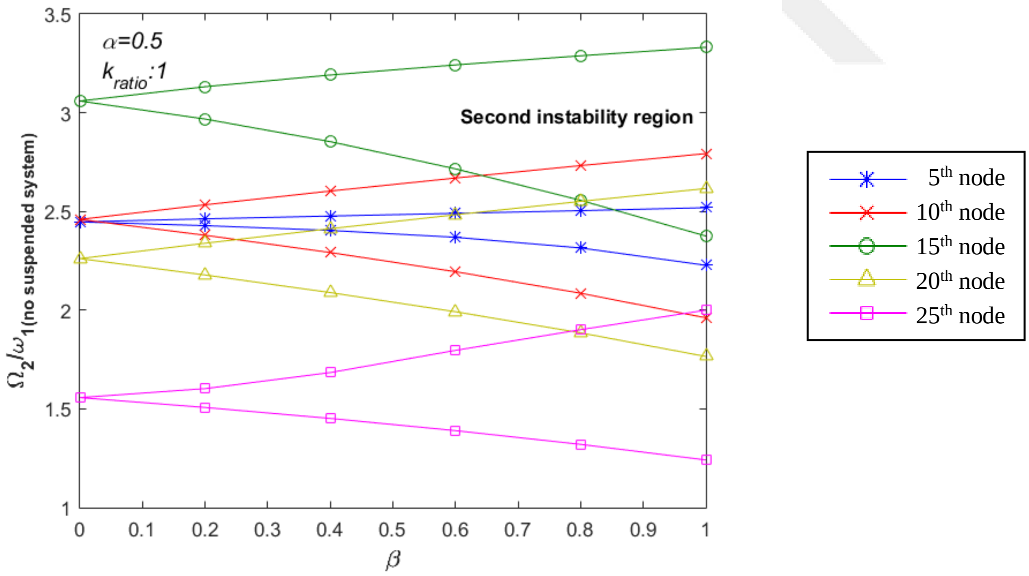

Figure 5.19 The effect of the location of the spring-mass system on the second stability regions of the curved beam with one suspended spring-mass system, α=0.5 (E=2.069x10^{11}N/m^2, ν=0.3, ρ=7836.8kg/m^3, b=0.02m, t=0.01m, θ=120º, R=1m, m_s=2 kg, k_{ratio}=1)

5.2.1 The Effect of Subtended Angle (θ)

In this section, the effect of subtended angle of the curved beam with the suspended spring-mass system on the first and second stability regions are shown in Figures 5.20 - 5.23. For this survey, the spring-mass system is suspended on the 25th node like as Figure 5.2 (b). Mass of the spring-mass system is 2 kg and the stiffness coefficient ratio k_{ratio} equals 1.

Figures 5.20 and 5.21 show the stability regions for the system that doesn't have a static load while Figures 5.22 and 5.23 show the stability regions in case of static loading.

As seen from these figures, if the suspended spring-mass system is attached on the curved beam, the dynamic instability region is narrower than the case that is no suspended system. When the subtended angle of the curved beam increases, the dynamic instability region moves towards the origin and widens. In the case of static loading, the dynamic stability regions narrow and move towards the origin.

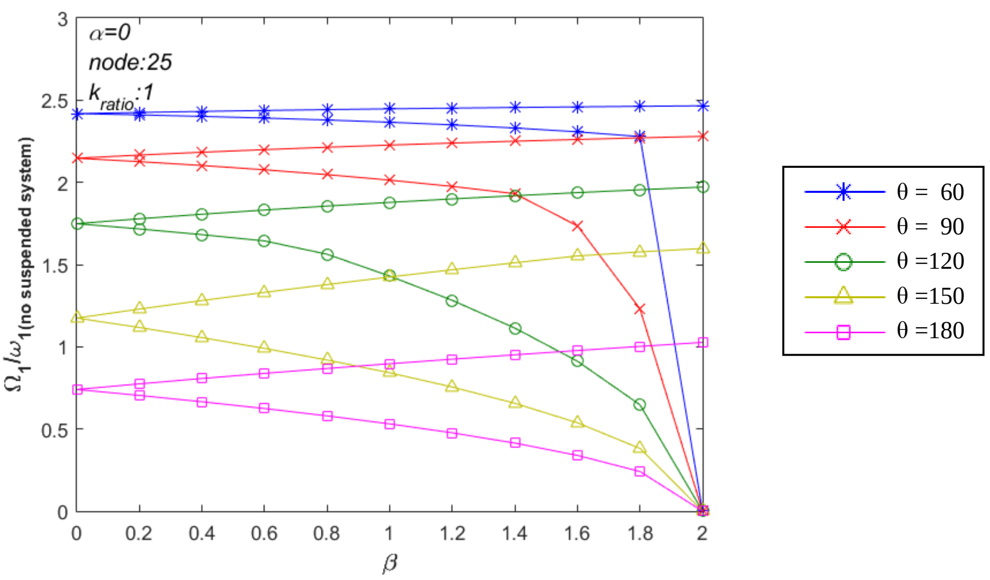

Figure 5.20 The effect of the subtended angle on the first stability regions of the curved beam with one suspended spring-mass system, α=0 (E=2.069x10^{11}N/m^2, ν=0.3, ρ=7836.8 kg/m^3, b=0.02m, t=0.01m, R=1m, m_s=2 kg, k_{ratio}=1)

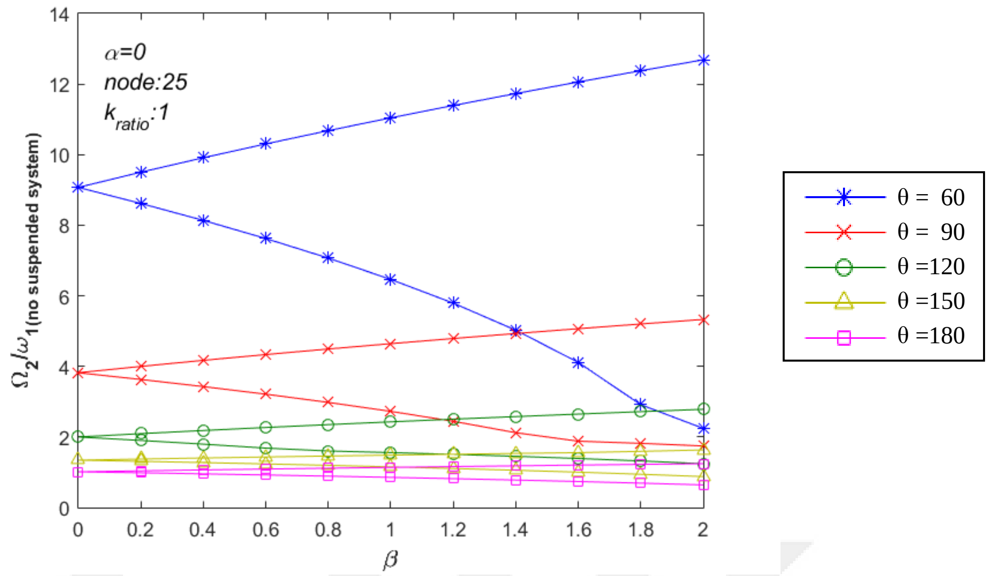

Figure 5.21 The effect of the subtended angle on the second stability regions of the curved beam with one suspended spring-mass system, α=0 (E=2.069x10^{11}N/m^2, ν=0.3, ρ=7836.8 kg/m^3, b=0.02m, t=0.01m, R=1m, m_s=2 kg, k_{ratio}=1)

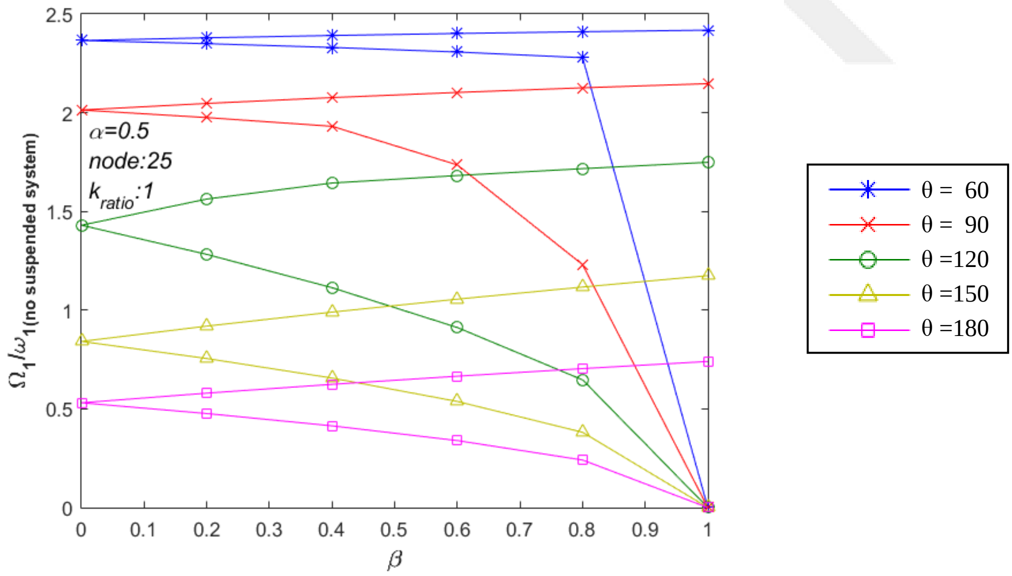

Figure 5.22 The effect of the subtended angle on the first stability regions of the curved beam with one suspended spring-mass system α=0.5, (E=2.069x10^{11}N/m^2, ν=0.3, ρ=7836.8 kg/m^3, b=0.02m, t=0.01m, R=1m, m_s=2 kg, k_{ratio}=1)

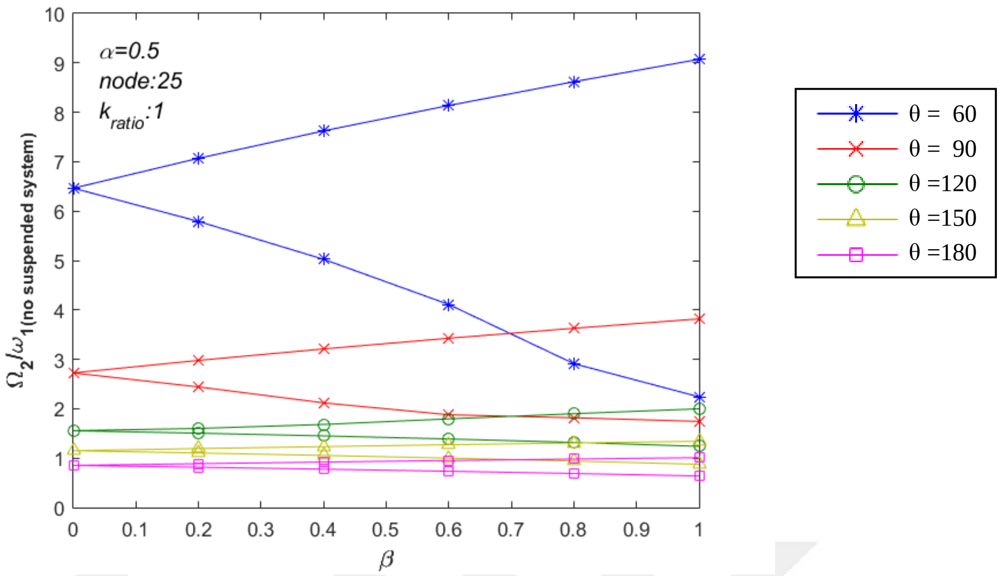

Figure 5.23 The effect of the subtended angle on the second stability regions of the curved beam with one suspended spring-mass system α=0.5, (E=2.069x10^{11}N/m^2, ν=0.3, ρ=7836.8 kg/m^3, b=0.02m, t=0.01m, R=1m, m_s=2 kg, k_{ratio}=1)

5.2.2 The Effect of Radius of the Curved Beam

In this section, the effect of radius of the curved beam with the suspended spring-mass system on the first and second stability regions are shown in Figures 5.24 - 5.27. For this survey, the spring-mass system is suspended on the 25th node like as Figure 5.2 (b). The mass of suspended system is 2 kg and the stiffness coefficient ratio k_{ratio} equals 1.

Figures 5.24 and 5.25 show the stability regions for the system that doesn't have a static load while Figures 5.26 and 5.27 show the stability regions in case of static loading. There is a similar effect between the radius and the curved beam. If the radius increases, the instability region narrows, and moves towards the origin.

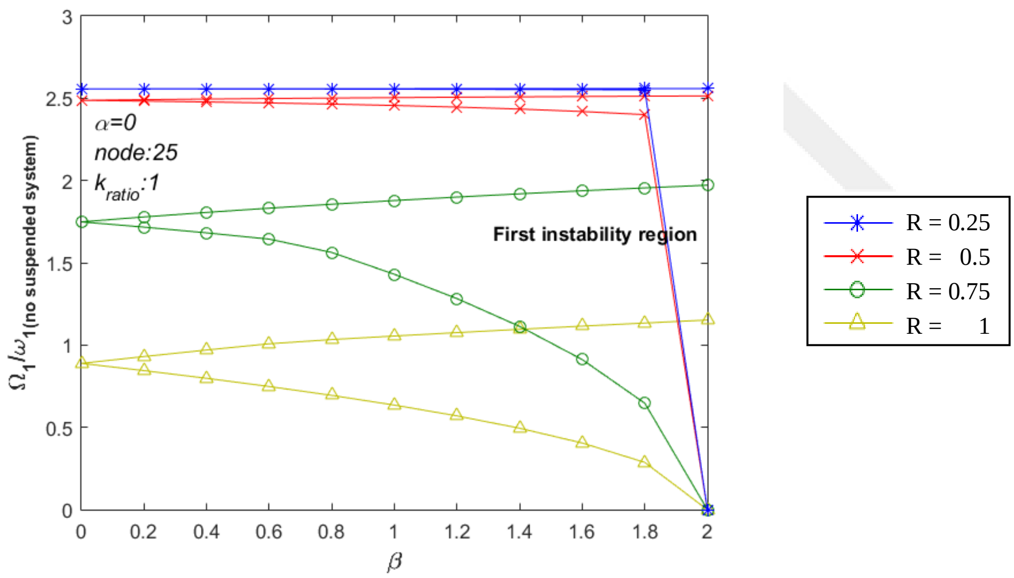

Figure 5.24 The effect of the radius of the curved beam on the first stability regions of the curved beam with one suspended spring-mass system, α=0 (E=2.069x10^{11}N/m^2, ν=0.3, ρ=7836.8 kg/m^3, b=0.02m, t=0.01m, θ=120º, m_s=2 kg, k_{ratio}=1)

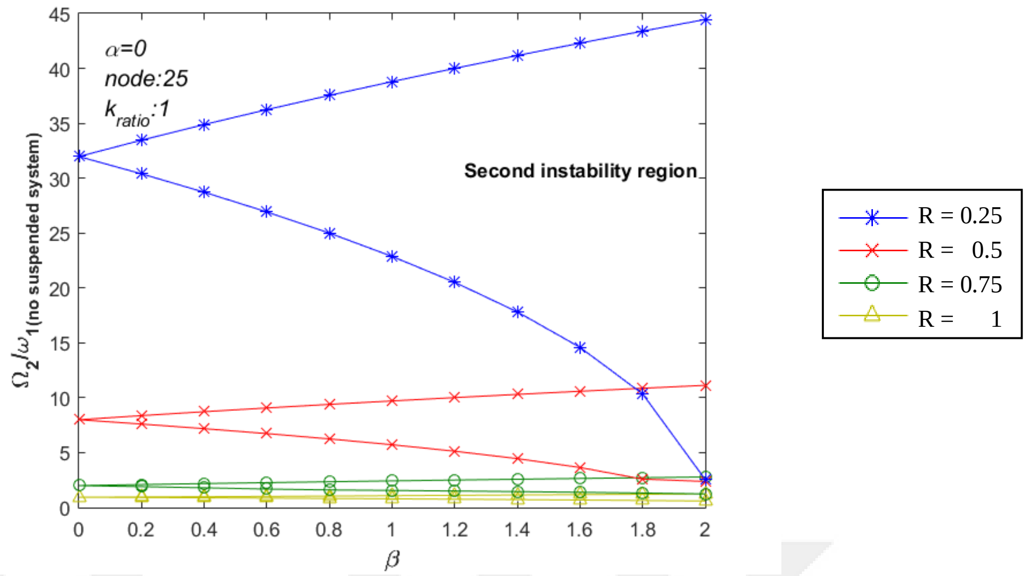

Figure 5.25 The effect of the radius of the curved beam on the second stability regions of the curved beam with one suspended spring-mass system, α=0 (E=2.069x10^{11}N/m^2, ν=0.3, ρ=7836.8 kg/m^3, b=0.02m, t=0.01m, θ=120º, m_s=2 kg, k_{ratio}=1)

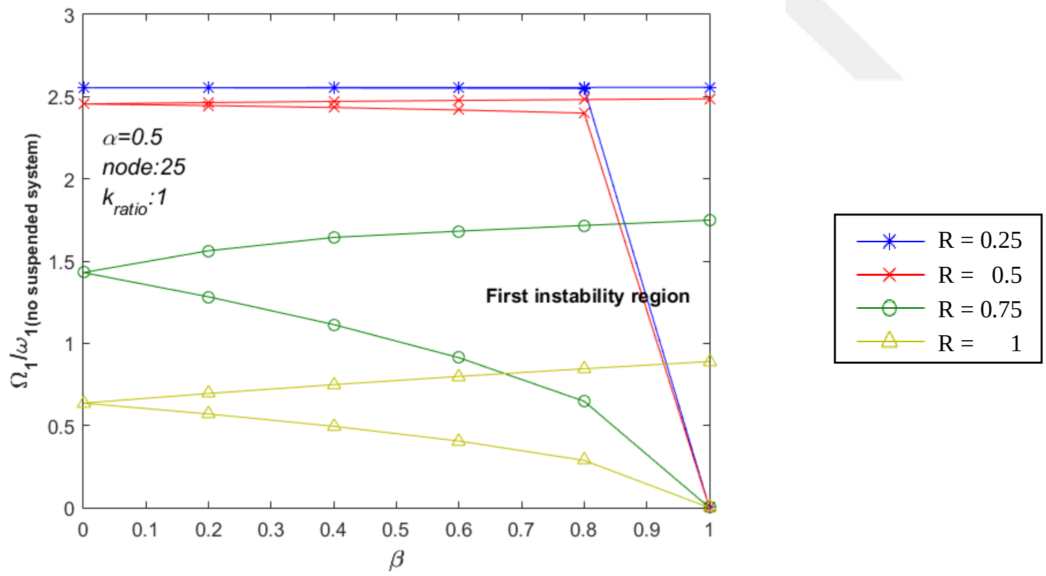

Figure 5.26 The effect of the radius of the curved beam on the first stability regions of the curved beam with one suspended spring-mass system, α=0 (E=2.069x10^{11}N/m^2, ν=0.3, ρ=7836.8 kg/m^3, b=0.02m, t=0.01m, θ=120º, m_s=2 kg, k_{ratio}=1)

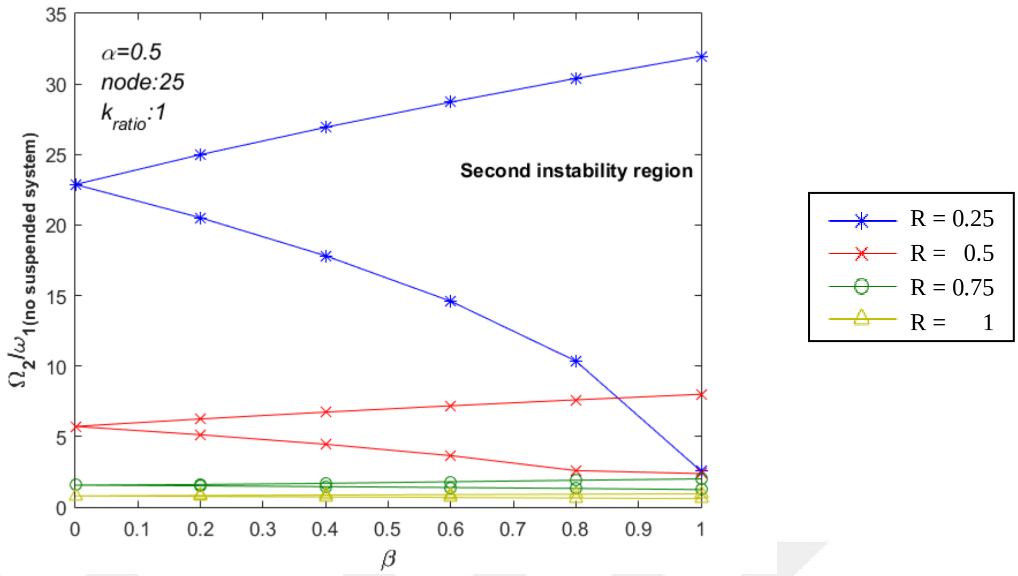

Figure 5.27 The effect of the radius of the curved beam on the second stability regions of the curved beam with one suspended spring-mass system, α=0 (E=2.069x10^{11}N/m^2, ν=0.3, ρ=7836.8 kg/m^3, b=0.02m, t=0.01m, θ=120º, m_s=2 kg, k_{ratio}=1)

5.2.3 The Effect of the Stiffness Coefficient of the Suspended Spring-Mass System

The stiffness coefficient of suspended spring has a significant effect on the dynamic stability regions. To understand this effect, the various stiffness coefficient ratio k_{ratio} have been employed in the spring-mass system and the stability regions are shown in Figures 5.28 – 5.35. In addition, the stability regions have been investigated for two different locations of one spring-mass system where are at 13th, and 25th nodes. When the static loading doesn't exist, the dynamic stability regions for the spring-mass system at 13th node become as shown in Figures 5.28 and 5.29 with respect to various stiffness coefficient ratios k_{ratio}.

When the static loading doesn't exist, the dynamic stability regions of the curved beam with the spring-mass system at the 13th node are shown in Figures 5.28 and 5.29. Figures 5.30 and 5.31 show the dynamic stability regions of the curved beam with the spring-mass system at the 25th node for the same type of load. On the other hand, if the static loading exists, the dynamic stability regions of the system with the spring-mass system at the 13th node are shown in Figures 5.32 and 5.33. Figures 5.34 and 5.35 show that the dynamic stability regions of the curved beam with the spring-mass system at the 25th node.

As seen from these figures, as long as the stiffness coefficient of suspended spring increases, the first instability region widens and moves away from the origin. According to Figure 5.31, the second instability region narrows when the ratio of the stiffness coefficient increases. Besides that, the upper borders of all cases intersect at all values of β.

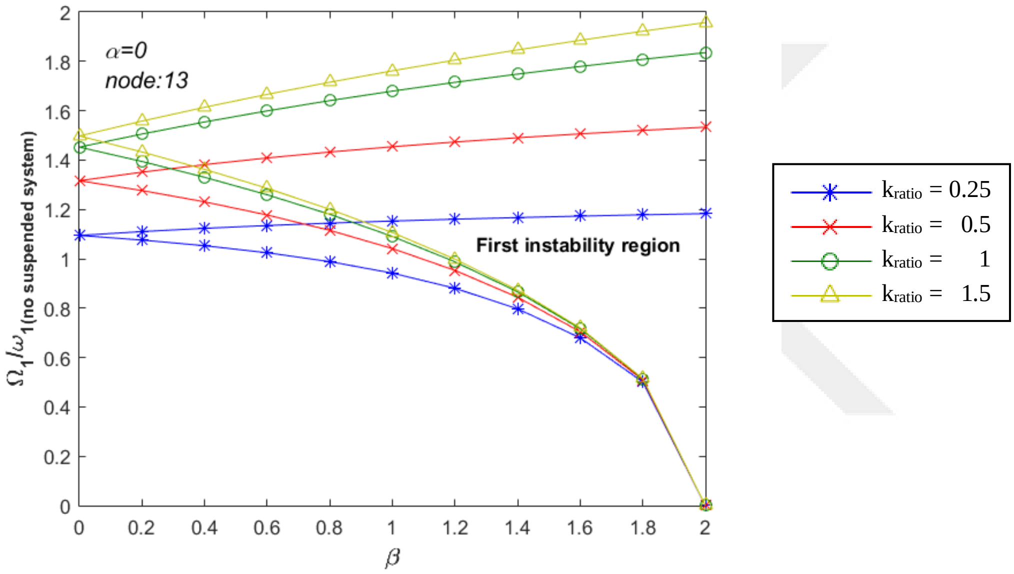

Figure 5.28 The effect of stiffness ratio of suspended spring on the first stability regions of the curved beam with one suspended spring-mass system, α=0 (E=2.069x10^{11}N/m^2, ν=0.3, ρ=7836.8 kg/m^3, b=0.02m, t=0.01m, θ=120°, R=1m, m_s=2 kg)

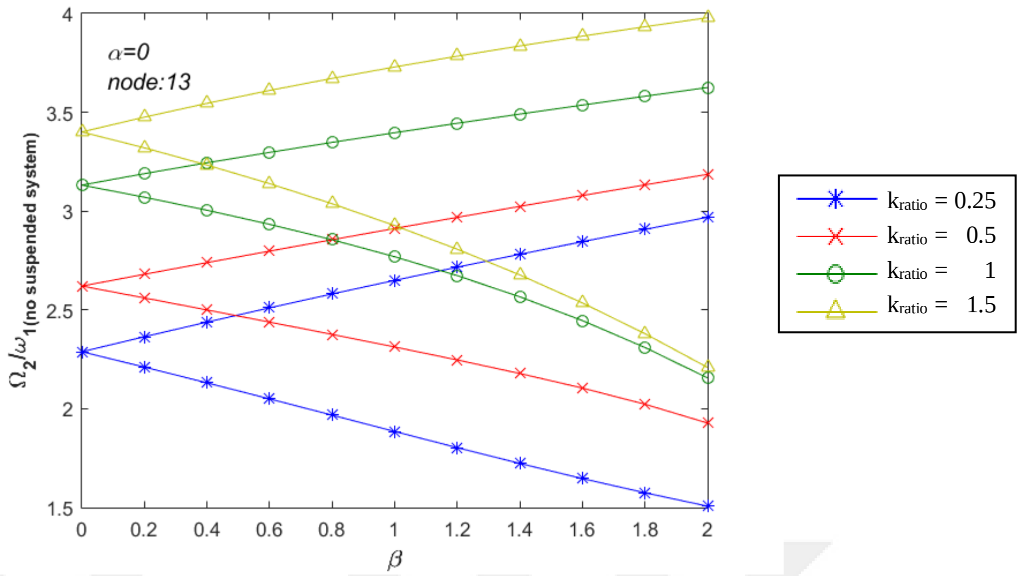

Figure 5.29 The effect of stiffness ratio of suspended spring on the second stability regions of the curved beam with one suspended spring-mass system, α=0 (E=2.069x10^{11}N/m^2, ν=0.3, ρ=7836.8 kg/m^3, b=0.02m, t=0.01m, θ=120º, R=1m, m_s=2 kg)

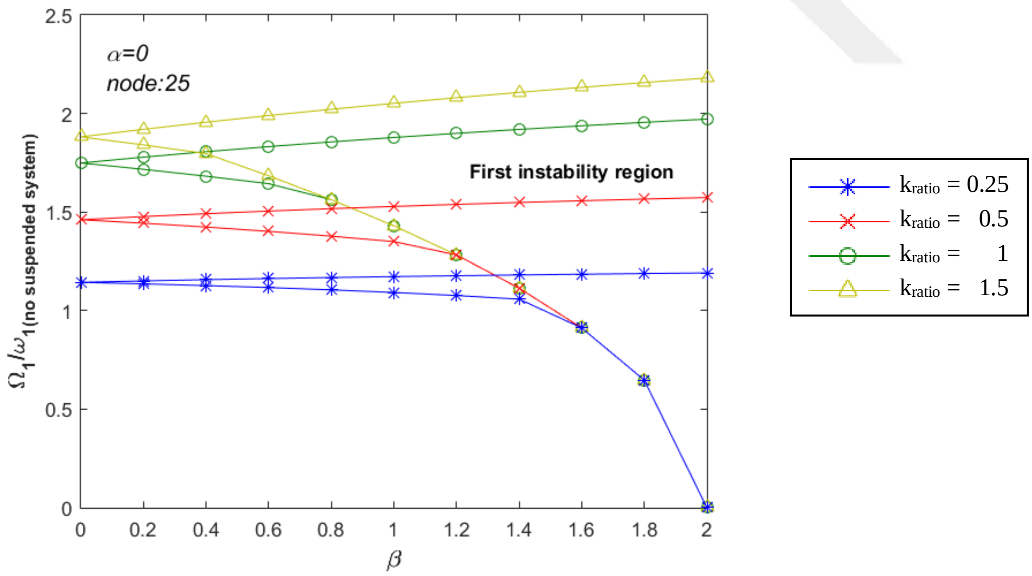

Figure 5.30 The effect of stiffness ratio of suspended spring on the first stability regions of the curved beam with one suspended spring-mass system, α=0 (E=2.069x10^{11}N/m^2, ν=0.3, ρ=7836.8 kg/m^3, b=0.02m, t=0.01m, θ=120º, R=1m, m_s=2 kg)

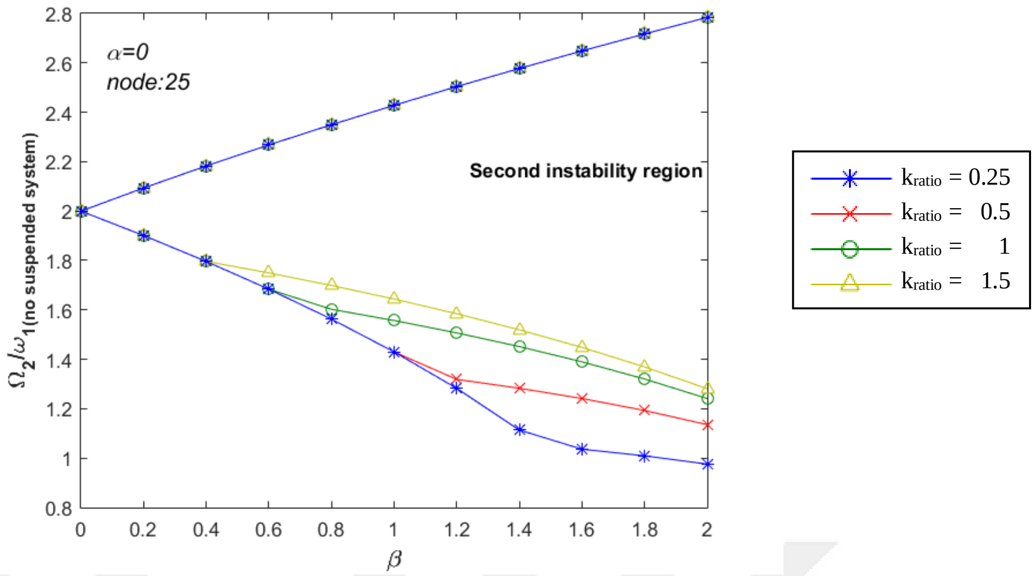

Figure 5.31 The effect of stiffness ratio of suspended spring on the second stability regions of the curved beam with one suspended spring-mass system, α=0 (E=2.069x10^{11}N/m^2, ν=0.3, ρ=7836.8 kg/m^3, b=0.02m, t=0.01m, θ=120º, R=1m, m_s=2 kg)

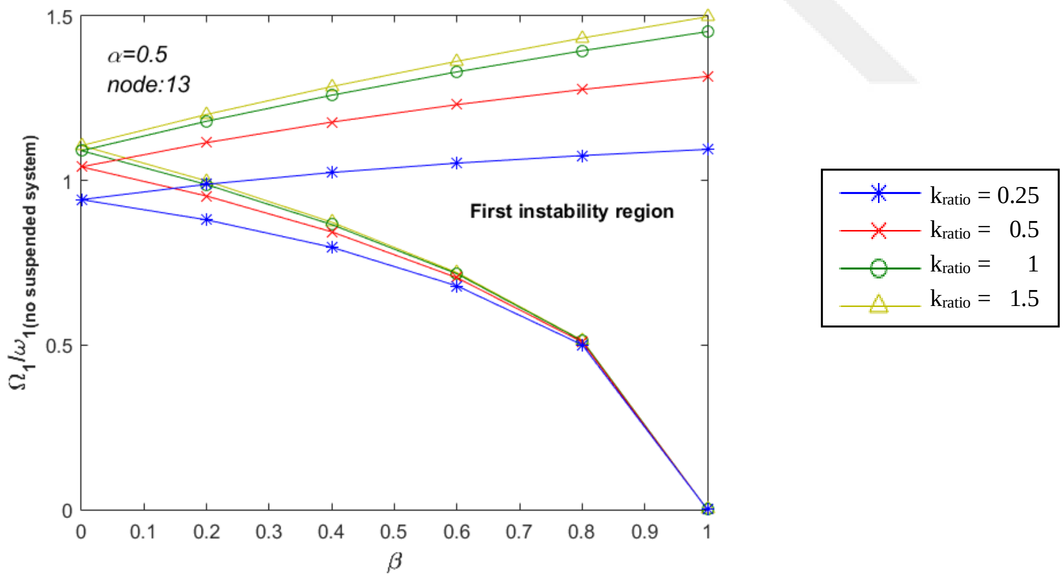

Figure 5.32 The effect of stiffness ratio of suspended spring on the first stability regions of the curved beam with one suspended spring-mass system, α=0.5 (E=2.069x10^{11}N/m^2, ν=0.3, ρ=7836.8 kg/m^3, b=0.02m, t=0.01m, θ=120º, R=1m, m_s=2 kg)

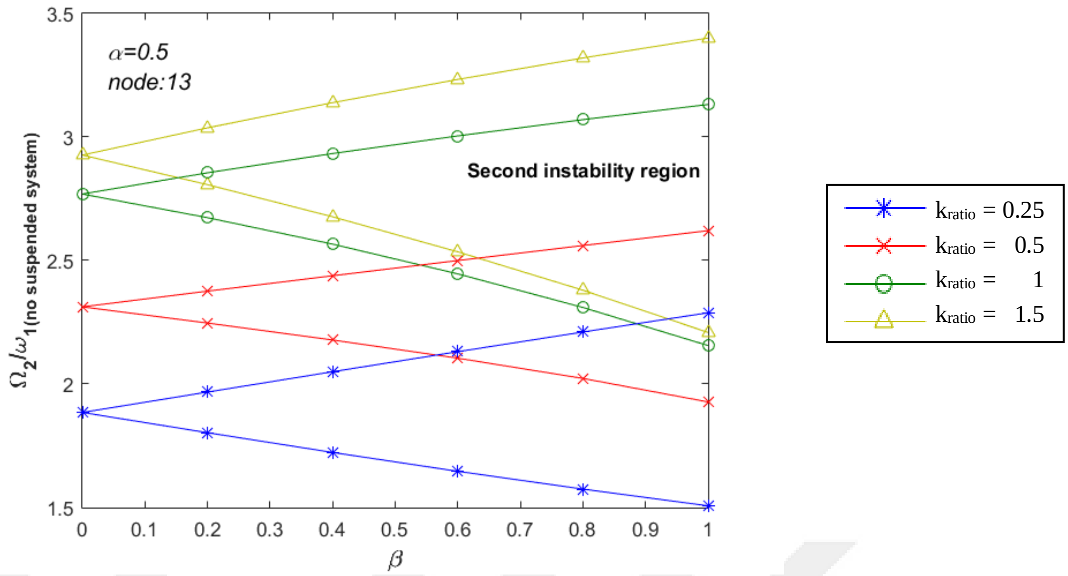

Figure 5.33 The effect of stiffness ratio of suspended spring on the second stability regions of the curved beam with one suspended spring-mass system, α=0.5 (E=2.069x10^{11}N/m^2, ν=0.3, ρ=7836.8 kg/m^3, b=0.02m, t=0.01m, θ=120º, R=1m, m_s=2 kg)

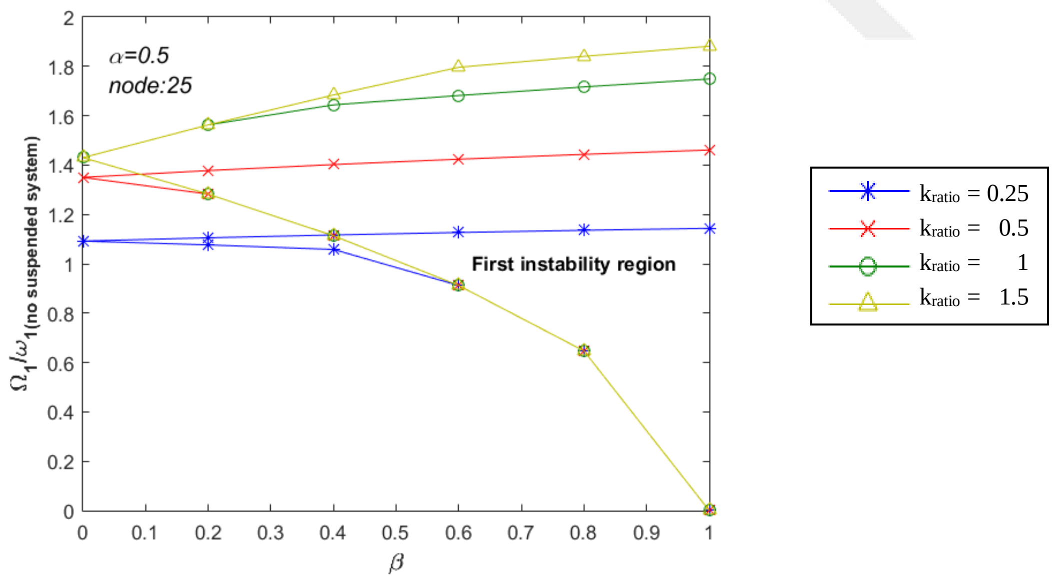

Figure 5.34 The effect of stiffness ratio of suspended spring on the first stability regions of the curved beam with one suspended spring-mass system, α=0.5 (E=2.069x10^{11}N/m^2, ν=0.3, ρ=7836.8 kg/m^3, b=0.02m, t=0.01m, θ=120º, R=1m, m_s=2 kg)

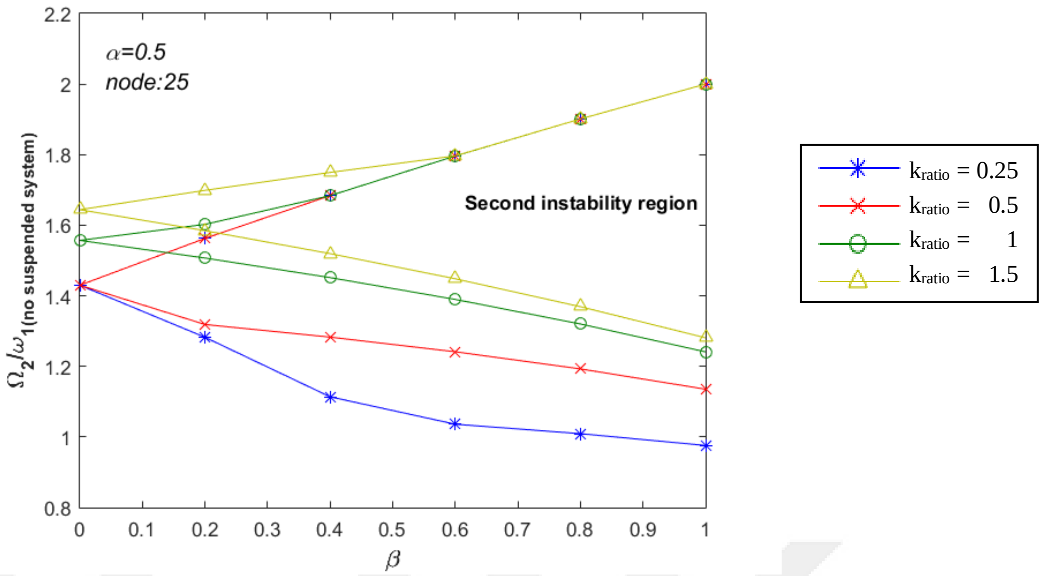

Figure 5.35 The effect of stiffness ratio of suspended spring on the second stability regions of the curved beam with one suspended spring-mass system, α=0.5 (E=2.069x1011N/m2, ν=0.3, ρ=7836.8 kg/m3, b=0.02m, t=0.01m, θ=120º, R=1m, ms=2 kg)

CHAPTER SIX
DYNAMIC STABILITY ANALYSIS FOR A COMPOSITE CURVED BEAM

6.1 Composite Structures

Composite is defined as brought close together in macroscopic level and comprised of two or more than constituents that don't dissolve in one another. These materials consist of two constituents named as reinforcing phase and matrix. The reinforcing phase has a discrete form like fiber, pieces or flake while the matrix has a continuous form generally. Composites are especially preferred by the aeronautical industry, the marine industry due to both high-resistant and lightweight. Graphite/epoxy, Kevlar/epoxy, boron/aluminum, and fiberglass/epoxy composites are examples of these.

6.1.1 The effective flexural modulus for a two-dimensional unidirectional lamina

A unidirectional lamina is considered as the orthotropic material. When the lamina is thin and not exposed to load on out of the plane, there can be assumed the in-plane stress case for the lamina. Therefore, the general strain-stress relationship for a two-dimensional body is (Kaw, 2006)

$$\begin{Bmatrix} \varepsilon_1 \\ \varepsilon_2 \\ \gamma_{12} \end{Bmatrix} = \begin{bmatrix} S_{11} & S_{12} & 0 \\ S_{12} & S_{22} & 0 \\ 0 & 0 & S_{66} \end{bmatrix} \begin{Bmatrix} \sigma_1 \\ \sigma_2 \\ \tau_{12} \end{Bmatrix} \tag{6.1}$$

where S_{ij} is the elements of the compliance matrix. If Equation 6.1 is inverted, the stress-strain equation is obtained as

$$\begin{Bmatrix} \sigma_1 \\ \sigma_2 \\ \tau_{12} \end{Bmatrix} = \begin{bmatrix} Q_{11} & Q_{12} & 0 \\ Q_{12} & Q_{22} & 0 \\ 0 & 0 & Q_{66} \end{bmatrix} \begin{Bmatrix} \varepsilon_1 \\ \varepsilon_2 \\ \gamma_{12} \end{Bmatrix} \tag{6.2}$$

where the Q_{ij} is the reduced stiffness coefficients that associate with the compliance coefficients shown as below.

$$Q_{11} = \frac{S_{22}}{S_{11}S_{22} - S_{12}^2} \tag{6.3}$$

$$Q_{12} = -\frac{S_{12}}{S_{11}S_{22} - S_{12}^2} \tag{6.4}$$

$$Q_{22} = \frac{S_{11}}{S_{11}S_{22} - S_{12}^2} \tag{6.5}$$

$$Q_{66} = \frac{1}{S_{66}} \tag{6.6}$$

For a unidimensional lamina, the engineering elastics constants *are* E_1, E_2, v_{12}, and G_{12} that are named as the longitudinal Young's modulus in direction *x* shown in Figure 6.1, the transverse Young's modulus in direction *z* shown in Figure 6.1, the major Poisson's ratio, and in-plane shear modulus, respectively. The four independent elements of the compliance matrix S of Equation 6.1 depend as follows on these four independent engineering elastic constants that measured experimentally.

$$S_{11} = \frac{1}{E_1} \tag{6.7}$$

$$S_{12} = -\frac{\upsilon_{12}}{E_1} \tag{6.8}$$

$$S_{22} = \frac{1}{E_2} \tag{6.9}$$

$$S_{66} = \frac{1}{G_{12}} \tag{6.10}$$

Additionally, the stiffness coefficients Q_{ij} can be rewritten using the Equations 6.7-6.10 as follows

$$Q_{11} = \frac{E_1}{1-\upsilon_{21}\upsilon_{12}} \tag{6.11}$$

$$Q_{12} = \frac{\upsilon_{12}E_2}{1-\upsilon_{21}\upsilon_{12}} \tag{6.12}$$

$$Q_{22} = \frac{E_2}{1-\upsilon_{21}\upsilon_{12}} \tag{6.13}$$

$$Q_{66} = G_{12} \tag{6.14}$$

where v_{21} is the minor Poisson's ratio and can be calculated from the following equation.

$$\upsilon_{21} = \frac{E_2}{E_1}\upsilon_{12} \tag{6.15}$$

The lamina may be placed with an α angle in order to provide the high-rigidity and high-strength. In this condition, the stiffness coefficients Q_{ij} should be transformed to the reduced stiffness coefficients $Q_{ij}*$ by using equations below.

$$Q_{11}^{\ *} = Q_{11}c^4 + Q_{22}s^4 + 2\left(Q_{12} + 2Q_{66}\right)s^2c^2 \tag{6.16}$$

$$Q_{12}^{\ *} = \left(Q_{11} + Q_{22} - 4Q_{66}\right)s^2c^2 + Q_{12}\left(s^4 + c^4\right) \tag{6.17}$$

$$Q_{22}^{\ *} = Q_{11}s^4 + Q_{22}c^4 + 2\left(Q_{12} + 2Q_{66}\right)s^2c^2 \tag{6.18}$$

$$Q_{12}^{\ *} = \left(Q_{11} + Q_{22} - 2Q_{12} - 2Q_{66}\right)s^2c^2 + Q_{66}\left(s^4 + c^4\right) \tag{6.19}$$

where c and s signify $cos\alpha$ and $sin\alpha$ terms, respectively.

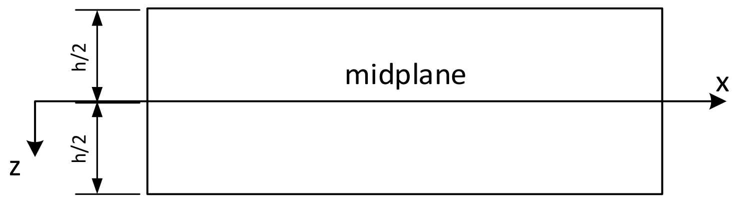

Figure 6.1 The coordinates of an orthotropic lamina

For an orthotropic lamina which is thin and is loaded only in its plane shown as Figure 6.1, the global strains in the top surface are expressed as follows

$$\begin{Bmatrix} \varepsilon_x \\ \varepsilon_y \\ \gamma_{xy} \end{Bmatrix} = \begin{Bmatrix} \dfrac{\partial u_0}{\partial x} \\ \dfrac{\partial v_0}{\partial y} \\ \dfrac{\partial u_0}{\partial x} + \dfrac{\partial v_0}{\partial y} \end{Bmatrix} + z \begin{Bmatrix} -\dfrac{\partial^2 \omega_0}{\partial x^2} \\ -\dfrac{\partial^2 \omega_0}{\partial y^2} \\ -2\dfrac{\partial^2 \omega_0}{\partial x \partial y} \end{Bmatrix} \tag{6.20}$$

u_0, v_0, and ω_0 are the displacement of x,y,z directions in mid-plane, respectively. In Equation 6.20, the first terms on right-hand sides explain the strain of mid-plane while the second terms imply the midplane curvatures. In this case, Equation 6.20 is expressed as

$$\begin{Bmatrix} \varepsilon_x \\ \varepsilon_y \\ \gamma_{xy} \end{Bmatrix} = \begin{Bmatrix} \varepsilon_x^0 \\ \varepsilon_y^0 \\ \gamma_{xy}^0 \end{Bmatrix} + z \begin{Bmatrix} \kappa_x \\ \kappa_y \\ \kappa_{xy} \end{Bmatrix} \tag{6.21}$$

The relation of forces and, moments acted on a lamina and the strains and, curvatures of the lamina is determined with Equation 6.22.

$$\begin{Bmatrix} N_x \\ N_y \\ N_{xy} \\ M_x \\ M_y \\ M_{xy} \end{Bmatrix} = \begin{bmatrix} A_{11} & A_{12} & A_{16} & B_{11} & B_{12} & B_{16} \\ A_{12} & A_{22} & A_{26} & B_{12} & B_{22} & B_{26} \\ A_{16} & A_{26} & A_{66} & B_{16} & B_{26} & B_{66} \\ B_{11} & B_{12} & B_{16} & D_{11} & D_{12} & D_{16} \\ B_{12} & B_{22} & B_{26} & D_{12} & D_{22} & D_{26} \\ B_{16} & B_{26} & B_{66} & D_{16} & D_{26} & D_{66} \end{bmatrix} \begin{Bmatrix} \varepsilon_x^0 \\ \varepsilon_y^0 \\ \gamma_{xy}^0 \\ \kappa_x \\ \kappa_y \\ \kappa_{xy} \end{Bmatrix} \tag{6.22}$$

In there, the resultant in-plane forces are associated with the in-plane strains by means of the extensional stiffness matrix **A**, while the bending stiffness matrix **D** couples the resultant bending moments to the plate curvatures. Besides that, the coupling stiffness matrix **B** relates the force and moment terms to the midplane strains and midplane curvatures.

The coupling stiffness matrix **B** equals zero for a symmetrical lamina according to the classical laminated plate theory when the resultant in-plane forces and the in-plane strains are assumed to be zero. Thus, using Equation 6.22, the bending compliance matrix **D*** can be obtained from Equation 6.23.

$$\begin{Bmatrix} \kappa_x \\ \kappa_y \\ \kappa_{xy} \end{Bmatrix} = \begin{bmatrix} D^*_{11} & D^*_{12} & D^*_{16} \\ D^*_{12} & D^*_{22} & D^*_{26} \\ D^*_{16} & D^*_{26} & D^*_{66} \end{bmatrix} \begin{Bmatrix} M_x \\ M_y \\ M_{xy} \end{Bmatrix} \tag{6.23}$$

In Equation 6.23, $D^*_{ij} = D^{-1}_{ij}$ and the D_{ij} is defined as

$$D_{ij} = \frac{1}{3}\sum_{k=1}^{n}\left[\left(Q_{ij}^{\ *}\right)\right]_k \left(h_k^3 - h_{k-1}^3\right) \tag{6.24}$$

where $i = 1,2,6$ and $j = 1,2,6$ for n number of layers seen in Figure 6.2. The laminated plate theory assumes that $M_y = 0$ and $M_{xy} = 0$.

$$\begin{Bmatrix} \kappa_x \\ \kappa_y \\ \kappa_{xy} \end{Bmatrix} = \begin{bmatrix} D^*_{11} & D^*_{12} & D^*_{16} \\ D^*_{12} & D^*_{22} & D^*_{26} \\ D^*_{16} & D^*_{26} & D^*_{66} \end{bmatrix} \begin{Bmatrix} M_x \\ 0 \\ 0 \end{Bmatrix} \tag{6.25}$$

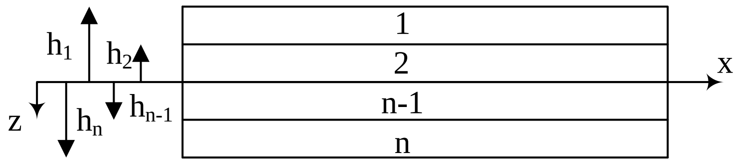

Figure 6.2 The layers of a beam

From Equation 6.25,

$$\kappa_x = D^*_{11} M_x \tag{6.26}$$

As a result, the effective flexural modulus are obtained as

$$E_f \equiv \frac{12 M_x}{\kappa_x h^3} = \frac{12}{h^3 D^*_{11}} \tag{6.27}$$

6.2 Free Vibration Analysis of a Composite Curved Beam

There are presented the natural frequency results of the composite curved beam in order to be a reference for the investigation of dynamic stability regions. The results of the first five natural frequency of present work are compared with ANSYS results in Table 6.1 and as seen from the table, agreements are good.

Table 6.1 The comparison of frequency results between the present composite curved beam and ANSYS models (E_1=35x10^9 N/m^2, E_2=9x10^9 N/m^2 , G_{12} = 4.7x10^9 N/m^2 , ν_{12}=0.28, ρ=1850 kg/m^3, b=0.02m, t=0.01m, R=1m)

		Frequency (Hz)				
		Mode				
Stacking Sequence		1	2	3	4	5
0°/0°/0°/0°	ANSYS	23.688	47.199	85.931	128.260	185.030
	Present Work	23.675	47.156	85.798	127.968	184.420
90°/90°/90°/90°	ANSYS	12.019	23.960	43.644	65.186	94.110
	Present Work	12.005	23.913	43.507	64.892	93.518
0°/90°/90°/0°	ANSYS	22.601	45.017	81.970	115.310	122.260
	Present Work	22.593	45.001	81.877	122.120	175.992
90°/0°/0°/90°	ANSYS	14.048	28.011	51.010	76.226	109.980
	Present Work	14.033	27.953	50.858	75.855	109.317
0°/45°/-45°/0°	ANSYS	22.740	45.298	82.481	121.160	123.050
	Present Work	22.773	45.360	82.530	123.094	177.396
0°/60°/-60°/0°	ANSYS	22.611	45.039	82.011	116.880	122.330
	Present Work	22.603	45.021	81.912	122.174	176.069

The composite curved beam has been studied for the six different laminated composite curved beams. The utilized orientations are denoted by C1, C2, C3, C4, C5, C6 as follows:

C1=0°/0°/0°/0°

C2=90°/90°/90°/90°

C3=0°/90°/90°/0°

C4=90°/0°/0°/90°

C5=0°/45°/-45°/0°

C6=0°/60°/-60°/0°

6.3 Dynamic Stability Region of the Composite Curved Beam

For the composite curved beam, the effect of dynamic stability parameter (β) on the dynamic stability regions are shown with graphics in Figures 6.3 – 6.6. These effects are figured out two cases in which the static load parameter is zero and 0.5. In case that the static parameter is zero, change of the dynamic stability regions are represented in Figures 6.3 and 6.4 and also in case that the static parameter is 0.5, change of the dynamic stability regions are represented in Figures 6.5 and 6.6.

From these figures, it can be seen that the initial disturbing frequency of composite curved beams having C2, C4, C3, C6, C5, and C1 type fiber orientations increases, respectively. The dynamic instability regions of the composite curved beam with suspended spring-mass system widen for C2, C4, C3, C6, C5, and C1, respectively. When the static load parameter is 0.5, sequences of instability region of the composite curved beam moves towards the origin and narrows.

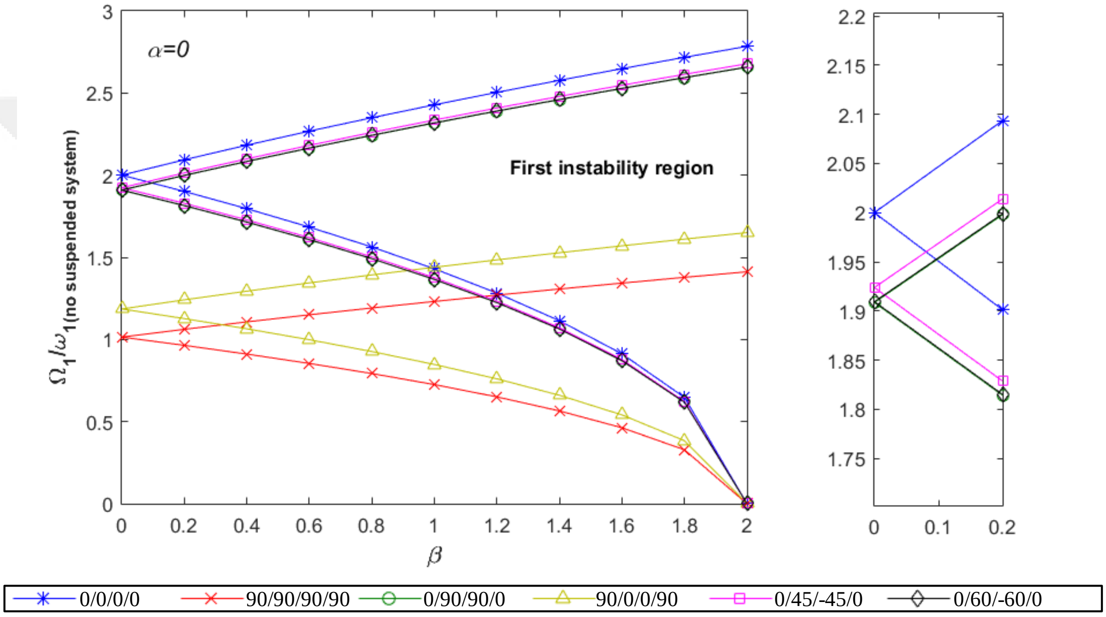

Figure 6.3 The effect of the orientation angle on the first stability regions of the curved composite beam, α=0 (E_1=3.5x10^{10}N/m^2, E_2=9x10^9N/m^2, G_{12}=4.7x10^9N/m^2, G_{23}=3.5x10^9N/m^2, ν_{12}=0.28, ρ=1850 kg/m^3, b=0.02m, t=0.01m, θ=120º, R=1m)

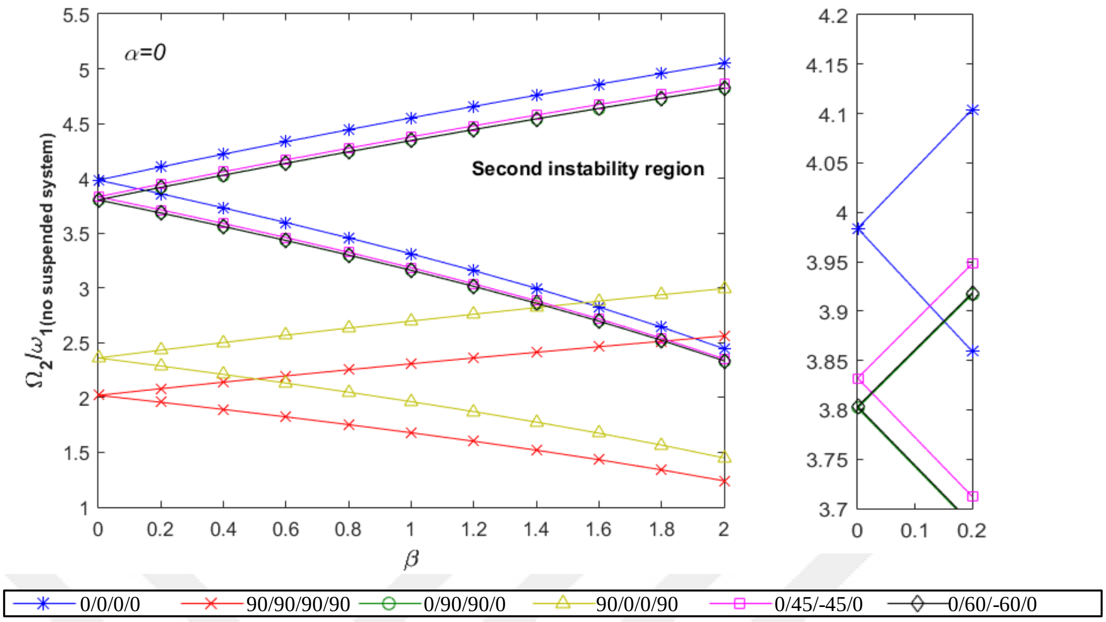

Figure 6.4 The effect of the orientation angle on the second stability regions of the curved composite beam, α=0 (E_1=3.5x10^{10}N/m^2, E_2=9x10^{9}N/m^2, G_{12}=4.7x10^{9}N/m^2, G_{23}=3.5x10^{9}N/m^2, ν_{12}=0.28, ρ=1850 kg/m^3, b=0.02m, t=0.01m, θ=120º, R=1m)

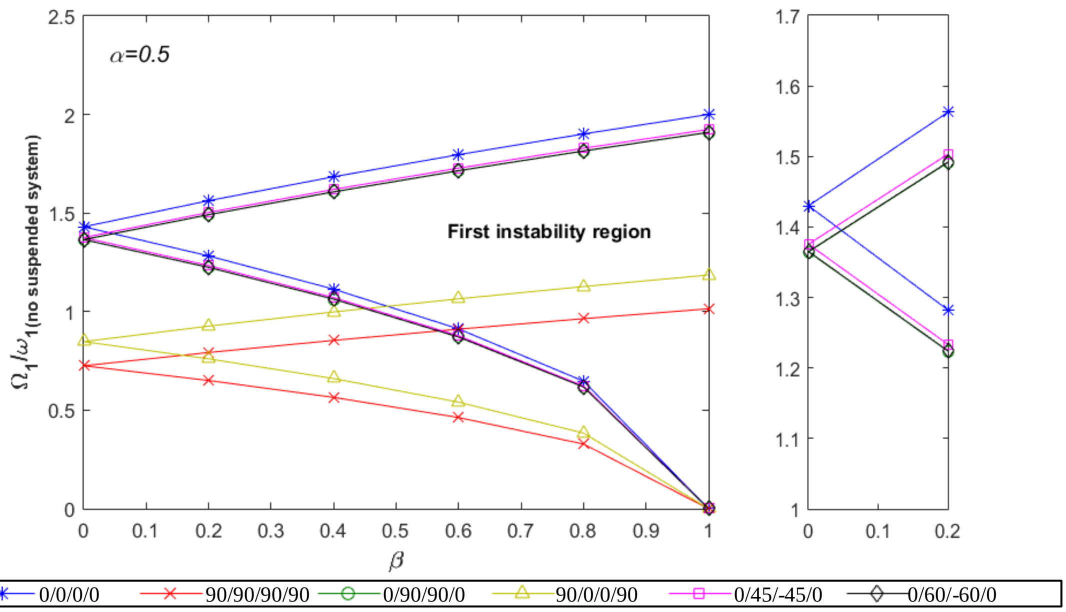

Figure 6.5 The effect of the orientation angle on the first stability regions of the curved composite beam, α=0.5 (E_1=3.5x10^{10}N/m^2, E_2=9x10^{9}N/m^2, G_{12}=4.7x10^{9}N/m^2, G_{23}=3.5x10^{9}N/m^2, ν_{12}=0.28, ρ=1850 kg/m^3, b=0.02m, t=0.01m, θ=120º, R=1m)

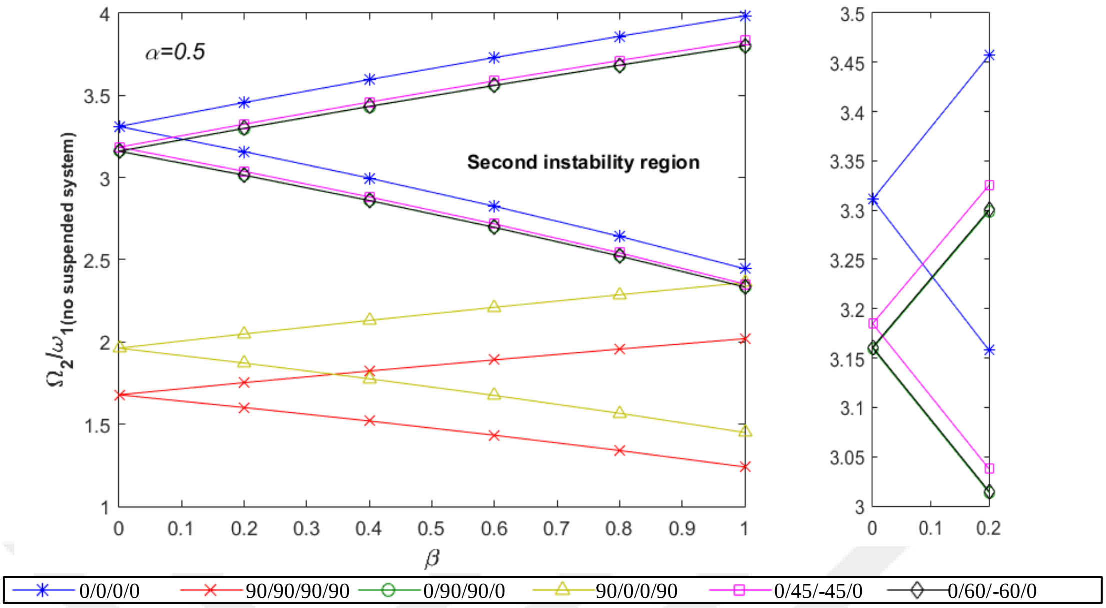

Figure 6.6 The effect of the orientation angle on the second stability regions of the curved composite beam angles, α=0.5 ($E_1=3.5\times10^{10}N/m^2$, $E_2=9\times10^9N/m^2$, $G_{12}=4.7\times10^9N/m^2$, $G_{23}=3.5\times10^9N/m^2$, $\nu_{12}=0.28$, $\rho=1850\ kg/m^3$, b=0.02m, t=0.01m, θ=120º, R=1m)

6.4 Dynamic Stability Region of the Curved Composite Beam with Suspended System

In this section, the effects of the number and location of the spring-mass system, fiber orientation angle are investigated on the stability region. The dynamic stability regions are shown with respect to the ratio of disturbing frequency to the natural frequency of *C1* curved beam without a suspended spring-mass system furthermore, the radius of the curved beam is 1 meter and the subtended angle is 120°.

The dynamic stability regions which are given in Figures 6.7 - 6.10 show the effect of the number of the suspended spring-mass system on the dynamic stability regions of the composite curved beam. For this reason, there is illustrated three different cases. In the first case, the curved beam doesn't have a suspended system, in the second case, the curved beam has one suspended system and in the last case, the curved beam has three suspended systems. The suspended mass is 2 kg and the stiffness coefficient ratio

k_{ratio} equals 1. Figures 6.7 and 6.8 express the case of no static loading while Figures 6.9 and 6.10 show the case of static loading.

As seen from these figures, if the composite curved beam has one or more the suspended spring-mass system, the dynamic instability region narrows and moves towards the origin. If the static load parameter increases, the dynamic instability regions of the composite curved beam are scattered and move towards the origin.

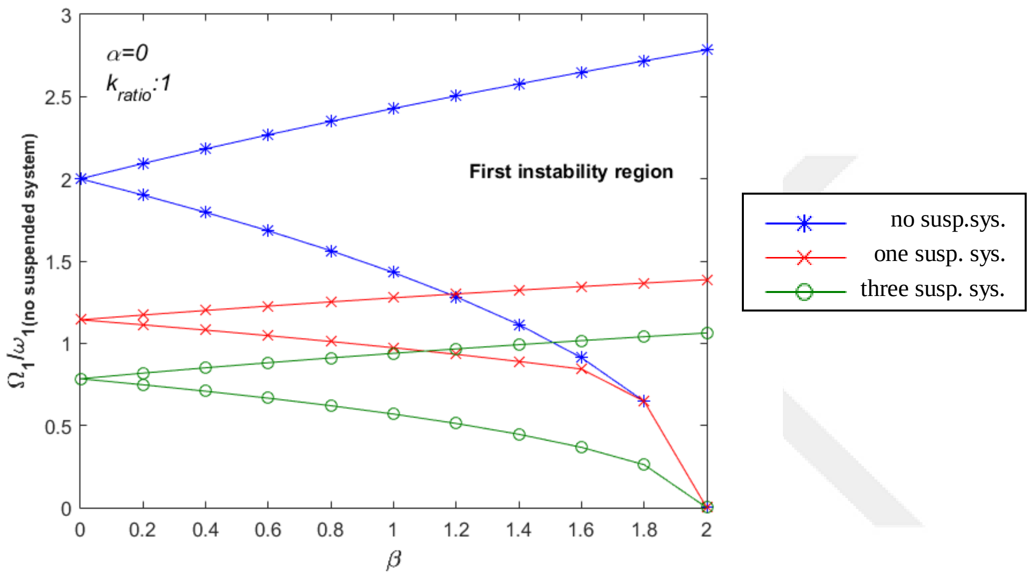

Figure 6.7 The effect of number of the spring-mass system on the first stability regions of the curved composite beam, α=0 (E_1=3.5x10^{10}N/m^2, E_2=9x10^9N/m^2, G_{12}=4.7x10^9N/m^2, G_{23}=3.5x10^9N/m^2, ν_{12}=0.28, ρ=1850 kg/m^3, b=0.02m, t=0.01m, θ=120º, R=1m, m_s=2 kg, k_{ratio}=1)

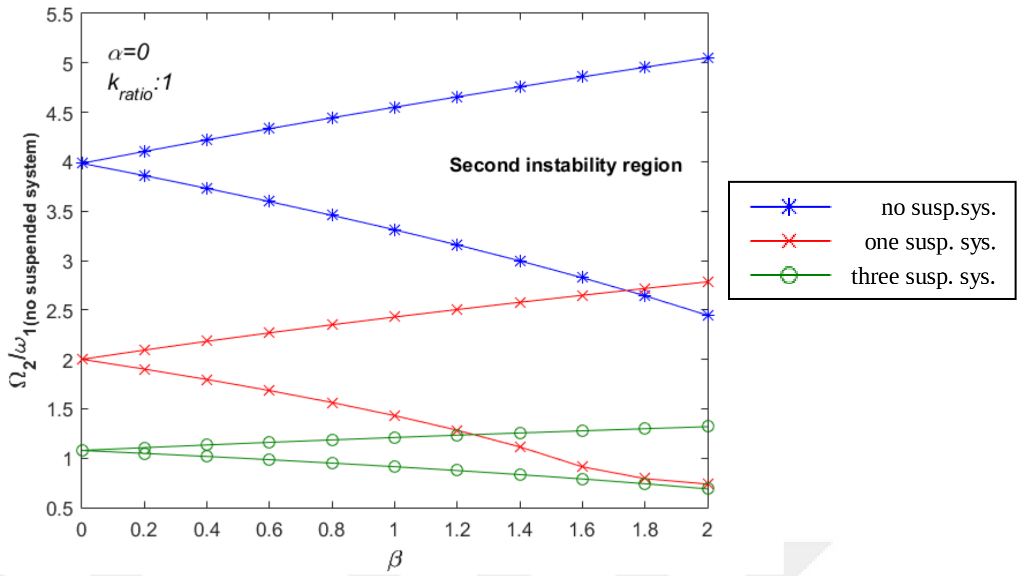

Figure 6.8 The effect of number of the spring-mass system on the second stability regions of the curved composite beam, α=0 (E_1=3.5x10^{10}N/m^2, E_2=9x10^{9}N/m^2, G_{12}=4.7x10^{9}N/m^2, G_{23}=3.5x10^{9}N/m^2, ν_{12}=0.28, ρ=1850 kg/m^3, b=0.02m, t=0.01m, θ=120º, R=1m, m_s=2 kg, kratio=1)

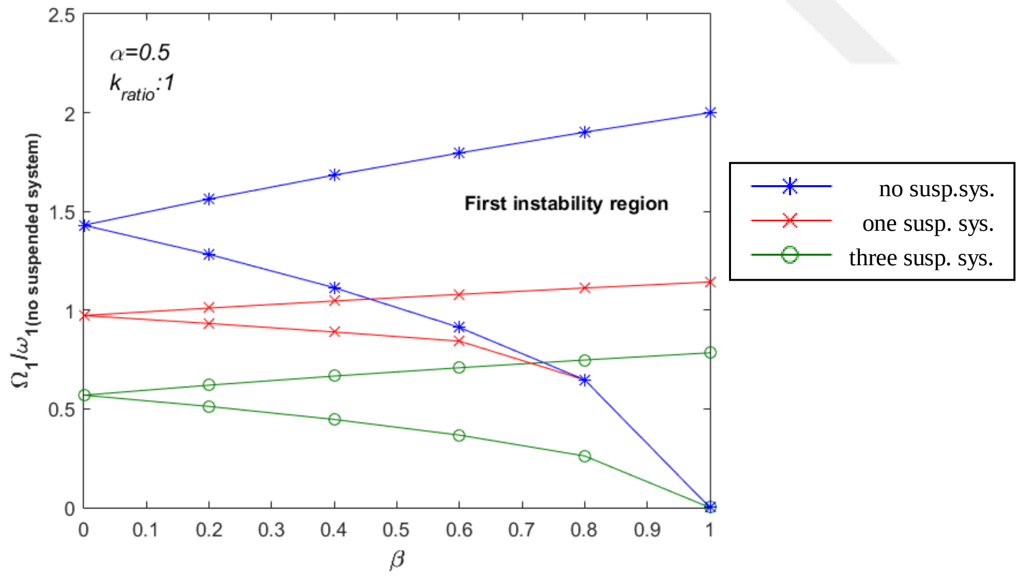

Figure 6.9 The effect of number of the spring-mass system on the first stability regions of the curved composite beam, α=0.5 (E_1=3.5x10^{10}N/m^2, E_2=9x10^{9}N/m^2, G_{12}=4.7x10^{9}N/m^2, G_{23}=3.5x10^{9}N/m^2, ν_{12}=0.28, ρ=1850 kg/m^3, b=0.02m, t=0.01m, θ=120º, R=1m, m_s=2 kg, k_{ratio}=1)

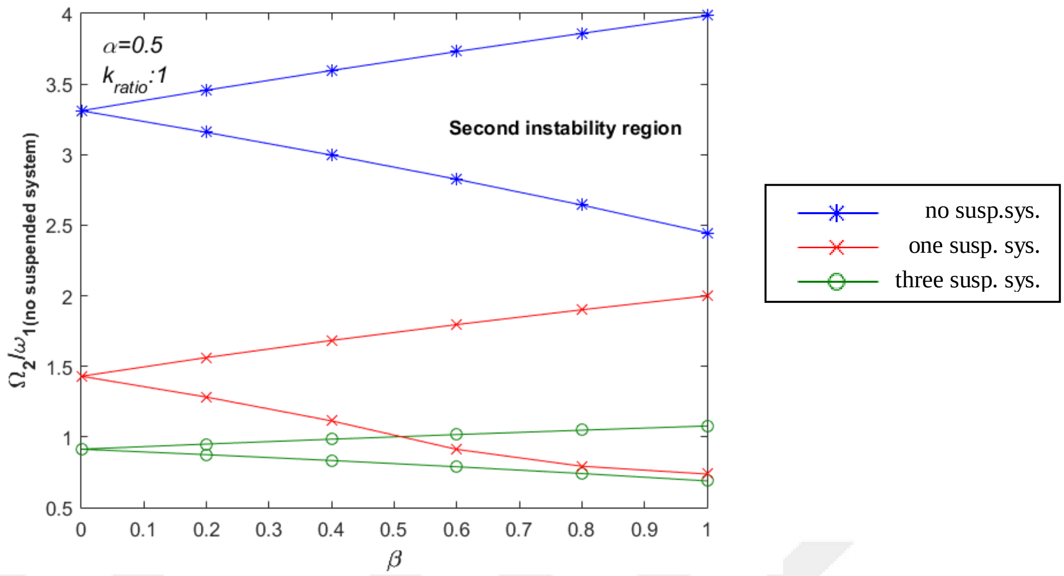

Figure 6.10 The effect of number of the spring-mass system on the second stability regions of the curved composite beam, α=0.5 (E_1=3.5x10^{10}N/m^2, E_2=9x10^9N/m^2, G_{12}=4.7x10^9N/m^2, G_{23}=3.5x10^9N/m^2, ν_{12}=0.28, ρ=1850 kg/m^3, b=0.02m, t=0.01m, θ=120º, R=1m, m_s=2 kg, k_{ratio}=1)

To assess the effect of location of the spring-mass system on the first and second stability regions of composite curved beam, only one spring-mass system has been suspended on various node of the system showing in Figure 5.2 (a). Besides that, the stability regions have been given with respect to the fiber orientation angles along with the different locations. The effect of the location of the spring-mass system on the stability regions is shown in Figures 6.11 and 6.12 for no static load. The effect of the location of the spring-mass system on the stability regions for static loading is indicated in Figures 6.13 and 6.14. For all of the situations, having static load and no static load, the ratio of stiffness coefficient ratio kratio is selected as 1 and the mass of suspended spring is 2 kg.

As seen from these figures, as long as the suspended spring-mass system is attached further away from non-vibrating nodes in terms of the mode shape of the composite curved beam, the dynamic instability region is narrower and closer to the origin from other cases.

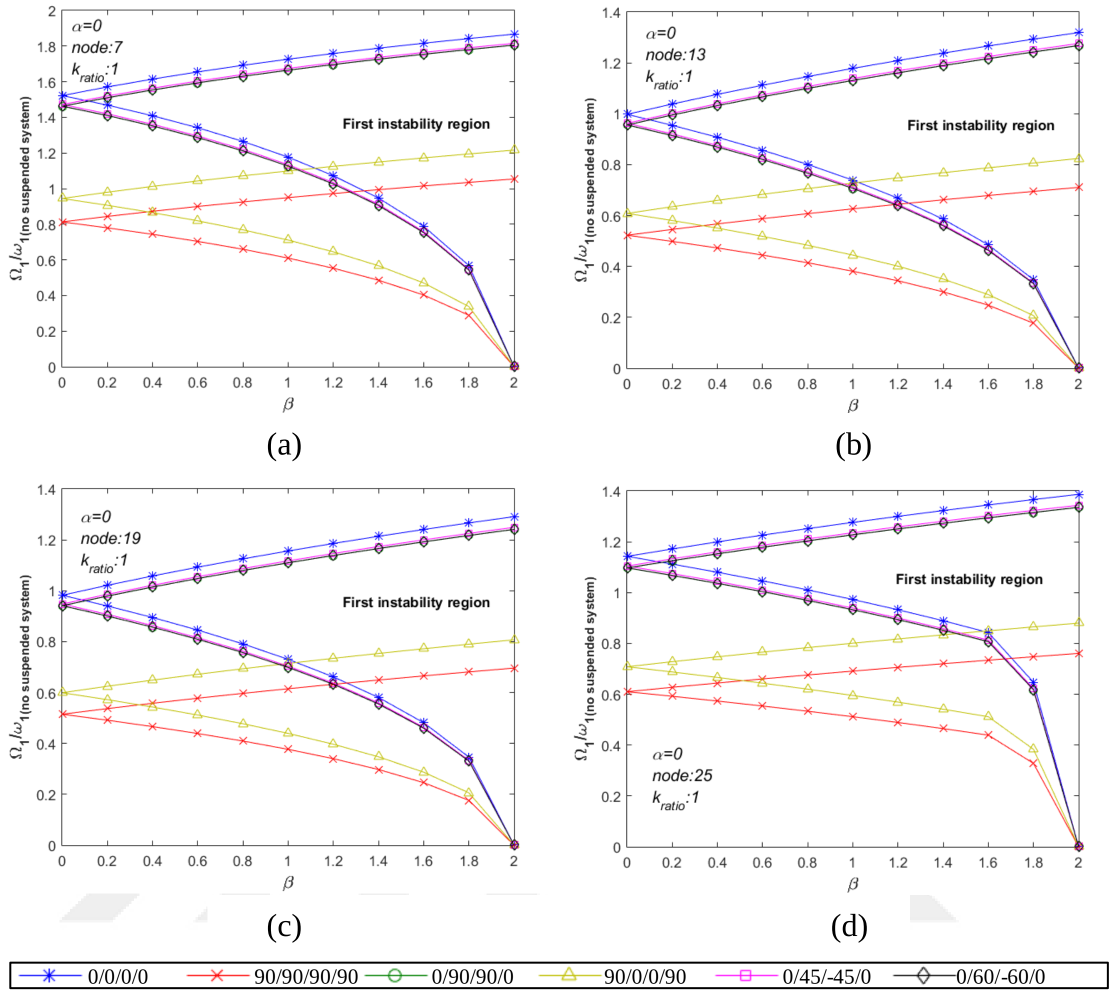

Figure 6.11 The effect of the fiber angles on the first stability regions of the curved composite beam with one suspended system, $\alpha=0$ ($E_1=3.5\text{x}10^{10}$N/m^2, $E_2=9\text{x}10^9$N/m^2, $G_{12}=4.7\text{x}10^9$N/m^2, $G_{23}=3.5\text{x}10^9$N/m^2, $\nu_{12}=0.28$, $\rho=1850$ kg/m^3, b=0.02m, t=0.01m, $\theta=120^o$, R=1m, $m_s=2$ kg, $k_{ratio}=1$)

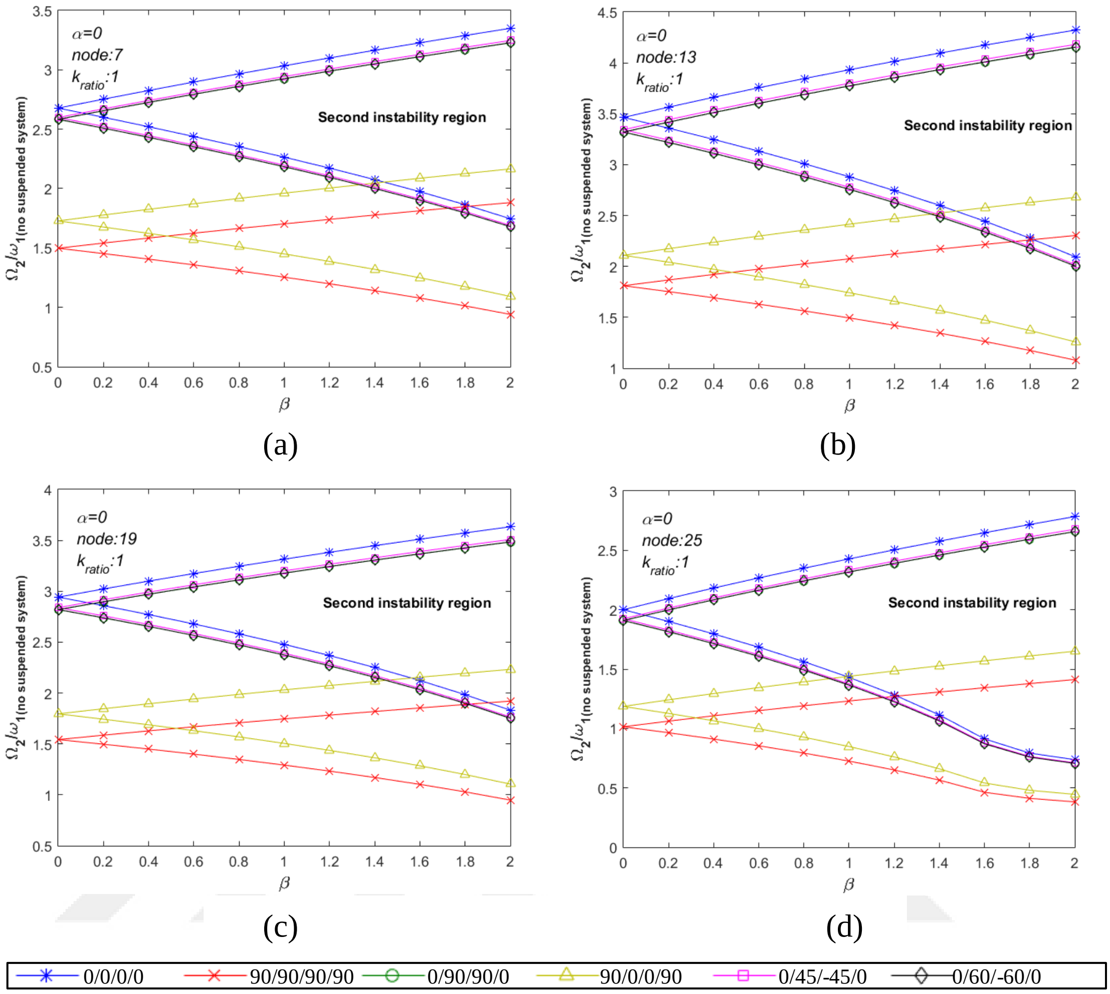

Figure 6.12 The effect of the fiber angles on the second stability regions of the curved composite beam with one suspended system, α=0 (E_1=3.5x10^{10}N/m^2, E_2=9x10^9N/m^2, G_{12}=4.7x10^9N/m^2, G_{23}=3.5x10^9N/m^2, ν_{12}=0.28, ρ=1850 kg/m^3, b=0.02m, t=0.01m, θ=120º, R=1m, m_s=2 kg, k_{ratio}=1)

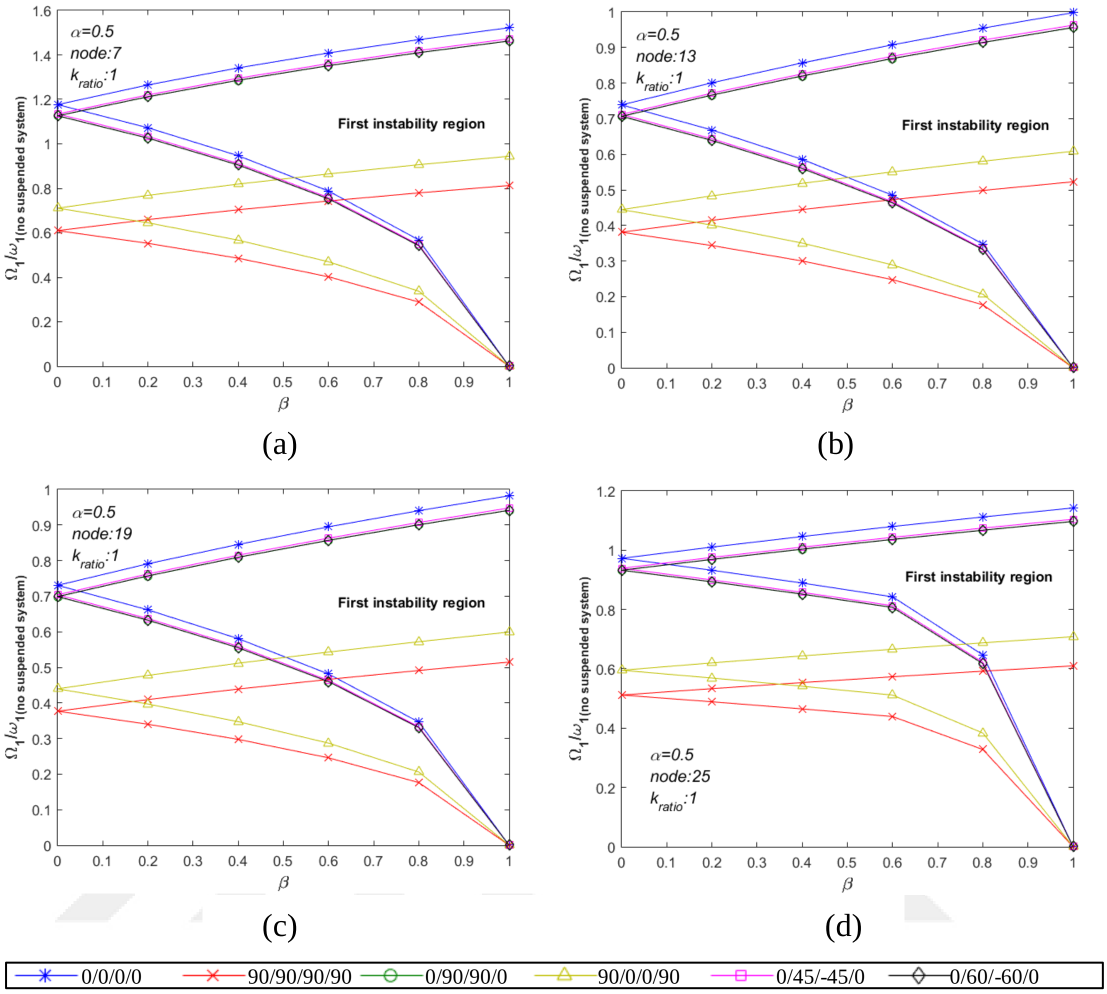

Figure 6.13 The effect of the fiber angles on the first stability regions of the curved composite beam with one suspended system, α=0.5 (E_1=3.5x10^{10}N/m^2, E_2=9x10^9N/m^2, G_{12}=4.7x10^9N/m^2, G_{23}=3.5x10^9N/m^2, ν_{12}=0.28, ρ=1850 kg/m^3, b=0.02m, t=0.01m, θ=120º, R=1m, m_s=2 kg, k_{ratio}=1)

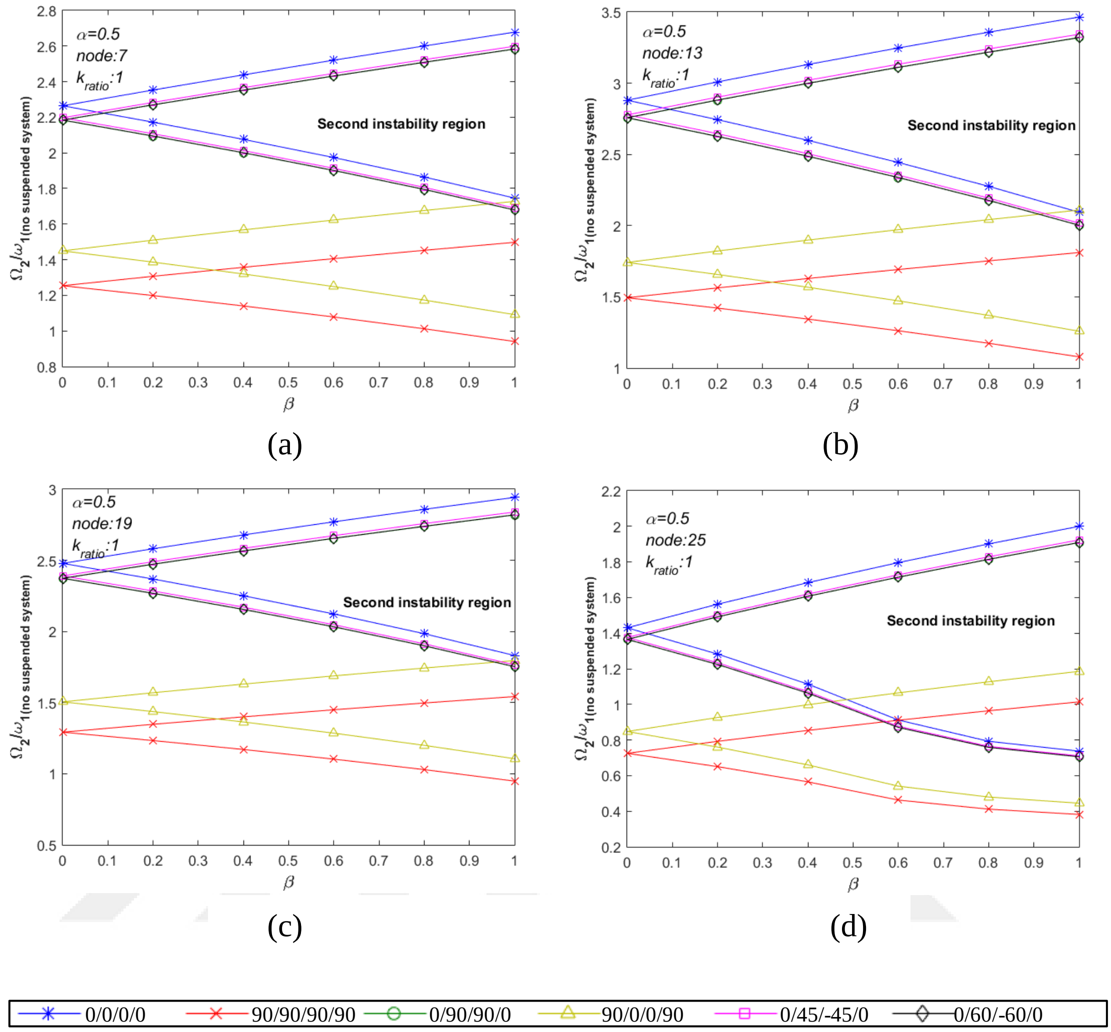

Figure 6.14 The effect of the fiber angles on the second stability regions of the curved composite beam with one suspended system, α=0.5 ($E_1=3.5\times10^{10}$N/m^2, $E_2=9\times10^9$N/m^2, $G_{12}=4.7\times10^9$N/m^2, $G_{23}=3.5\times10^9$N/m^2, $\nu_{12}=0.28$, ρ=1850 kg/m^3, b=0.02m, t=0.01m, θ=120º, R=1m, m_s=2 kg, k_{ratio}=1)

Figures 6.15 – 6.18 show the dynamic stability regions of the composite curved beam that has three suspended spring-mass system shown in Figure 5.2 (c). The effect of three suspended spring-mass system has been investigated for the different orientation angles. Figures 6.15 and 6.16 present the stability regions in the case of no static load while Figures 6.17 and 6.18 show the case with the static load. As seen from Figure 6.15, the instability regions of composite curved beam widen for C2, C4, C3, C6, C5, and C1, respectively in case of three suspended system. If the three spring-mass systems are attached, the dynamic instability region of composite curved beam narrows and moves towards the origin.

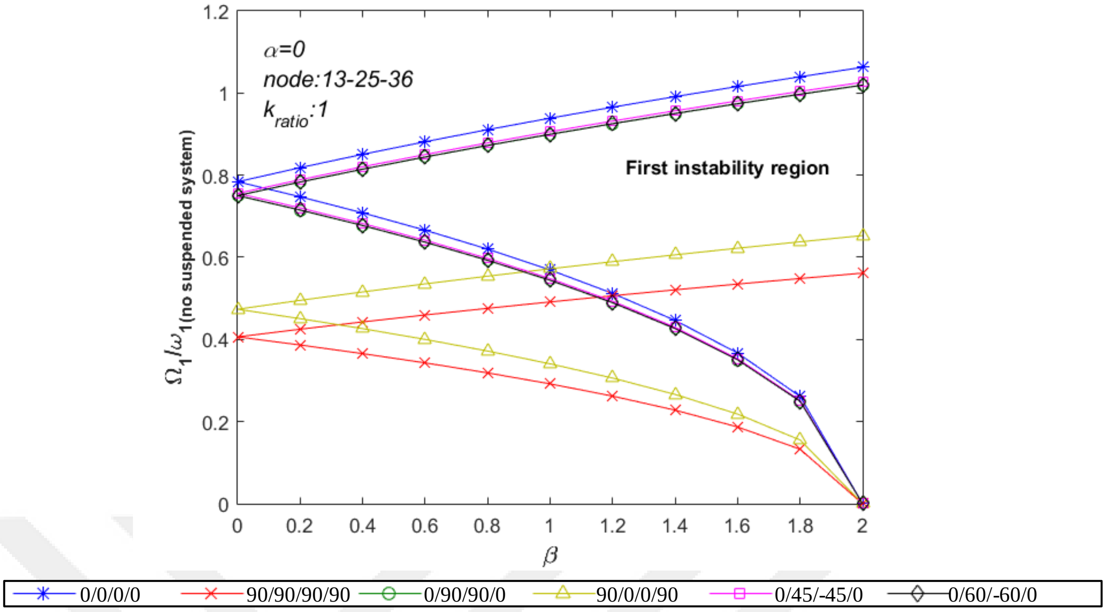

Figure 6.15 The effect of the fiber angles on the first stability regions of the curved composite beam with three suspended systems, α=0 ($E_1=3.5x10^{10}N/m^2$, $E_2=9x10^9N/m^2$, $G_{12}=4.7x10^9N/m^2$, $G_{23}=3.5x10^9N/m^2$, $\nu_{12}=0.28$, ρ=1850 kg/m^3, b=0.02m, t=0.01m, θ=120º, R=1m, m_s=2 kg, k_{ratio}=1)

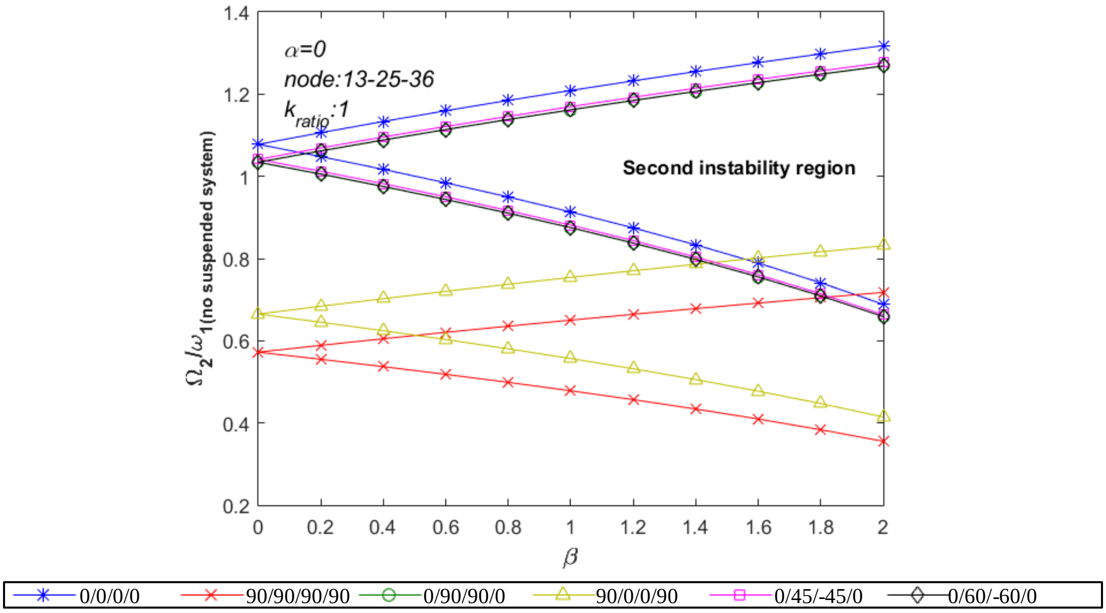

Figure 6.16 The effect of the fiber angles on the second stability regions of the curved composite beam with three suspended systems, α=0 ($E_1=3.5x10^{10}N/m^2$, $E_2=9x10^9N/m^2$, $G_{12}=4.7x10^9N/m^2$, $G_{23}=3.5x10^9N/m^2$, $\nu_{12}=0.28$, ρ=1850 kg/m^3, b=0.02m, t=0.01m, θ=120º, R=1m, m_s=2 kg, k_{ratio}=1)

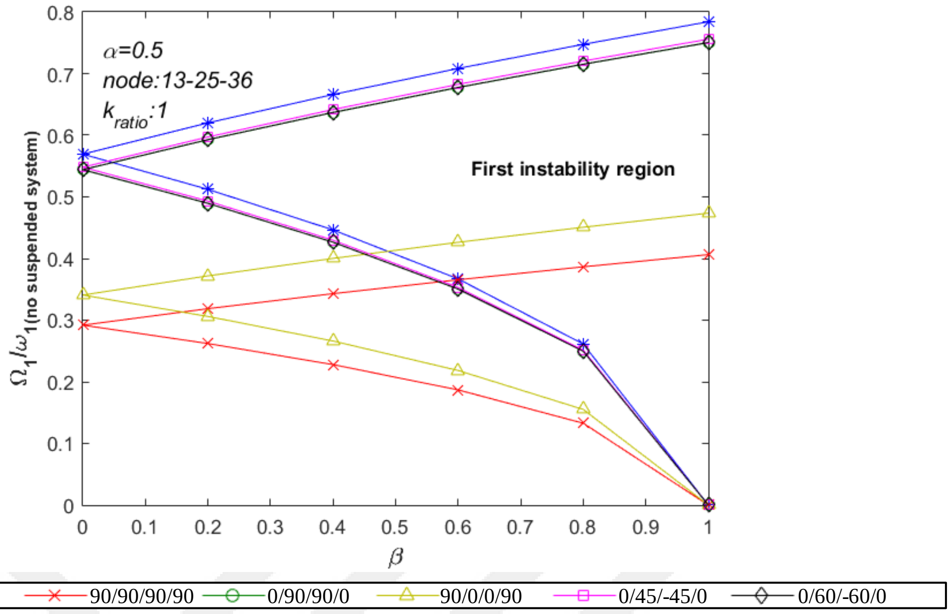

Figure 6.17 The effect of the fiber angles on the first stability regions of the curved composite beam with three suspended systems, α=0.5 (E_1=3.5x10^{10}N/m^2, E_2=9x10^9N/m^2, G_{12}=4.7x10^9N/m^2, G_{23}=3.5x10^9N/m^2, ν_{12}=0.28, ρ=1850 kg/m^3, b=0.02m, t=0.01m, θ=120º, R=1m, m_s=2 kg, k_{ratio}=1)

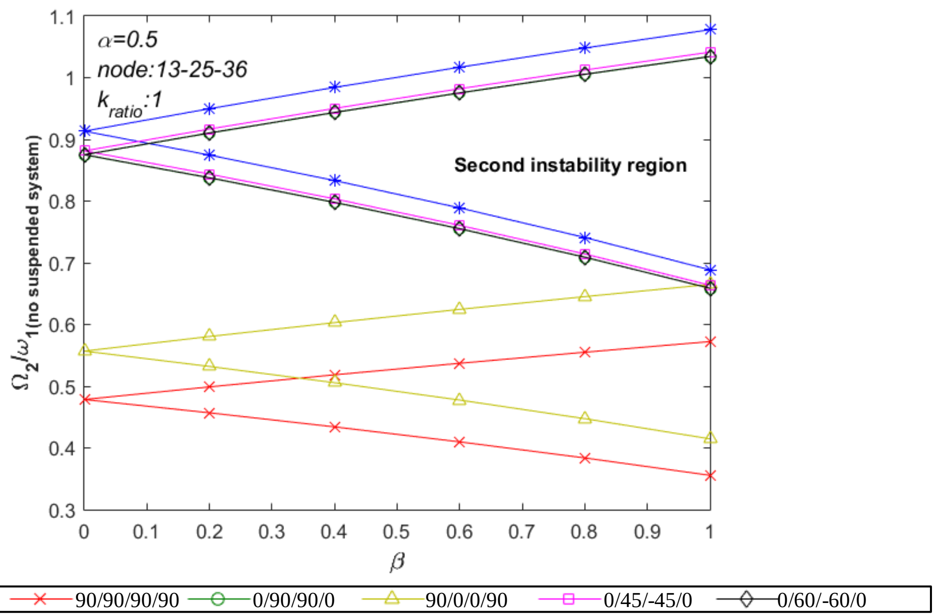

Figure 6.18 The effect of the fiber angles on the second stability regions of the curved composite beam with three suspended systems, α=0.5 (E_1=3.5x10^{10}N/m^2, E_2=9x10^9N/m^2, G_{12}=4.7x10^9N/m^2, G_{23}=3.5x10^9N/m^2, ν_{12}=0.28, ρ=1850 kg/m^3, b=0.02m, t=0.01m, θ=120º, R=1m, m_s=2 kg, k_{ratio}=1)

CHAPTER SEVEN
CONCLUSION

In this study, the dynamic stability of Euler-Bernoulli curved beam that has the suspended spring-mass system is investigated for both isotropic material and layered composite by using the finite element method. The conclusions are presented below:

- The location and number of suspended spring-mass systems are significant parameters for the natural frequency of curved beam with suspended spring-mass system. When the spring mass system is suspended on the vibrational nodes of curved beams, there is no effect on the natural frequencies.
- The suspension of the spring-mass system on the curved beam leads to constriction on the dynamic instability regions. If the number of the suspended spring-mass system is increased, the dynamic instability region shrinks further and the initial disturbing frequency moves towards the origin.
- When the static loading parameter equals to 0.5, the dynamic instability regions of the curved beam is narrower than the no static loading case and moves towards to the origin. Moreover, when the spring-mass system is suspended on curved beam, these effects are more considerable.
- As long as the suspended spring-mass system is attached further away from non-vibrating nodes in terms of the mode shape of the curved beam, the dynamic instability region is narrower and closer to the origin from other cases.
- If the subtended angle and radius of the curved beam reduce, the curved beam becomes more stable. In such a case, the appeared dynamic instability region belongs to the suspended spring-mass system. This region is excessively small and the initial disturbing frequency is seen far away from the origin.
- The reduction of the stiffness coefficient of the spring-mass system results in an ascendance the initial disturbing frequency as soon as a spread of dynamic instability region.

- The dynamic instability regions of the composite curved beam with suspended spring-mass system widen for the fiber orientation, C2, C4, C3, C6, C5, and C1, respectively.
- The initial disturbing frequency for the composite curved beam with suspended spring-mass system moves away from the origin with respect to the fiber orientation, C2, C4, C3, C6, C5, and C1, respectively.
- The dynamic instability regions of the composite curved beam with the suspended spring-mass system are in line with each other in cases of C3, C5, and C6.

REFERENCES

Abbas, B.A.H. (1977). *Mechanical vibration and dynamic stability of complex structures by finite element method*. Ph.D. Thesis, Surrey University, Surrey.

Ahmed, K. M. (1971). Free vibration of curved sandwich beams by the method of finite elements. *Journal of Sound and Vibration, 18* (1), 61-74.

Briseghella, L., Majorana, C. E., & Pellegrino, C. (1998). Dynamic stability of elastic structures: a finite element approach. *Computers & Structures*, *69* (1), 11-25.

Bolotin, V.V. (1962). *The dynamic stability of elastic systems.* San Francisco: Holden-Day, Inc.

Castle, B. (2006). *Tyne Bridge*. Retrieved November 23, 2018, from https://en.wikipedia.org/wiki/Tyne_Bridge.

Çankaya, P., Sabuncu, M., & Öztürk, H. (2017). Asılı Kütle-Yay Sistemlerine Sahip Eğri Çubuğun Titreşim Analizi. *Symposium: 18. Ulusal Makine Teorisi Sempozyumu*, (387-391).

Gunyar, A., Ozturk, H., Sabuncu, M., (2012). Kompozit Eğri Çubukların Doğal Frekans ve Burkulma Yükü Analizi. *DEU Mühendislik Fakültesi Mühendislik Bilimleri Dergisi*, *14*, (42), 33-42.

Gunyar, A., Ozturk, H., Sabuncu, M., (2012). Dynamic stability analysis of laminated curved beams. *DEU Mühendislik Fakültesi Mühendislik Bilimleri Dergisi*, *14*, (42), 43-55.

Howard, D.P. (2013). *Gateshead Millennium Bridge*. Retrieved November 23, 2018, from https://commons.wikimedia.org/wiki/Category:Gateshead_Millennium_Bridge.

Kaw, A. K. (2005). *Mechanics of composite materials.* CRC press.

Kawakami, M., Sakiyama, T., Matsuda, H., & Morita, C. (1995). In-plane and out-of-plane free vibrations of curved beams with variable sections. *Journal of Sound and Vibration, 187* (3), 381-401.

Lim, N. H., & Kang, Y. J. (2004). Out of plane stability of circular arches. *International Journal of Mechanical Sciences, 46* (8), 1115-1137.

Petyt, M., & Fleischer, C. C. (1971). Free vibration of a curved beam. *Journal of Sound and Vibration, 18* (1), 17-30.

Poon, W. Y., Ng, C. F., & Lee, Y. Y. (2002). Dynamic stability of a curved beam under sinusoidal loading. *Proceedings of the Institution of Mechanical Engineers, Part G: Journal of Aerospace Engineering, 216* (4), 209-217.

Rao, S. S. (2011). *Mechanical Vibrations*. Miami: Pearson.

Ravishankar, J. S. (2015). *Airplane Skeleton.* Retrieved November 23, 2018, from https://www.flickr.com/photos/jsravishankar/17119879092.

Reddy, J. N., (1997). *Mechanics of laminated composite plates theory and analysis*. New York: CRS Press.

Sabir, A. B., & Ashwell, D. G. (1971). A comparison of curved beam finite elements when used in vibration problems. *Journal of Sound and Vibration, 18* (4), 555-563.

Sabuncu, M. (1978). *Vibration characteristics of rotating aerofoil cross-section bladed-disc assembly*. PhD Thesis, Surrey University, Surrey.

Öztürk, H., Yeşilyurt, İ., & Sabuncu, M. (2006). In-plane stability analysis of non-uniform cross-sectioned curved beams. *Journal of Sound and Vibration, 296* (1-2), 277-291.

Yoo, C. H., Kang, Y. J., & Davidson, J. S. (1996). Buckling analysis of curved beams by finite-element discretization. *Journal of Engineering Mechanics, 122* (8), 762-770.

APPENDICES

NOMENCLATURE

A	cross-sectional area of the curved beam
b	width of the curved beam
E	elasticity module of the curved beam
E_f	Effective flexural modulus of the composite curved beam
I_{xx}	moment of area of cross-section of the curved beam
k_s	suspended stiffness coefficient
k_c	equivalent stiffness coefficient of the curved beam
k_{cr}	ratio critical buckling load parameter
K_e	global elastic stiffness matrix
k_e	elastic stiffness matrix of the elemental finite element
k_g	geometric stiffness coefficient of the curved beam
k_{ratio}	ratio of the stiffness coefficients
L	transformation matrix
l	length of the finite element
m_s	suspended mass
M	global mass (inertia) matrix
m_e	mass matrix of the elemental finite element
$P(t)$	periodic load
P_{cr}	critical buckling load
q	generalized coordinates
R	radius of the curved beam
t	thickness of the curved beam
T	kinetic energy
U	strain energy
v	axial displacement
w	radial displacement
α	static load parameter
β	dynamic load parameter
θ	subtended angle of the curved beam (opening angle)

ρ	density of the curved beam
φ	the opening angle of the finite element
ψ	rotation of tangent
Ω	disturbing frequency
ω	the natural frequency